UNIVERSITY OF CALIFORNIA

SANTA CRUZ

STRUCTURAL STUDIES OF RETINOBLASTOMA PROTEIN PHOSPHORYLATION

A dissertation submitted in partial satisfaction
of the requirements for the degree of

DOCTOR OF PHILOSOPHY

in

CHEMISTRY

by

Jason R. Burke

September 2012

The dissertation of Jason R. Burke is approved:

_____
Professor Glenn L. Millhauser, Chair

_____
Professor Seth M. Rubin, Advisor

_____
Professor R. Scott Lokey

_____
Tyrus Miller
Vice Provost and Dean of Graduate Studies

Table of Contents

Page

List of Figures

Page

List of Tables

Page

Abstract

The Retinoblastoma Protein (Rb) is a sentinel of the cell division process. When phosphorylated, Rb is inactivated and physically releases its protein-binding partner, E2F; a potent transcription factor that up-regulates many of the genes required for DNA synthesis and cell division. Aberrant deregulation of Rb, either through the loss of functional Rb or the persistence of hyper-phosphorylated Rb, is a common event in the development and progression of cancer. This study uses protein X-ray crystallography, NMR, ITC and SAXS to characterize three distinct structural changes to Rb that are caused by certain phosphorylation events. Specifically, we find phosphorylation of S608 induces the formation of a helix within the pocket linker region of Rb, which competitively inhibits E2F-binding. T373 phosphorylation promotes a docking interaction between Rb's two structured domains; this causes an allosteric change to a critical E2F-binding surface of Rb and dramatically weakens the Rb-E2F interaction. Lastly, phosphorylation of Rb's C-terminus at S788 and S795 also promotes an intramolecular interaction that destabilizes the Rb-E2F complex. These three distinct phosphorylation-induced mechanisms provide supporting evidence for structure-based theories of how Rb phosphorylation promotes the release and activation of E2Fs. A knowledge of these mechanisms is the first step in understanding how Rb may be therapeutically targeted to regain its function in cancer cells.

Acknowledgments

I acknowledge my research advisor and mentor, Dr. Seth Rubin. Thanks Seth, for taking me under your wing and teaching me-hands-on-about protein crystallography, NMR, and all the other stuff that went into the making of this thesis. Thanks for your extensive help with projects presented in this thesis, encouraging me to pursue my own ideas, and lastly, the many thought-provoking and enjoyable discussions we've had on the "Grand Unified Theory of Rb" over the years.

Thank you to my committee members, Dr. Glenn Millhauser and Dr. Scott Lokey, for your advice and encouragement throughout my time as a graduate student.

Thanks to the facility managers who assisted me with experiment design and data acquisition: Dr. Jeffery Pelton at the Central California 900MHz NMR facility, Qiangli Zhang at the UCSC Mass Spec facility, and James Loo at the UCSC NMR facility.

Thank you to all the members of the Millhauser lab, and specifically Dr. Matt Nix and Dr. Darren Thompson for teaching me the art of peptide synthesis and purification with a peptide that turned out to be exceptionally difficult to both synthesize and purify.

I am grateful to the members of the Rubin lab, past and present, for your daily ideas, support, encouragement, jokes, good taste in music and

great personalities. For this, thanks to my fellow current grad students, Alex Hirschi, Tyler Liban and Denise Lorish, and former students/post-docs: Dr. Eva Balog, Danielle Grey and Dr. Kyle Brown. Thanks to Jaclyn Schmidt, who rotated in the lab and worked with me on NMR experiments. Special thanks to my undergraduate assistants Alison Deshong and Tamara Restrepo who have made the most excellent contributions to chapters 2 and 4 of this thesis, respectively. Thanks to the other undergraduates I have mentored over the years, who have also made every day that we worked together at the bench feel like a productive day: Kenneth Sexton, Danaldo Salis, and Andrew Caldwell.

Thank you to my family. To my brother, Joseph, for your support and good ideas. Thanks to my aunt, Katherine Rowell, for your encouragement and discussions about science, both of which have been great motivating factors in my life. Thank you to my cousins Sharon and Tom Martin, Michelle Mellinger, Rebecca Martin, Lisa Gendron and Nicole Draper for your love and support.

This thesis is dedicated to the memory of my mother, Wendy Suzanne Rowell Burke, who passed away from complications related to Acute Myelogenous Leukemia on January 27th, 2012.

Chapter 1: Introduction

1.1 Rb and cancer

For over three decades now, the retinoblastoma protein (Rb) has been an important focal point of cancer research. The initial the discovery of Rb and revelations about its function changed our fundamental understanding of cancer biology. This introductory section on Rb and cancer will briefly introduce the discovery of Rb, theories on how it functions as a tumor suppressor, and the effects of Rb loss in different cancers.

1.1.1 Rb is a tumor suppressor protein

Rb was the first protein to be identified as a tumor suppressor. Prior to its discovery, the preeminent cancer model attributed mutant, constitutively-active and growth-promoting proteins to be the main cause of cancer (Hanahan and Weinberg 2011). By contrast, the discovery of a tumor suppressing protein heralded a model in which cancer can develop from the loss of a protein whose normal function is to prevent the formation of tumors. The discovery of Rb was spurred by Alfred Knudson's now famous "two hit hypothesis". In this hypothesis, Knudson proposed that individuals with familial retinoblastoma sometimes inherit only a signal functional copy of an important tumor suppressing allele and are therefore predisposed to earlier development of bilateral retinoblastoma via a sporadic "second hit" to that

allele (Knudson 1971). Knudson's hypothesis started a race to find the then-unknown gene. In the 1980s, the task of finding an unknown gene missing from a small group of cancer patients was monumental (it has been well-chronicled in the book Natural Obsessions). Once the gene was cloned it was found to be mutant homozygous in retinoblastoma patients (Dunn et al. 1988; Friend et al. 1986).

After the discovery of the RB1 gene, researchers began to wonder how a tumor suppressor protein functions. Similar to many known oncoproteins at the time, the protein product of the RB1 gene was identified as a phosphoprotein located in the nucleus of the cell (Lee et al. 1987). Subsequent studies revealed Rb is phosphorylated at the G_1-S boundary of the cell cycle (Buchkovich et al. 1989; Chen et al. 1989; DeCaprio et al. 1989; Mihara et al. 1989). The timing of Rb phosphorylation is concomitant with a critical growth-restriction point in the cell cycle: a moment late G_1 in which the cell commits to a round of cell division regardless of the removal of growth-factors (Pardee et al. 1989). Additional work showed that the E2F transcription factor physically associates with Rb (Bagchi et al. 1991; Bandara et al. 1991), and this interaction is dependent upon the phosphorylation state of Rb (Chellappan et al. 1991). The functional significance of the Rb-E2F interaction was elucidated when it was found that unphosphorylated Rb but not phosphorylated Rb causes repression of E2F-mediated promoters (Hamel et al. 1992; Helin et al. 1993), and importantly, that E2F promoters regulate

many of the genes required for S-phase (Nevins 1992). Taken together, this core body of initial research strongly implies that Rb's tumor suppressor activity is reflective of its ability to sequester E2F in the absence of mitogenic growth signals, whereby it negatively regulates the critical G_1-S transition of the cell-cycle. Likewise, this research also suggests that in a healthy cell, Rb has the essential role of responding to growth signals by becoming phosphorylated and releasing E2F, thereby promoting a timely transition in to S-phase.

While these early studies suggest a role for Rb that is consistent with tumor suppression, modern research indicates that Rb's roll in cancer may be far more complex. Recent studies correlate the loss of functional Rb with several newly-identified hallmarks of cancer. In addition to the suppression of cell division, these include: prevention of cellular senescence, promotion of angiogenesis, increased metastatic potential, and chromosomal instability (Burkhart and Sage. 2008). Many of these effects may be caused by the deregulation of transcription-promoting E2Fs, which are over-expressed in the majority of cancers and are suspected to be oncogenic in their own right (Chen et al. 2009). Accordingly, recent studies have shown that E2Fs regulate genes important for differentiation, development, apoptosis, metabolism, and chromatin remodeling (Burkhart and Sage. 2008; Chen et al. 2009; Hernando et al. 2004). Therefore, there are clear indications that Rb's

tumor suppressing function reflects its ability to control E2F-mediated transcription.

A separate line of research argues that Rb's tumor suppressor function may be separate from it's cell cycle dependent regulation of E2F. The basis of this theory comes from work which shows that a "LxCxE-binding site" on Rb is non-essential for the E2F-mediated G1-S transition of the cell cycle (Chen et al. 2000; Dick et al. 2000). Separate research suggests that Rb may use this special "LxCxE-binding site" to recruit chromatin modifiers and heterochromatin regulators such as HP1, SUV39H1 and DNMT1 to E2F promoters or heterochromatin (Gonzalo et al. 2005; Nielsen et al. 2001; McCabe et al. 2005). Mice lacking functional Rb and its pocket protein homologues are not viable and exhibit genomic instability, chromosome missegregation, and specific changes in histone methylation patterns on heterochromatin (Gonzalo et al. 2005). Astonishingly, very similar research shows that mutations to 3 residues within Rb's "LxCxE-binding site" can recapitulate the phenotypic changes to heterochromatin observed in triple knock-out mice, despite the fact that these mice are viable and seem healthy (Isaac et al. 2006). Notably, Rb's pocket protein homologues, p107 and p130, are compensatory to some functions of Rb but not others, and are not considered tumor suppressors although they also have an "LxCxE-binding site" (Cobrink 2005; Rayman et al. 2002). Separate investigations into Rb's tumor suppression function suggest that Rb may have a unique role in

regulating senescence by facilitating the formation of distinct heterochromatin structures and silencing E2F promoters (Narita et al. 2003). Again, by employing the same simple "LxCxE-binding site" mutant mice, Talluri et al, (2010) show impairment of both heterochromatinization and repression of E2F-responsive promotors in senescent cells, thereby narrowing down the requirement for Rb-mediated senescence to "LxCxE-binding". Despite this simplification, recent work further distinguishes that Rb loss in senescent cells correlates with increased transcription of E2F-controlled DNA synthesis genes, suggesting that transcriptional regulation of this subset of E2F promotors may be an important tumor suppressor function of Rb in senescence (Chicas et al. 2010). Whether or not LxCxE mediates chromatin modifications at these promotors to induce senescence, we will have to wait and see.

In light of the work that indicates the LxCxE site carries with it a critical tumor suppressor function, it is interesting to note that the LxCxE site is not a frequent site of missense mutations in tumors relative to the E2F-binding cleft (Lee et al. 1998). However, the "LxCxE-binding site" is one of Rb's most highly-conserved regions (Lee et al. 1998); an observation which has garnered wild speculation that the "LxCxE-binding site" hosts a variety of critical cellular proteins, each with its own "LxCxE motif" (Morris and Dyson 2001). Despite such speculation, definitive functional interactions which are mediated directly through "LxCxE" are left wanting. Indeed there are

contradictions over whether or not HDAC binds here directly (Dick et al. 2000; Harbour et al. 1999). In addition, my personal investigations have failed to detect the interaction between recombinant Rb and HP1 reported by Nielsen et al. (2001). Therefore, an entirely different possibility is that the "LxCxE-binding site" plays a role in regulating Rb-E2F complexes through a functionally-important but "weak" interaction, which has escaped detection from the infamous "pull-down" assays that have been used to characterize the Rb-E2F complex (Haung et al. 1993). Importantly, the same studies which originally claimed to parse LxCxE and E2F function also observed many instances in which "LxCxE-site" mutants are less effective than wild-type Rb in repressing E2F-mediated transcription (Chen et al., 2000; Dick et al, 2000). Furthermore, there are distinctions in the ways in which Rb binds different E2Fs that have functional consequences (Cecchini and Dick. 2011; Dick and Dyson. 2003; Hallstrom et al. 2003); it has been suggested that these interactions are mediated directly through the LxCxE site (Xiao et al. 2003).

1.1.3 Rb is a target of oncogenic viruses

The importance of Rb's tumor suppression function has been underscored by the fact that Rb is a primary target for deregulation by two potentially oncogenic viruses. Certain subtypes of the human papillomavirus (HPV) are considered to be the main etiological factor for cervical cancer and are associated with other epithelial cancers (zur Hausen H. 2002). Likewise,

it has been suggested that the Simian virus 40 (SV40) plays a role in mesotheliomas, although this idea is somewhat controversial (Felsani et al. 2006). The adenovirus is also known to target Rb; however, it has the interesting distinction of commonly causing respiratory infections in children, not cancer.

Despite differences in the oncogenic potential of these three virus families, each virus expresses a specific protein that interacts with Rb and it's homologues p107 and p130, principally through an LxCxE sequence (Felsani et al. 2006). The LxCxE motif is necessary for each viral protein to bind Rb with any appreciable affinity; however, LxCxE binding alone is not sufficient to disrupt Rb-E2F interactions. For this function, each viral protein has a unique sequence or domain (Huang et al. 1993; Ikeda et al. 1993; Phelps et al. 1992; Zalvide et al. 1998). For example, the adenovirus E1A protein contains a conserved N-terminal sequence which binds Rb similar to E2F (Ikeda et al. 1993; Liu et al. 2007). Likewise, HPV's E7 protein is thought to make multiple weak interactions that contribute to the overall disruption of Rb-E2F complexes (Liu et al. 2006; Huang et al. 1993; Phelps et al. 1992). Notably, HPV also mediates degradation of Rb in order to transform cells, suggesting that functional deregulation of Rb alone is not sufficient to cause cancer (Felsani et al. 2006).

1.1.3 Inactivation of Rb is ubiquitous in cancer

It is well established that the loss of functional Rb, through either gene mutation, chromosome deletion, or constitutive hyperphosphorylation, occurs in nearly all human cancers. Initially, loss-of-function mutations and genetic deletions of Rb were found to correlate with retinoblastoma, osteosarcoma, and distinct types of lung cancer (Friend et al. 1986; Harbour et al. 1988; Horowitz et. al. 1990). We now know that Rb loss in these types of cancer plays a unique role in the initial transformation of healthy cells in to cancer cells (Burkhart and Sage 2008). In addition, Rb is mutated in 15-50% of cases of prostate cancer, breast cancer, liver cancer, bladder cancer, glial cancer, adenocarcinomas, and chronic myelogenous leukemia. In these cancers, Rb loss often correlates with more progressive and invasive outcomes (Burkhart and Sage 2008). In several other cancers such as myeloma and pancreatic cancer, Rb is not frequently mutated; however, hallmarks of cancer may also arise from sporadic mutations to growth signaling proteins that ultimately deregulate Rb (Hanahan and Weinberg 2011). For example, in pancreatic cancer, the frequent loss the CDK4 inhibitor protein, p16INKa, leads to aberrant kinase activity and Rb hyperphosphorylation (Sherr 1996). Likewise, mutations in CDK4 which prevent regulation by p16INKa have been found in melanoma (Zou et al. 1996). Breast cancers sometimes exhibit an over abundance of cyclin E due to mutations in protein degradation machinery, which results in sustained Rb

hyperphosphorylation and is correlated with a poor prognosis (Sherr 1996). Therefore, although Rb's tumor suppressor function was identified as a virtue of its absence in retinoblastoma, we now know that Rb deregulation is ubiquitous in cancer. However, it is still poorly understood why Rb loss has distinct effects in different cancers.

1.2 Rb phosphorylation

Cell cycle progression through G_1-M is controlled primarily by the timely expression of cyclins D, E and A, each of which forms activating complexes with a specific cyclin dependent kinase (CDK) capable of phosphorylating Rb. During the cell cycle, Rb is phosphorylated in late G_1 by cyclinD-CDK4 and cyclinE-CDK2, resulting in the disruption of Rb-E2F complexes and the activation of E2F. Rb phosphorylation is then maintained by cyclinA-CDK2 until late G_2 when Rb is dephosphorylated by PP1 phosphatase. Rb has 16 CDK-consensus phosphorylation sites, many of which occur in pairs (mysteriously), and all of which exist within flexible loops and linkers of the protein. Rb also contains two similarly-structured alpha helical domains: the well-studied "pocket domain" is critical for E2F binding, while the N-terminal domain is important for E2F release. The C-terminal domain is intrinsically unstructured; however, it also interacts with E2F and recruits kinases to Rb. The work presented in this thesis identifies key phosphorylation events which disrupt Rb-E2F complexes through unique

molecular mechanisms. All of our work is done using purified proteins *in vitro,* and is predated by research which sought to detail the cellular context of Rb phosphorylation. Therefore, this introductory section reviews cell-based investigations which suggest Rb is phosphorylated differentially, both temporally and spatially, by different cyclin-CDK complexes. It is notable that these studies are sometimes contradictory in their findings. Nevertheless, the work reviewed in this section is relevant to this thesis not only because it provides a comprehensive background and reveals our motivation for these studies, more importantly, it suggests the mechanisms we've discovered might have specific timings and distinct functions in the cell.

1.2.1 Site-specific Rb phosphorylation by Cyclin-CDKs

The protein kinase family that phosphorylate Rb was found by the virtue of work with yeast that revealed cdc2 (cell division control protein 2) is essential for G_1-S and G_2-M transitions of the cell cycle (Nurse et al. 1976). Experiments using human cdc2 (Cyclin Dependent Kinase 1, or CDK1) and trypsin-generated Rb peptides show that Rb can be phosphorylated by CDK1 *in vitro* (Lin et. al. 1991). A similar study elegantly correlated this result to phosphorylation by CDK1 *in vivo* (in cultured cells), and additionally mapped some of these phosphorylation events to CDK consensus sites within Rb: S249/T252/T373/S807/S811 (Lees et al. 1991). At the time of this work, Rb phosphorylation was barely understood; however, the authors of this seminal

study prophetically proclaimed, “Although it is not yet known whether E2F binds to the same regions, this observation suggests that phosphorylation induces the dissociation of these factors by bringing about a major conformational change” (Lees et al. 1991).

The first study to support the growing notion that Rb is phosphorylated and functionally regulated by Cyclin-CDK complexes famously employed an osteosacroma cell line (SaOS-2) lacking endogenous Rb. Using these special cells, Hinds et al. (1992) show ectopic expression of Rb is sufficient to arrest cell proliferation, while ectopic expression of Rb with either cyclin A or E restores proliferation. *In vitro* experiments confirm Rb can also be phosphorylated by complexes of cyclinD-CDK4/6 (Kato et al. 1993), and that cyclinD1 even exhibits a unique physical association with Rb (Dowdy et al. 1993).

The first experiment to suggest that cyclinD-CDK4 and cyclinE-CDK2 may be playing unique roles in the phosphorylation of Rb, revealed that deletion of the cyclinD or cyclinE homologue in *saccharomyces cerevisiae* prevents human Rb from becoming fully phosphorylated (Hatakeyama et. al. 1994). This hypothesis was later supported by a landmark study from Lundberg and Weinberg (1998), who show selective inhibition of cyclinE-CDK2 in the presence of cyclinD-CDK4 allows for only partial phosphorylation of Rb. Furthermore, this partial “priming” phosphorylation event by cyclinD-CDK4 is required for cyclinE-CDK2 to then fully phosphorylate Rb and

inactivate E2F binding. Together, these results suggest that Rb is initially only partially phosphorylated by cyclinD-CDK4 (Lundberg and Weinberg suspected site-specifically), before cyclinE-CDK2 is up regulated later in G_1 to finish the job.

Separate groups of researchers used phosphopeptide mapping techniques to arrive at somewhat disparate conclusions about about whether Rb phosphorylation by cyclins D, E and A is, in fact, site-specific. Within the site-specific camp, experiments using Rb peptides phosphorylated *in vitro* show that each cyclin-CDK complex can phosphorylate a specific subset of Rb's phosphoacceptor sites: cyclinD-CDK4 phosphorylates all but S612 and T821; cyclinA-CDK2 and cyclinE-CDK2 are more selective and phosphorylate only S608, S612, S795, T821, and T373, S612, S795, T821, respectively (Zarkowska et al. 1997a). Additionally, a monoclonal antibody specific for phosphorylation at residue S608 shows this site is preferentially phosphorylated by cyclinD-CDK4 or cyclinA-CDK2 but not cyclinE-CDK2 (Zarkowska et al. 1997b). A separate group of researches attempting to answer the same question agree that cyclinD-CDK4 phosphorylates Rb in a site-specific fashion; however, in contrast to Zarkowska et al., they find that only cyclinD-CDK4 and not cyclinA-CDK2 or cyclinE-CDK2 is specific for S795 (Connell-Crowley et al. 1997). Subsequent work also suggests that S795 is preferentially phosphorylated over other phosphorylation sites in Rb by cyclinD-CDK4 (Grafstrom et al. 1999). A separate study employed *in vitro*

peptide phosphorylation experiments combined with *in vivo* analysis of specific phosphorylation events to conclude that S780 is the critical target of cyclinD-CDK4 (Kitagawa et al. 1996). Overall, this cluster of similar studies disagrees over the exact site specificities of cyclins D, E and A for Rb; however, the majority of studies presented here do agree that S795 is a preferred phosphorylation site for cyclinD-CDK4.

In the non-site specific Rb phosphorylation camp, a more qualitative and biologically-oriented *in vivo* approach to asking whether cyclins D,E and A differentially phosphorylate Rb showed that different ectopically expressed cyclin-CDK complexes produce identical proteolytic phosphopeptide maps of Rb; an indication that these different cyclin-CDK complexes might all phosphorylate Rb in the same fashion (Horton et. al. 1995). While this cell-based "*in vivo"* study largely contradicts the conclusions drawn from the *in vitro* peptide work, there are caveats to each set of experiments which call into question their accuracy in representing the true biological system. Firstly, phosphorylation of Rb peptides *in vitro* is far less efficient and therefore not necessarily representative of a reaction in which full-length Rb is phosphorylated (Grafstrom et al. 1999). This further suggests that *in vitro* peptide phosphorylation reactions are often missing an important lager protein context which may direct or enhance phosphorylation at specific sites. Secondly, *in vivo* ectopic over-expression of kinases in SaOS2 cells can produce artificial kinase-substrate ratios that may promote

hyperphosphorylation of the substrate in a manner that is not necessarily reflective of the true endogenous activity of those proteins. For example, Lundberg and Weinberg (1998) stated that by using an ectopic expression system with either cyclinE or D, they were able to drive Rb phosphorylation to completion; however, when they used endogenous levels of the cyclin-cdks and controlled the enzyme activity through over-expression of specific cyclin-cdk inhibitor proteins, they found that neither cyclinD-CDK4 or cyclinE-CDK2 could fully phosphorylate Rb on its own.

Since the initial discovery that Rb can be phosphorylated *in vitro* by any of the cyclin-cdk complexes which predominate throughout the cell cycle, only two carefully-controlled studies have revealed the intriguing distinction that, *in vivo*, both cyclinD-CDK4, and cyclinE-CDK2 are necessary to fully phosphorylate and thereby deactivate Rb at the G_1-S transition (Hatakeyama et al. 1994; Lundberg and Weinberg 1998). These results imply that Rb must be phosphorylated in a manner that is sequential and/or cooperative. Unfortunately, studies in to site-specific phosphorylation of Rb by these cyclin-CDK complexes have yielded only one quasi-consistent result: that cyclinD-CDK4 may have a preference for phosphorylating Rb at S795 (Connell-Crowley et al. 1997; Grafstrom et al. 1999; Zarkowska et al. 1997a). Modern investigations have begun to focus on the important roles of Rb that extend beyond cell-cycle regulation. Accordingly, one long-standing hypothesis has been that distinct phosphorylation events can give rise to specific

phosphoisoforms of Rb, each with unique binding epitopes that may produce distinct signaling outputs (Mittnacht et al. 1994). On the other hand, the sequential phosphorylation regime of Rb might simply represent an esoteric biological control mechanism that exists only to safeguard the critical G_1-S transition from aberrant kinase activity. Either way, more careful biological investigations are required to adequately reveal the details and purpose of the initial site-specific phosphorylation events promoted by CyclinD-CDK4.

1.2.2 The different functions of specific Rb phosphorylation events

Since the initial discovery that Rb-E2F binding is negatively regulated by the phosphorylation of Rb (Chellappan et al. 1991), a persistent set of questions with mechanistic qualities has occupied the minds of Rb researchers: Which phosphorylation sites are necessary for dissociating Rb-E2F complexes? Are certain Rb phosphorylation sites (or sets of phosphorylation sites) redundant in this function? Do select Rb phosphorylation sites regulate non-E2F activities? Studies over two intervening decades have lent support to the notion that certain phosphorylation sites are indeed better than others at dissociating Rb-E2F complexes. Likewise, the hypothesis that Rb phosphorylation regulates some non-E2F activities has also been supported-sort of. However, the answer to whether or not phosphorylation at different sites is functionally redundant has been more elusive, and while some studies have identified general functional

redundancies, a detailed knowledge of the specific role and timing of each phosphorylation event is likely required to begin to truly understand the complex interplay between different phosphorylation sites.

A study by Knudsen and Wang was the first to suggest that certain phosphorylation sites have roles outside of the regulation of Rb-E2F binding; they described how phosphorylation at S807/S811 promotes the dissociation of Rb complexes with c-Abl, while phosphorylation at T821/T826 dissociates Rb from viral oncoproteins containing an 'LxCxE' motif (Knudsen and Wang 1996). While the role of S807/S811 phosphorylation in disrupting Rb complexes with c-Abl has not been well-supported since this initial finding, many investigations have focused on the role of T821/T826 phosphorylation. The crystal structure of Rb bound to an LxCxE peptide reveals a close physical proximity between the LxCxE peptide and a conserved lysine patch on Rb that the authors suggested might serve as a binding site for phosphorylated T821/T826 (Lee et al. 1998). Later work suggests phosphorylation at T821/T826 is capable of disrupting interactions between Rb and histone deacetylase (HDAC), which contains an 'LxCxE' motif (Harbour and Dean 1999); however, this result has been challenged multiple times (Dick et al. 2000; Kennedy et al. 2001; Rayman et al. 2002). Most recently, quantitative binding studies confirm that phosphorylation of T821/T826 enhances the affinity of the RbC-terminus for the Rb pocket domain (Rubin et al. 2005).

Initial work that sought to parse specific phosphorylation events with the disruption Rb-E2F complexes reveals two distinct mechanisms for phosphorylation-induced dissociation of Rb-E2F complexes: one involving the C-terminus of Rb and the other involving pocket linker region of Rb (Knudsen and Wang 1997). Specifically, this study was the first to show that by using alanine substitutions to the 7 most C-terminal phosphoacceptor sites of Rb, phosphorylated Rb (lacking the structured N-terminal domain) looses its ability to dissociate E2F1 and instead binds E2F1 similar to unphosphorylated Rb. Additionally, these researchers propose Rb-E2F complexes also dissociate due to phosphorylation of the pocket linker sites in Rb (S608 and S612), which they assert, requires the presence of the structured N-terminal domain. Subsequent work claims to support this hypothesis and has shown that U2-OS cells transfected with Rb lacking C-terminal phosphorylation sites exhibit *slightly retarded* colony formation when compared with wild-type (Chew et al. 1998).

Follow-up work by Brenda Gallie and coworkers convincingly used mouse Rb to show mutations to T373 or S807/S811 or 821/826 partially suppresses E2F reporter activity in the presence of cyclinE-CDK2; however, they found that the suppression effect is greatest with the greatest number of mutations: T252/T356/S608/S612/S788/S795/S807/S811 (Brown et al. 1998). Thus, they generally concluded, “Our data suggest that regulation of the pRb-

E2F interaction on DNA by phosphorylation of pRB occurs by accumulation of phosphate groups on the pRB molecule".

More recently, several papers by Joe Baldassare and coworkers have challenged the hypothesis that multiple phosphorylation events are required to dissociate Rb-E2F complexes. Initially, this group showed that a set of four phosphorylation sites, previously identified as specific for cyclinE-CDK2 (Zarkowska et al. 1997a), is sufficient to relieve Rb-mediated repression of E2F activity (Keenan et al. 2004). Follow-up work employed reverse mutational analysis to generate several Rb constructs with only one or two of Rb's sixteen possible phosphoacceptor sites. By using these constructs in a variety of assays, Lents et al. (2006) made the surprising discovery that phosphorylation at T373 alone is sufficient to fully restore E2F activation and progress cells into S-phase. In addition, this study revealed that all Rb constructs containing S795 partially restored E2F reporter activity and only S608 in combination with S795 showed significantly greater E2F reporter activity than S795 alone. Later work by the same group found that phosphorylation of T356 alone can also partially restore activity in a cyclin E reporter assay (Gorges et al. 2008), expanding the theory that select individual phosphorylation sites have the power to partially restore E2F activity. Furthermore, several phosphorylation sites were unable to restore any E2F activity in these assays, including: S249, T252, S608+S612, and 821+826 (Gorges et al. 2008; Lents et al. 2006). Overall, the work by

Baldassare and coworkers has dramatically advanced the theory originally put forward by Knudsen and Wang by revealing that T373 phosphorylation alone is *sufficient* to fully activate E2F. Notably, they did not ask whether T373 phosphorylation is *necessary* for full activation of E2F; however, separate work has shown that mutation of the equivalent site in murine Rb significantly abrogates E2F reporter activity (Brown et al. 1999); indicating that T373 phosphorylation is indeed necessary and sufficient for full activation of E2F.

Taken together, cell-based investigations in to the specific functions of Rb's phosphorylation sites have revealed that the majority of phosphorylation events promote the activation of E2F-mediated transcription. Certain phosphorylation events seem important for partial activation of E2F-mediated transcription; T356, S608, S612, S795, S807, S811, T821, T826 have all been shown to have an effect either alone or in the context of additional phosphorylation events. T373 is perhaps unique in its ability to fully activate E2F-mediated transcription alone, suggesting that it may act as a master switch for turning off Rb and turning on E2F. In addition, since there seems to be a functionally-mysterious sequence to Rb phosphorylation by cyclinD-CDK4 then cyclinE-CDK2, it is enticing to speculate how T373 phosphorylation fits in. Research along these lines has shown that either cyclinD-CDK4 or cyclinE-CDK2 can phosphorylate T373 *in vitro* and *in vivo* (Lents et al. 2006; Zarkowska et al. 1997a). However, one cell-based

designed to parse these cyclin-CDK specificities further revealed that T373 phosphorylation appears to coincide with a peak in cyclinD-CDK4 activity (Gorges et al. 2008). This seems counter-intuitive to the mechanism of E2F activation, since one might expect early and less-potent phosphorylation events by cyclinD-CDK4 ramp-up E2F activity before E2F is definitively switched-on with T373 phosphorylation by cyclinE-CDK2. However, the authors of this study propose that since T373 phosphorylation alone can control E2F activation, other phosphorylation events must have unique functions which are activated in response to separate cell-signaling events (Gorges et al. 2008). This notion gets back to the paradigm disparity over the role of the Rb's multisite phosphorylation: Does phosphorylation itself have one function, or many functions? And, are there specific cyclin-CDK complexes that selectively phosphorylate Rb to achieve different functional outcomes, or, is there large-scale redundancy in this system?

1.2.3 Rb phosphorylation: redundant or specific?

Degeneracy in biology is defined by structurally unique elements that perform similar functions. Famous examples of degeneracy in biochemistry are found within the genetic code, in which various nucleotide sequences code for the same amino acid; protein folding, in which similar protein folds can arise from very different amino acid sequences; and in enzymes, in which structurally unique active sites are capable of catalyzing the same reaction

(Edelman and Gally 2001). Investigations that have selectively removed certain murine CDKs and cyclins indicate that these proteins might present another good example of biological degeneracy. Specifically, knockouts for Cdk2-/- or Cdk4-/- each produce perfectly viable mice (Berthet et al. 2003; Tsutsui et al. 1999). In contrast, double knockout mice for Cdk2-/-Cdk4-/- are embryonic lethal, and show a progressive decline in Rb phosphorylation which leads to the impairment of cell cycle progression (Berthet et al. 2006). Together, these mouse studies indicate that cyclinD-CDK4 and cyclinE-CDK2 are capable of regulating Rb in a manner that is functionally redundant. Consequently, a recent review of all mouse CDK and cyclin knockout literature states, “Extensive analyses of these mouse models revealed that most of the Cdks and cyclins, originally thought essential for cell-cycle regulation, are in fact largely dispensable” (Satyanarayana and Kaldis 2009). Similarly, many aspects of Rb regulation also seem like examples of biological degeneracy: from compensatory phosphorylation machinery to the often compensatory functions of the pocket proteins, to the multiple E2Fs, to the seemingly functionally-redundant multiple phosphorylation events.

On the other hand, there is growing evidence that a variety of kinase complexes regulate Rb phosphorylation in unique, poorly understood ways. Of particular interest is one well-founded study which suggests that Rb is phosphorylated at S807/S811 by cyclinC-Cdk3, in order to facilitate the G_0-G_1 cell cycle transition (Ren and Rollins 2004). Very recently, studies of neurons

have also revealed that CDK5/p35 can phosphorylate Rb and increase the activity of E2F (Futatsugi et al. 2012). Furthermore, several studies have documented rapid Rb phosphorylation by p38MAPK in response to the activation of Fas receptor signaling or apoptosis cascades (Hou et al. 2002; Nath et al. 2003; Wang et al. 1999). One study even concluded that phosphorylation at S780/S795/S807/S811 is needed to promote the formation of pro-apoptotic Rb-E2F1 complexes in response to DNA damage (Ianari et al. 2009). Therefore, a picture of context-dependent, tissue-specific and signaling-specific roles for Rb regulatory proteins and phosphorylation events may be coming into focus. This hypothesis is particularly attractive when considering that although several cyclins and CDKs are dispensable for mouse viability, none have been found that are dispensable for meiosis (Satyanarayana and Kaldis 2009). Similarly, while E2F1 and E2F3 seem compensatory in their cell-cycle functions, they also play distinct roles in development (Trimarchi and Lees 2001). Therefore, perhaps we will find that Rb phosphorylation events are similar in the respect that they each have distinct, albeit subtle, tissue-specific and development-specific roles.

1.3 Rb-E2F structure-function relationships

Within the Rb-E2F complex, two essential Rb-E2F interfaces have been the basis of several structure and function studies. The Rb pocket domain binds the E2F transactivation domain ($E2F^{TD}$) to repress transcription,

and the RbC-terminus binds the E2F marked box domain. Many studies suggest these two interfaces are targets for regulation by phosphorylation of Rb. Beyond these two primary interactions, Rb-E2F complexes are comprised of more subtle interactions that have not been well-characterized, and which may also be targets of phosphorylation. To understand how specific phosphorylation events differentially activate E2F in cell-based assays, it is critical to understand the distinct binding interactions that constitute Rb-E2F complexes. This section reviews structural studies of Rb-E2F complexes and the functional implications of these studies.

1.3.1 Rb-E2F complexes

The first attempt to dissect the Rb-E2F interaction revealed that the pocket domain and C-terminus of Rb together comprise the minimal region required for growth suppression as well as E2F binding (Qin et al. 1992). The first structure of Rb's pocket domain showed how the A and B subdomains comprise tandem cyclin folds, separated by a flexible, 60-residue loop (Lee et al. 1998). Two subsequent studies presented crystal structures the Rb pocket domain in complex with the transactivation domains of E2Fs 1 and 2 (Lee et al. 2002; Xiao et al. 2003). Importantly, these structures were predated by work that identified the minimal 18-residue transactivation domain of E2F ($E2F^{TD}$), which is sufficient to bind Rb to inhibit transcription, or alternatively, bind the TATA binding protein (TBP), CBP or TFIIB and thereby activate

transcription at E2F-controlled promoters (Hagemeier et al. 1993; Trouche et al. 1996). The structural studies revealed $E2F^{TD}$ binds to Rb pocket in a highly-conserved and positively charged A-B subdomain cleft, which is frequently mutated in cancer (Lee et al. 1998; Lee et al. 2002, Xiao et al. 2003). The 18-residue $E2F^{TD}$ peptide is highly negatively charged and, when bound to Rb pocket, forms a short helix at its C-terminus and an extended conformation at its N-terminus (Figure 1.1, B). The sidechains of the E2F peptide are most buried near its N and C terminal residues, indicating a bipartite binding interaction (Lee et al. 2002). The significance of this bipartite binding is now understood in the context of the phosphorylation-induced $E2F^{TD}$ release mechanism, in which distinct phosphorylation events separately compete off these two buried interfaces from Rb pocket (chapter 2 and chapter 4 of this thesis). Further analysis of the Rb pocket-$E2F^{TD}$ structures reveals the C-terminal segment of $E2F^{TD}$ primarily contacts the A subdomain, and the N-terminal segment contacts both the A and B subdomains. Again, this interaction is interesting in the context of a different phosphorylation-induced $E2F^{TD}$ release mechanism, in which an allosteric change alters the A-B binding cleft geometry, so to weaken $E2F^{TD}$ binding (Chapter 3).

The second structurally-characterized Rb-E2F binding interface consists of a 35-residue peptide of $RbC^{829-864}$ (termed $Rb^{C\text{-}Core}$) bound via a strand-loop-helix motif to the E2F1-DP1 heterodimer (Rubin et al. 2005;

Figure 1.1, C). Functional studies indicate that this interaction may be specific for E2F1 (Cecchini and Dick 2011; Dick and Dyson 2003). Accordingly, E2F1's marked box domain is unique from other E2F marked box domains in that it is required to induce apoptosis in response to excessive proliferation or DNA damage (Hallstrom et al. 2003). Separate work suggests that other E2F marked box domains may also have specific activities since they exhibit promoter preferences by binding distinct transcription factors (Schlisio et al. 2002; Giangrande et al. 2003).

There are indications in the literature of several lesser-studied interactions between Rb and E2F that may be targets of Rb phosphorylation. Of particular interest is $RbC^{786\text{-}800}$ (termed RbC^{N}). The presence of this RbC fragment greatly enhances the $Rb^{C\text{-}Core}$-E2F-$DP1^{MB/CC}$ interaction (Rubin et al. 2005); however there are no structural studies which indicate how RbC^{N} binds to E2F-$DP1^{MB/CC}$. Notably, this interaction between RbC^{N} and E2F-$DP1^{MB/CC}$ is dramatically weakened by phosphorylation of S788/S795, perhaps contributing to dissociation of the whole RbC-E2F-$DP1^{MB/CC}$ complex (Rubin et al. 2005). Nuclear magnetic resonance studies presented in chapter 4 confirm an interaction between RbC^{N} and E2F-$DP1^{MB/CC}$, which is disrupted by phosphorylation. Furthermore, this study indicates that phosphorylation of RbC^{N} also promotes an association with Rb pocket that disrupts $E2F^{TD}$ binding. Together, these results indicate that S788/S795

phosphorylation may uniquely contribute to the disruption of two separate Rb-E2F interfaces: Rb pocket-E2F^{TD} and RbC^{N} and E2F-DP1^{MB}(Figure 1.1, D-E).

A separate, lesser-studied Rb-E2F interaction exists between the E2F marked box domain and Rb pocket at the “LxCxE-binding site” (Xiao et al. 2003). This study shows Rb pocket-E2F binding is inhibited in the presence of the E7^{LxCxE} peptide, but only when E2F^{MB} is present, indicating that E2F^{MB} binds to Rb pocket via the “LxCxE-binding site”. An earlier study shows the same result using a GST pull-down assay (Hagemeier et al. 1993). One obvious concern over these experiments is whether or not this E2F construct is properly folded due to the lack of it’s coil-coiled domain as seen in the crystal structure of heterodimeric E2F-DP1 (Rubin et al. 2005). Work presented in this thesis revamps this experiment by showing E2F-DP1$^{MB/CC}$ bound to Rb pocket impairs E7^{LxCxE} peptide binding to Rb, in comparison to when E2F is absent (Chapter 4). Therefore, this result supports earlier findings that E2F^{MB} does contact the “LxCxE-binding site”. This result is particularly interesting because phosphorylated T821/T826 are known to target the LxCxE binding site on Rb pocket (Harbour et al. 1999; Knudsen and Wang. 1996; Rubin et al. 2005), and mutation of T821/T826 has been shown to decrease E2F activity in a reporter assay (Brown et al. 1999). Therefore, it seems plausible that T821/T826 phosphorylation may play a role in disrupting this potential Rb-E2F interaction.

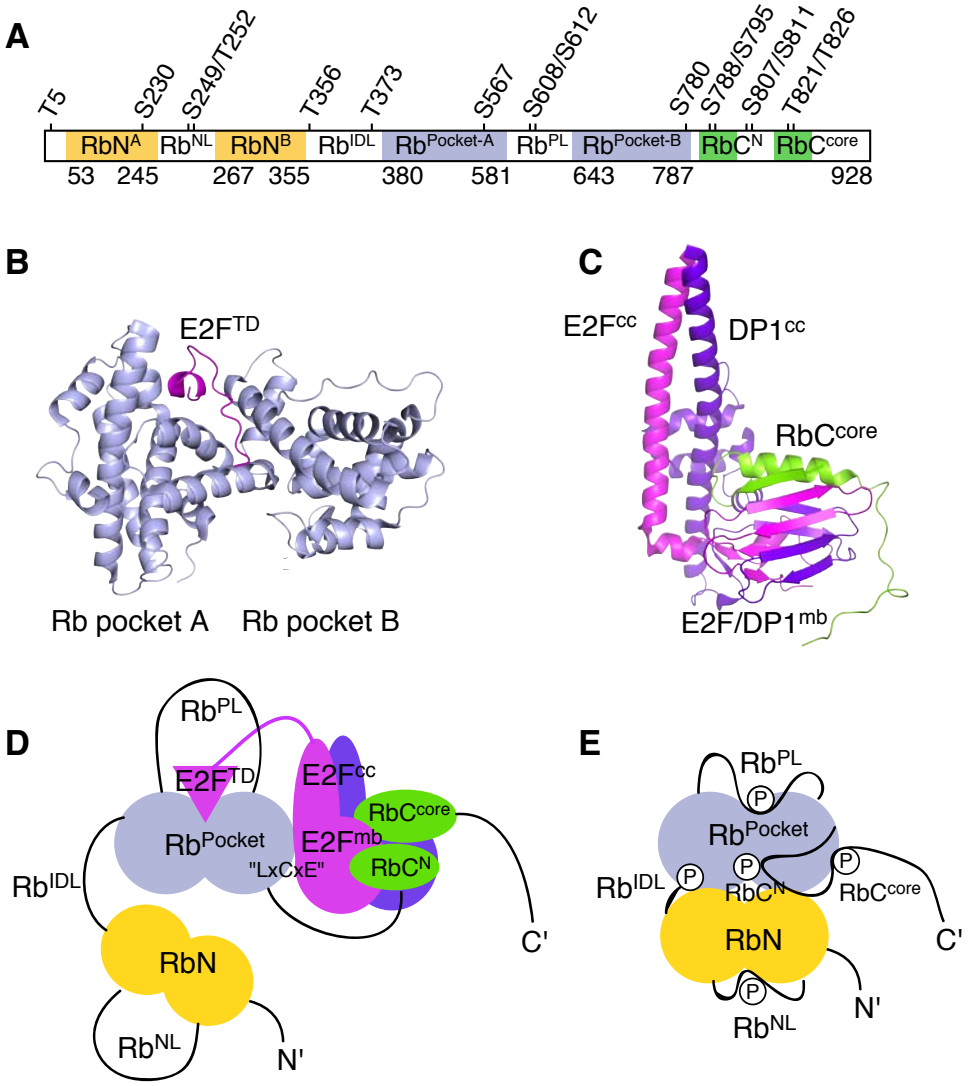

Figure 1.1. Rb-E2F structure-function details. (**A**) Schematic of full-length Rb. Distinct structured domains are colored, unstructured regions of the protein are white. Rb's phosphorylation sites occur primarily in unstructured regions of the protein and in pairs. (**B**) Crystal structure of the pocket domain bound to the E2F transactivation domain (Lee et al. 2002; PDB: 1N4M). (**C**) Crystal structure of RbC^{core} bound to E2F1-$DP1^{cc/mb}$ (Rubin et al. 2005; PDB: 2AZE). (**D**) Summary of Rb-E2F binding interactions. (**E**) Summary of Rb phosphorylation events that promote intramolecular binding and disrupt Rb-E2F interfaces.

1.3.2 Rb pocket-E2F^{TD} - a proposed mechanism of dissociation

Prior to the work presented in this thesis, there has been only one comprehensive mechanistic study of how phosphorylation regulates the Rb-E2F^{TD} interface. This study reported that S567 phosphorylation singularly regulates the activation of E2F by destabilizing binding between the Rb pocket A and B subdomains (Harbour et al,. 1999). While initially impressive, this hypothesis began to fall apart when a bona fide crystal structure of Rb's pocket domain revealed, "Phosphorylation of S567 appears unfavorable because its side chain is not solvent accessible and its side-chain hydroxyl group makes two hydrogen bonds to backbone amide and carbonyl groups in a rigid portion of the structure" (Lee et al. 1998). Additionally, there has long been a lack of independent research which corroborates that S567 is actually phosphorylated, either *in vivo* or *in vitro*. Therefore, a mechanistic understanding of how phosphorylation regulates the Rb-E2F^{TD} complex really begins with the work presented in this thesis.

1.4 Direction of research

1.4.1 Approach

The primary goal of this research has been to identify the structural mechanisms underpinning the phosphorylation-induced dissociation of the Rb-E2F^{TD} complex. In approaching this question from a biochemical standpoint, we use functional truncates of whole domains or unstructured

peptides to study binding between different Rb-E2F interfaces. We quantify the binding affinities of different Rb-E2F interactions and determine the effects of phosphorylation on these binding affinities using isothermal titration calorimetry (ITC). Similarly, we use nuclear magnetic resonance (NMR) to characterize phosphorylation-induced binding interactions between Rb peptides and the Rb pocket domain. Small Angle X-ray Scattering (SAXS) is used to observe large-scale conformational changes that occur as a result of certain phosphorylation events. Finally, we use protein X-ray crystallography to reveal the atomic details of the unique phosphorylation-driven intramolecular interactions which dissociate Rb-E2F complexes.

1.4.2 Background experiments

Work in our lab, which pre-dated the work of this thesis, shows that phosphorylation of full-length Rb causes a 200-fold reduction in the binding affinity of the E2F1 transactivation domain peptide when compared to unphosphorylated Rb (Table 1.1, rows 1&2). Domain truncates of Rb reveal that when the N-terminal domain is removed, the overall effect of phosphorylation is approximately 15-fold (Table 1.1, rows 1&3). This 15-fold weakening of Rb-E2F1^{TD} binding is similar to the effect of phosphorylating the pocket domain alone (Table 1.1, rows 1&4). When the C-terminus alone is removed, phosphorylated Rb retains the full 200-fold inhibition of E2F1^{TD} binding (Table 1.1, rows 1&4). These in vitro experiments reveal that multiple,

distinct mechanisms exist for dissociating Rb-E2F1^{TD}. Furthermore, some of these mechanisms are clearly cooperative.

Rb construct	Domain truncate	Kd E2F1^{TD}
unphos Rb$^{55-928}$	-	0.04 ± 0.06 μM
phos Rb$^{55-928}$	-	11 ± 3 μM
phos Rb$^{380-928}$	RbN	0.62 ± 0.03 μM
phos Rb$^{380-787}$	RbN + RbC	0.7 ± 0.4 μM
phos Rb$^{55-787}$	RbC	13 ± 3 μM

Table 1.1. Summary of E2F1^{TD} binding to Rb truncates.

1.4.3 Summary of findings presented in chapters

Chapter 2 examines how phosphorylation of the Rb pocket linker (Rb^{PL}: S608/S612) weakens E2F1^{TD} binding to Rb pocket. Specifically, we use NMR to show phosphorylation of Rb^{PL} promotes binding to Rb pocket that is incompatible with E2F^{TD} binding. Using ITC and NMR, we then identify several conserved residues around the phosphorylation sites of Rb^{PL}, and within the pocket domain, that are critical for phosphorylated Rb^{PL}-Rb pocket binding and inhibition of E2F^{TD} binding. Lastly, present the crystal structure solution of Rb^{PL} bound to Rb pocket. The structure reveals that phosphorylated Rb^{PL} binds almost exactly at the E2F^{TD} binding site and makes structurally analogous interactions with Rb pocket to block E2F^{TD} binding.

Chapter 3 focuses on the role of the inter-domain linker phosphorylation sites (Rb^{IDL}: T356/T373) in the regulation of Rb-$E2F^{TD}$. Using SAXS, we find that phosphorylation of T373 alone causes a global conformational change to Rb that is consistent with binding between the N-terminal domain and the pocket domain. The crystal structure solution of Rb phosphorylated at T373 reveals the N-terminal domain binds to the pocket domain to affect an allosteric change which opens the A-B cleft, thereby disrupting the $E2F^{TD}$ binding site. ITC experiments are used confirm weak $E2F1^{TD}$ binding to Rb pocket when this construct is phosphorylated and additionally support the proposed allosteric mechanism for $E2F1^{TD}$ dissociation. Chapter 3 also describes structural studies of the N-terminal domain using NMR, and attempts that have been made to crystallize this domain with Rb^{NL} phosphorylated.

Chapter 4 reveals that RbC phosphorylation also weakens the Rb-$E2F^{TD}$ interaction. We use ITC to evaluate several sites in RbC and ultimately show that S788/S795 are critical for this effect. NMR experiments show RbC^{N} peptide binding to Rb pocket is phosphorylation-dependent. Furthermore, we show phosphorylation of S788/S795 dissociates the RbC^{N} peptide from the E2F-DP1 complex; this is consistent with previous findings (Rubin et al. 2005). Additionally S788/S795 acts synergistically with S608/ S612 to disrupt binding between Rb pocket and $E2F1^{TD}$ by ITC. Attempts to crystallize the phosphorylated RbC^{N}-pocket interaction have been

unsuccessful, but are described nonetheless. Lastly, this chapter includes investigations in to interactions between E2F and Rb's "LxCxE-binding site"

The majority of work presented in chapters 2 and 3 has been published in two separate papers (Burke et al. 2010; Burke et al. 2012).

1.5 References

Bagchi S, Weinmann R, Raychaudhuri P. "The retinoblastoma protein copurifies with E2F1, an E1A-regulated inhibitor of the transcription factor E2F." *Cell* 65, 1063-1072. (1991)

Bandara LR and La Thangue NB. "Adenovirus E1a prevents the retinoblastoma gene product from complexing with a cellular transcription factor." *Nature* 351: 494-497. (1991)

Berthet C, Aleem E, Coppola V, Tessarollo L, Kaldis P. "Cdk2 knockout mice are viable." *Curr Biol.* 3(20), 1775-85. (2003)

Berthet C, Klarmann KD, Hilton MB, Suh HC, Keller JR, Kiyokawa H, Kaldis P. "Combined loss of Cdk2 and Cdk4 results in embryonic lethality and Rb hypophosphorylation." *Dev Cell.* 10(5), 563-73. (2006)

Brown VD, Phillips RA, Gallie BL. "Cumulative effect of phosphorylation of pRB on regulation of E2F activity." *Mol Cell Biol.* 19(5), 3246-56. (1999)

Brown VD, Gallie BL. "The B-domain lysine patch of pRB is required for binding to large T antigen and release of E2F by phosphorylation." *Mol Cell Biol.* 22(5), 1390-401. (2002)

Buchkovich K, Duffy LA, Harlow E. "The retinoblastoma protein is phosphorylated during specific phases of the cell cycle." *Cell* 58, 1097-1105. (1989)

Burke JR, Deshong AJ, Pelton JG, Rubin SM. "Phosphorylation-induced conformational changes in the retinoblastoma protein inhibit E2F transactivation domain binding." *J Biol Chem* 285(21):16286-93. (2010)

Burke JR, Hura GL, Rubin SM. “Structures of inactive retinoblastoma protein reveal multiple mechanisms for cell cycle control.” *Genes Dev.* 26(11):1156-66. (2012)

Burkhart DL and Sage J. “Cellular mechanisms of tumor suppression by the retinoblastoma gene.” *Nat Rev Cancer* 8(9): 671-682. (2008)

Cecchini MJ, Dick FA. “The biochemical basis of CDK phosphorylation-independent regulation of E2F1 by theretinoblastoma protein.” *Biochem J.* 434(2):297-308. (2011)

Chellappan SP, Hiebert S, Mudryj M, Horowitz JM, Nevins JR. “The E2F transcription factor is a cellular target for the RB protein.” *Cell* 65: 1053-1061. (1991)

Chen HZ, Tsai SY, Leone G. “Emerging roles of E2Fs in cancer: an exit from cell cycle control.” *Nat Rev Cancer* 9(11): 785-97. (2009)

Chen PL, Scully P, Shew JY, Wang JYJ, Lee WH. “Phosphorylation of the retinoblastoma gene product is modulated during the cell cycle and cellular differentiation.” *Cell* 58, 1193-1198. (1989)

Chen TT, Wang JYJ. “Establishment of irreversible growth arrest in myogenic differentiation requires RB LxCxE-binding function.” *Mol. Cell. Biol.* 20(15), 5571-80. (2000)

Chew YP, Ellis M, Wilkie S, Mittnacht S. “pRB phosphorylation mutants reveal role of pRB in regulating S phase completion by a mechanism independent of E2F.” *Oncogene* 17(17), 2177-86. (1998)

Chicas A, Wang X, Zhang C, McCurrach M, Zhao Z, Mert O, Dickins RA, Narita M, Zhang M, Lowe SW. “Dissecting the unique role of the retinoblastoma tumor suppressor during cellular senescence.” *Cancer Cell* 17(4), 376-87. (2010)

Cobrinik D. “Pocket proteins and cell cycle control.” *Oncogene* 24(17), 2796-809. (2005)

Connell-Crowley L, Harper JW, Goodrich DW. “Cyclin D1/Cdk4 regulates retinoblastoma protein-mediated cell cycle arrest by site-specific phosphorylation.” *Mol Biol Cell.* 8(2), 287-301. (1997)

DeCaprio JA, Ludlow JW, Lynch D, Furukawa Y, Grifin J, Piwnica-Worms H, Huang CM, Livingston DM. “The product of the retinoblastoma susceptibility gene has properties of a cell cycle regulatory element.” *Cell* 58, 1085-1095. (1989)

Dick FA, Sailhamer E, Dyson NJ. “Mutagenesis of the pRB pocket reveals that cell cycle arrest functions are separable from binding to viral oncoproteins.” *Mol Cell Biol.* 20(10), 3715-27. (2000)

Dick FA, Dyson N. “pRB contains an E2F1-specific binding domain that allows E2F1-induced apoptosis to be regulated separately from other E2F activities.” *Mol Cell.* 12(3), 639-49. (2003)

Dowdy SF, Hinds PW, Louie K, Reed SI, Arnold A, Weinberg RA. “Physical interaction of the retinoblastoma protein with human D cyclins.” *Cell* 73(3), 499-511. (1993)

Dunn JM, Phillips RA, Becker AJ, Gallie BL. “Identification of germline and somatic mutations affecting the retinoblastoma gene.” *Science* 241, 1797-800. (1988)

Edelman GM, Gally JA. “Degeneracy and complexity in biological systems.” *Proc Natl Acad Sci* 98(24), 13763-8. (2001)

Felsani A, Mileo AM, Paggi MG. “Retinoblastoma family proteins as key targets of the small DNA virus oncoproteins.” *Oncogene* 25(38), 5277-85. (2006)

Friend SH, Bernards R, Rogelj S, Weinberg RA, Rapaport JM, Albert DM, Dryja TP. “A human DNA segment with properties of the gene that predisposes to retinoblastoma and osteosarcoma.” *Nature* 323, 643-646. (1986)

Futatsugi A, Utreras E, Rudrabhatla P, Jaffe H, Pant HC, Kulkarni AB. “Cyclin-dependent kinase 5 regulates E2F transcription factor through phosphorylation of Rb protein in neurons.” *Cell Cycle* 11(8), 1603-10. (2012)

Gonzalo S, García-Cao M, Fraga MF, Schotta G, Peters AH, Cotter SE, Eguía R, Dean DC, Esteller M, Jenuwein T, Blasco MA. “Role of the RB1 family in stabalizing histone methylation at constitutive heterochromatin.” *Nat Cell. Biol.* 7(4), 420-8. (2005)

Gorges LL, Lents NH, Baldassare JJ. “The extreme COOH terminus of the retinoblastoma tumor suppressor protein pRb is required for phosphorylation on Thr-373 and activation of E2F. “ *Am J Physiol Cell Physiol.* 295(5), 1151-60. (2008)

Grafstrom RH, Pan W, Hoess RH. “Defining the substrate specificity of cdk4 kinase-cyclin D1 complex.” *Carcinogenesis* 20(2), 193-8. (1999)

Giangrande PH, Hallstrom TC, Tunyaplin C, Calame K, Nevins JR. “Identification of E-box factor TFE3 as a functional partner for the E2F3 transcription factor.” *Mol Cell Biol.* 23(11), 3707-20. (2003)

Hagemeier C, Cook A, Kouzarides T. “The retinoblastoma protein binds E2F residues required for activation in vivo and TBP binding in vitro.” *Nucleic Acids Res.* 21(22), 4998-5004. (1993)

Hallstrom TC, Nevins JR. “Specificity in the activation and control of transcription factor E2F-dependent apoptosis.” *Proc Natl Acad Sci* 100(19), 10848-53. (2003)

Hamel P, Gill RM, Phillips RA, Gallie BA. “Regions controlling hyperphosphorylation and conformation of the retinoblastoma gene product are independent of domains required for transcriptional repression.” *Oncogene 7:* 693- 701. (1992)

Hanahan D and Weinberg RA. “Hallmarks of cancer: the next generation.” *Cell* 144, 646-674. (2011)

Harbour JW, Lai SL, Whang-Peng J, Gazdar AF, Minna JD, Kaye FJ. “Abnormalities in structure and expression of the human retinoblastoma gene in SCLC.” *Science* 241, 353-7. (1988)

Harbour JW, Luo RX, Dei Santi A, Postigo AA, Dean DC. “Cdk phosphorylation triggers sequential intramolecular interactions that progressively block Rb functions as cells move through G1.” *Cell* 98(6), 859-69. (1999)

Hatakeyama M, Brill JA, Fink GR, Weinberg RA. “Collaboration of G1 cyclins in the functional inactivation of the retinoblastoma protein.” *Genes Dev.* 8(15), 1759-71. (1994)

Helin K, Lees JA, Vidal M, Dyson N, Harlow E, Fattaey A. "A cDNA encoding a pRB-binding protein with properties of the transcriptional factor E2F." *Cell* 70: 337- 350. (1992)

Hernando E, Nahlé Z, Juan G, Diaz-Rodriguez E, Alaminos M, Hemann M, Michel L, Mittal V, Gerald W, Benezra R, Lowe SW, Cordon-Cardo C. "Rb inactivation promotes genomic instability by uncoupling cell cycle progression from mitotic control." *Nature* 430: 797-802. (2004)

Hinds PW, Mittnacht S, Dulic V, Arnold A, Reed SI, Weinberg RA. "Regulation of retinoblastoma protein functions by ectopic expression of human cyclins." *Cell* 70(6), 993-1006. (1992)

Horowitz JM, Park SH, Bogenmann E, Cheng JC, Yandell DW, Kaye FJ, Minna JD, Dryja TP, Weinberg RA. "Frequent inactivation of the retinoblastoma anti-oncogene is restricted to a subset of human tumor cells." *Proc Natl Acad Sci* 87(7), 2775-9. (1990)

Horton LE, Qian Y, Templeton DJ. "G1 cyclins control the retinoblastoma gene product growth regulation activity via upstream mechanisms." *Cell Growth Differ.* 6(4), 395-407. (1995)

Hou ST, Xie X, Baggley A, Park DS, Chen G, Walker T. "Activation of the Rb/E2F1 pathway by the nonproliferative p38 MAPK during Fas (APO1/CD95)-mediated neuronal apoptosis." *J Biol Chem.* 277(50), 48764-70. (2002)

Huang PS, Patrick DR, Edwards G, Goodhart PJ, Huber HE, Miles L, Garsky VM, Oliff A, Heimbrook DC. "Protein domains governing interactions between E2F, the retinoblastoma gene product, and human papillomavirus type 16 E7 protein." *Mol Cell Biol.* 13(2), 953-60. (1993)

Ianari A, Natale T, Calo E, Ferretti E, Alesse E, Screpanti I, Haigis K, Gulino A, Lees JA. "Proapoptotic function of the retinoblastoma tumor suppressor protein." *Cancer Cell.* 15(3), 184-94. (2009)

Ikeda MA, Nevins JR. "Identification of distinct roles for separate E1A domains in disruption of E2F complexes." *Mol Cell Biol.* 13(11), 7029-35. (1993)

Isaac CE, Francis SM, Martens AL, Julian LM, Seifried LA, Erdmann N, Binné UK, Harrington L, Sicinski P, Bérubé NG, Dyson NJ, Dick FA. "The

retinoblastoma protein regulates pericentric heterochromatin." *Mol Cell Biol.* 26(9), 3659-71. (2006)

Kato JY, Matsushime H, Hiebert SW, Ewen ME, Sherr CJ. "Direct binding of cyclin D to the retinoblastoma gene product (pRb) and pRb phosphorylation by the cyclin D-dependent kinase CDK4." *Genes Dev.* 7(3), 331-42. (1993)

Keenan SM, Lents NH, Baldassare JJ. "Expression of cyclin E renders cyclin D-CDK4 dispensable for inactivation of the retinoblastoma tumor suppressor protein, activation of E2F, and G1-S phase progression." *J Biol Chem* 279(7), 5387-96. (2003)

Kennedy BK, Liu OW, Dick FA, Dyson N, Harlow E, Vidal M. "Histone deacetylase-dependent transcriptional repression by pRB in yeast occurs independently of interaction through the LXCXE binding cleft." *Proc Natl Acad Sci* 98(15), 8720-5. (2001)

Kitagawa M, Higashi H, Jung HK, Suzuki-Takahashi I, Ikeda M, Tamai K, Kato J, Segawa K, Yoshida E, Nishimura S, Taya Y. "The consensus motif for phosphorylation by cyclin D1-Cdk4 is different from that for phosphorylation by cyclin A/E-Cdk2." *EMBO J.* 15(24),7060-9. (1996)

Knudsen ES, Wang JY. "Differential regulation of retinoblastoma protein function by specific Cdk phosphorylation sites." *J Biol Chem.* 271(14), 8313-20. (1996)

Knudsen ES, Wang JY. "Dual mechanisms for the inhibition of E2F binding to RB by cyclin-dependent kinase-mediated RB phosphorylation." *Mol Cell Biol.* 17(10), 5771-83. (1997)

Knudson, A.G. "Mutation and cancer: statistical study of retinoblastoma." *Proc. Natl. Acad. Sci.* 68, 820-823. (1971)

Lee C, Chang JH, Lee HS, Cho Y. "Structural basis for the recognition of the E2F transactivation domain by the retinoblastoma tumor suppressor." *Genes Dev.* 16(24), 3199-212. (2002)

Lee JO, Russo AA, Pavletich NP. "Structure of the retinoblastoma tumour-suppressor pocket domain bound to a peptide from HPV E7." *Nature* 391, 859-65. (1998)

Lee WH, Shew JY, Hong F, Sery TW, Donoso LA, Young LJ, Bookstein R, and Lee EY. “The retinoblastoma susceptibility gene encodes a nuclear phosphoprotein associated with DNA binding activity.” *Nature* 329, 642-645. (1987)

Lees JA, Buchkovich KJ, Marshak DR, Anderson CW, and Harlow E. “The retinoblastoma protein is phosphorylated on multiple sites by human cdc2.” *EMBO J.* 10**,** 4279- 4290. (1991)

Lents NH, Gorges LL, Baldassare JJ. “Reverse mutational analysis reveals threonine-373 as a potentially sufficient phosphorylation site for inactivation of the retinoblastoma tumor suppressor protein (pRB).” *Cell Cycle* 5(15),1699-707. (2006)

Lin BT, Gruenwald YS, Morla A, Lee WH, Wang JYJ. “Retinoblastoma cancer suppressor gene product is a substrate of the cell cycle regulator cdc2 *kinase.” EMBO J.* 10**,** 857-864. (1991)

Liu X, Clements A, Zhao K, Marmorstein R. “Structure of the human Papillomavirus E7 oncoprotein and its mechanism for inactivation of the retinoblastoma tumor suppressor.” *J Biol Chem.* 281(1), 578-86. (2006)

Liu X, Marmorstein R. “Structure of the retinoblastoma protein bound to adenovirus E1A reveals the molecular basis for viral oncoprotein inactivation of a tumor suppressor.” *Genes Dev.* 21(21), 2711-6. (2007)

Lundberg AS, Weinberg RA. “Functional inactivation of the retinoblastoma protein requires sequential modification by at least two distinct cyclin- cdk complexes.” *Mol Cell Biol.* 18(2), 753-61. (1998)

McCabe MT, Davis JN, Day ML. “Regulation of DNA methyltransferase 1 by the pRb/E2F1 pathway.” *Cancer Res.* 65(9), 3624-32. (2005)

Mihara K, Cao XR, Yen A, Chandler S, Driscol B, Murphree AL, T'Ang A, Fung YKT. “Cell cycle-dependent regulation of phosphorylation of the human retinoblastoma gene product.” *Science* 246, 1300-1303. (1990)

Mittnacht S, Lees JA, Desai D, Harlow E, Morgan DO, Weinberg RA. “Distinct sub-populations of the retinoblastoma protein show a distinct pattern of phosphorylation.” *EMBO J.* 13(1), 118-27. (1994)

Morris EJ, Dyson NJ. “Retinoblastoma binding partners.” *Adv Cancer Res.* 82, 1-54. (2001)

Narita M, Nũnez S, Heard E, Narita M, Lin AW, Hearn SA, Spector DL, Hannon GJ, Lowe SW. “Rb-mediated heterochromatin formation and silencing of E2F target genes during cellular senescence.” *Cell* 113(6), 703-16. (2003)

Nath N, Wang S, Betts V, Knudsen E, Chellappan S. “ Apoptotic and mitogenic stimuli inactivate Rb by differential utilization of p38 and cyclin-dependent kinases.” *Oncogene* 22(38), 5986-94. (2003)

Nevins JR. “E2F: A link between the Rb tumor suppressor protein and viral oncoproteins.” *Science* 258: 424-429. (1992)

Nielsen SJ, Schneider R, Bauer UM, Bannister AJ, Morrison A, O'Carroll D, Firestein R, Cleary M, Jenuwein T, Herrera RE, Kouzarides T. “Rb targets histone H3 methylation and HP1 to promoters.” *Nature* 412,561-5. (2001)

Nurse P, Thuriaux P, Nasmyth K. “Genetic control of the cell division cycle in the fission yeast Schizosaccharomyces pombe.” *Mol. Gen. Genet.* 146, 167-178. (1976)

Phelps WC, Münger K, Yee CL, Barnes JA, Howley PM. “Structure-function analysis of the human papillomavirus type 16 E7 oncoprotein.” *J Virol.* 66(4), 2418-27. (1992)

Pardee AB. “G1 events and regulation of cell proliferation.” *Science* 246 (4930), 603-8. (1989)

Qin XQ, Chittenden T, Livingston DM, Kaelin WG Jr. “Identification of a growth suppression domain within the retinoblastoma gene product.” *Genes Dev.* 6(6), 953-64. (1992)

Rayman JB, Takahashi Y, Indjeian VB, Dannenberg JH, Catchpole S, Watson RJ, te Riele H, Dynlacht BD. “E2F mediates cell cycle-dependent transcriptional repression in vivo by recruitment of an HDAC1/mSin3B corepressor complex.” *Genes Dev.* 16(8), 933-47. (2002)

Ren S, Rollins BJ. “Cyclin C/cdk3 promotes Rb-dependent G0 exit.” *Cell* 17(2), 239-51. (2004)

Rubin SM, Gall AL, Zheng N, Pavletich NP. “Structure of the Rb C-terminal domain bound to E2F1-DP1: a mechanism for phosphorylation-induced E2F release.” *Cell* 123(6),1093-106. (2005)

Satyanarayana A, Kaldis P. “Mammalian cell-cycle regulation: several Cdks, numerous cyclins and diverse compensatory mechanisms.” *Oncogene* 28(33), 2925-39. (2009)

Schlisio S, Halperin T, Vidal M, Nevins JR. “Interaction of YY1 with E2Fs, mediated by RYBP, provides a mechanism for specificity of E2F function.” *EMBO J*. 21(21), 5775-86. (2002)

Sherr CJ. “Cancer cell types.” *Science* 274, 1672-7. (1996)

Talluri S, Isaac CE, Ahmad M, Henley SA, Francis SM, Martens AL, Bremner R, Dick FA. “A G1 checkpoint mediated by the retinoblastoma protein that is dispensable in terminal differentiation but essential for senescence.” *Mol Cell Biol.* 30(4), 948-60. (2010)

Tsutsui T, Hesabi B, Moons DS, Pandolfi PP, Hansel KS, Koff A, Kiyokawa H. “Targeted disruption of CDK4 delays cell cycle entry with enhanced p27(Kip1) activity.” *Mol Cell Biol. 1*9(10), 7011-9. (1999)

Trimarchi JM, Lees JA. “Sibling rivalry in the E2F family.” *Nat Rev Mol Cell Biol.* 3(1), 11-20. (2002)

Trouche D, Cook A, Kouzarides T. “The CBP co-activator stimulates E2F1/DP1 activity.” *Nucleic Acids Res.* 24(21), 4139-45. (1996)

Wang S, Nath N, Fusaro G, Chellappan S. “Rb and prohibitin target distinct regions of E2F1 for repression and respond to different upstream signals. *Mol Cell Biol.* 19(11), 7447-60. (1999)

Xiao B, Spencer J, Clements A, Ali-Khan N, Mittnacht S, Broceño C, Burghammer M, Perrakis A, Marmorstein R, Gamblin SJ. “Crystal structure of the retinoblastoma tumor suppressor protein bound to E2F and the molecular basis of its regulation.” *Proc Natl Acad Sci* 100(5), 2363-8. (2003)

Zalvide J, Stubdal H, DeCaprio JA. “The J domain of simian virus 40 large T antigen is required to functionally inactivate RB family proteins.” *Mol Cell Biol.* 18(3),1408-15. (1998)

Zarkowska T, Mittnacht S. “Differential phosphorylation of the retinoblastoma protein by G1/S cyclin-dependent kinases.” *J Biol Chem.* 272(19), 12738-46. (1997a)

Zarkowska T, Harlow E, Mittnacht S. “Monoclonal antibodies specific for underphosphorylated retinoblastoma protein identify a cell cycle regulated phosphorylation site targeted by CDKs.” *Oncogene* 1997 14(2), 249-54. (1997b)

Zuo L, Weger J, Yang Q, Goldstein AM, Tucker MA, Walker GJ, Hayward N, Dracopoli NC. “Germline mutations in the p16INK4a binding domain of CDK4 in familial melanoma.” *Nat Genet.* 12(1), 97-9. (1996)

zur Hausen H. “Papillomaviruses and cancer: from basic studies to clinical application.” *Nat Rev Cancer.* 2(5):342-50. (2002)

Chapter 2: Phosphorylation of Rb^{PL} (S608) promotes an intramolecular interaction that competes for $E2F^{TD}$ binding to Rb pocket.

2.1 Introduction

The principal function of retinoblastoma protein (Rb) is to sequester the transcription factor, E2F, and upon phosphorylation, release it in order to facilitate the cell cycle transition from G_1 to S phase. Early work in our lab revealed a minimal Rb construct consisting of the pocket domain and the pocket linker ($Rb^{380-787}$) is sufficient to both bind $E2F^{TD}$ similar to full-length Rb and, upon phosphorylation, significantly weaken this binding interaction (Table 1.1). Unlike full-length Rb, this protein construct expresses exceptionally well in *Escherichia coli*, making the study of this particular mechanism both tractable and inviting.

We began to study the role of S608/S612 phosphorylation through the use of site-directed mutagenesis coupled with ITC. In the context of our *in vitro* binding assay, we find that S608 is principally important for disrupting the interaction between $E2F^{TD}$ and Rb pocket, while S612 is dispensable. Next, we use NMR to show phosphorylation-specific binding occurs between Rb's pocket linker (Rb^{PL}) and Rb pocket in a manner that is incompatible with $E2F^{TD}$ binding. Analysis of this interaction through chemical shift mapping studies further reveals a highly-conserved sequence of residues in Rb^{PL}, which are critical for this mechanism. Alanine scanning mutagenesis of this

sequence, combined with ITC, enabled us to identify a functional sequence motif within Rb^{PL} that is critical for inhibiting $E2F^{TD}$ binding to Rb pocket: DxYLS*P. Finally, through protein X-ray crystallography we are able to validate our model of competitive inhibition and reveal the atomic details of the Rb^{PL}-Rb pocket interface.

2.2 Results

2.2.1. Phosphorylation at S608 modulates binding between $E2F1^{TD}$ and Rb pocket.

Initially, we sought to determine whether phosphorylation of Rb^{PL} residues S608 and S612 weaken the binding affinity between $E2F1^{TD}$ and Rb's pocket domain. For this assay, we purified a single construct of Rb consisting of the pocket domain and Rb^{PL} ($Rb^{380\text{-}787}$). Dissociation constants were measured by ITC for $E2F1^{TD}$ binding to both unphosphorylated and phosphorylated $Rb^{380\text{-}787}$. A direct comparison of these dissociation constants clearly demonstrates that phosphorylation of residues S608 and S612 weakens the binding between $E2F1^{TD}$ and Rb pocket approximately 15-fold (Table 2.1, rows 1-2).

In order to determine the relative contribution of each phosphorylation site to the inhibition of $E2F1^{TD}$ binding to Rb pocket, we use $Rb^{380\text{-}787}$ with S608 and S612 individually mutated to alanine. Phosphorylation of S612 alone has a minor 3-fold effect, while phosphorylation of S608 alone is sufficient to reproduce the previously observed 15-fold effect (Table 2.1, rows

3-4). When both S608 and S612 are mutated to alanine we observe no reduction in binding between E2F1^{TD} and Rb pocket (Table 2.1, row 5). These experiments demonstrate that phosphorylation of Rb^{PL} reduces binding between E2F1^{TD} and Rb pocket 15-fold, and phosphorylation of S608 is both necessary and sufficient for this effect.

	Rb construct	mutations	K_d Rb-E2F1^{TD}	panel
1	unphos. Rb$^{380-787}$	-	0.05 ± 0.01 μM	A
2	phos. Rb$^{380-787}$	-	0.70 ± 0.40 μM	B
3	phos. Rb$^{380-787/S608A}$	S608A	0.15 ± 0.01 μM	C
4	phos. Rb$^{380-787/S612A}$	S612A	0.70 ± 0.10 μM	D
5	phos. Rb$^{380-787/S608A/S612A}$	S608A, S612A	0.06 ± 0.04 μM	E

Table 2.1. Phosphorylation of Rb^{PL} inhibits E2F1^{TD} binding to Rb pocket. This table shows the dissociation constants of E2F1^{TD} for each Rb pocket construct. Phosphorylation of Rb$^{380-787}$ reduces the binding affinity of E2F1^{TD} 15-fold. The reduction in binding affinity between E2F1^{TD} and Rb pocket is attributable to phosphorylation of S608 and not S612.

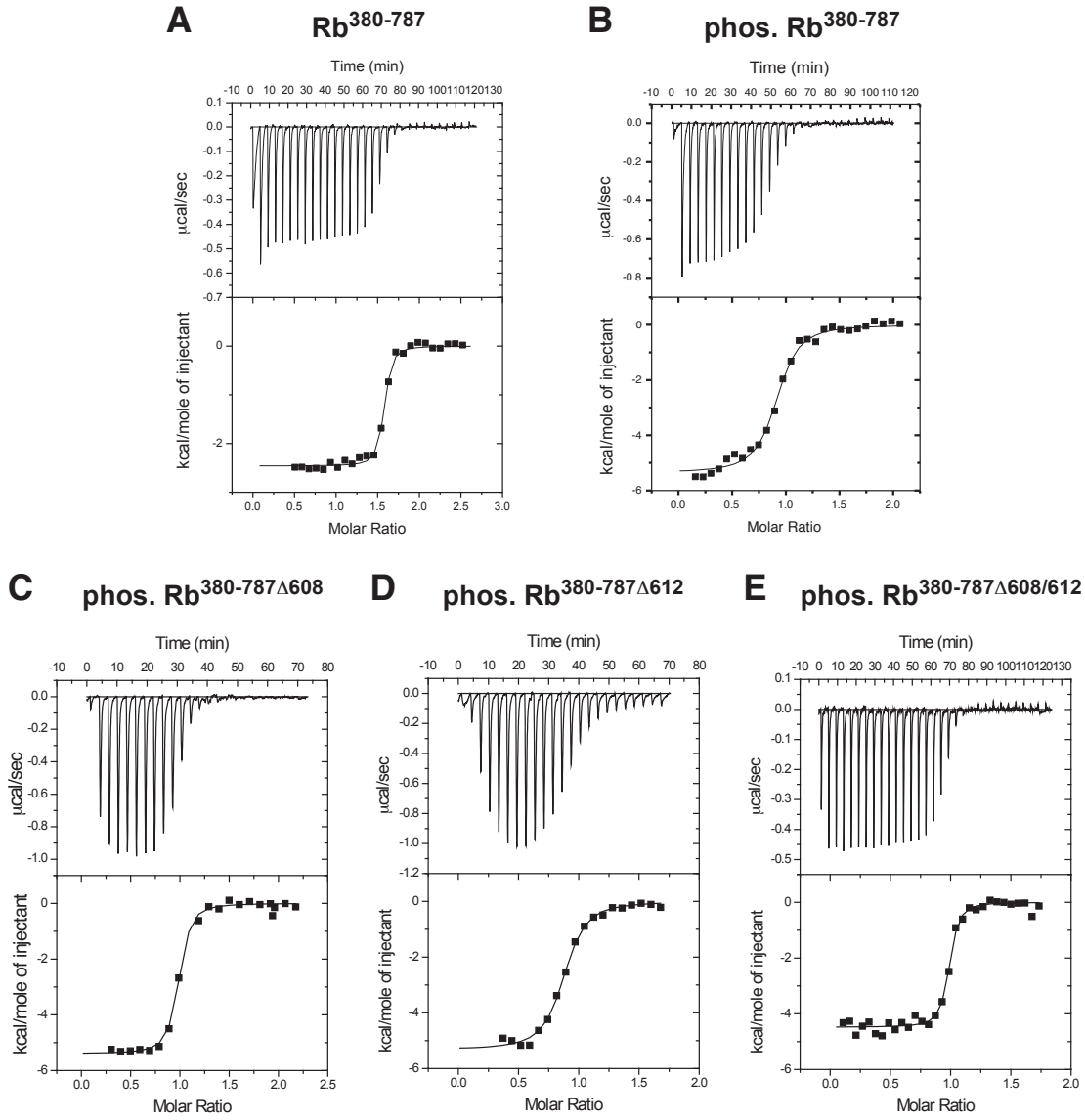

Figure 2.1. Representative ITC data presented in table 2.1.

2.2.2. Rb^{PL} binding to the pocket domain $E2F^{TD}$ binding site is phosphorylation-dependent

Since, the ITC data demonstrate phosphorylation of S608 significantly inhibits the binding interaction between $E2F1^{TD}$ and Rb pocket, we next sought to identify the mechanism of binding inhibition. One hypothesis is

phosphorylation of S608 promotes an intramolecular association between the Rb^{PL} and Rb pocket and weakens the binding affinity of $E2F1^{TD}$ for Rb pocket through competitive inhibition. To test for phospohrylation-dependent binding, Rb^{PL} and Rb pocket were separately expressed and purified, and nuclear magnetic resonance (NMR) experiments were used to observe *in-trans* binding interactions via chemical shift changes to ^{1}H -^{15}N heteronuclear single quantum coherence (HSQC) spectra. Rb Pocket is 42kDa and undergoes rapid signal relaxation by NMR. We therefore conducted a series ^{1}H-^{15}N HSQC-TROSY experiments on the 900MHz magnet at the Central California NMR Facility. These experiments were designed with the goal of optimizing ^{1}H-^{15}N HSQC signal intensity. Additionally, in preparation for these experiments, a special Rb pocket construct lacking Rb^{PL} ($Rb^{362\text{-}787\Delta578\text{-}642}$, or $Rb^{362\text{-}787\Delta PL}$) was expressed in *e.coli* and grown with $^{15}NH_4Cl$ and $^{2}D_2O$. Previous unpublished work in our lab has shown that excision of the pocket linker is a crucial step to obtaining an interpretable ^{1}H -^{15}N HSQC-TROSY spectrum of Rb pocket.

Comparison of ^{1}H-^{15}N HSQC-TROSY spectra of ^{15}N-labeled Rb pocket alone, and in the presence of 1.5 and 4 molar equivalents of unlabeled, phosphorylated Rb^{PL}, reveals that a distinct subset of Rb pocket amide proton peaks shift and broaden in a manner that is dependent upon the concentration of phophorylated Rb^{PL} (Figure 2.2). By comparison, this effect is minor when we instead use unphosphorylated Rb^{PL} (Figure 2.3). The

shifting and broadening of selective amide proton peaks is suggestive of a binding interaction on the fast to intermediate exchange NMR time scale; this indicates a moderate to weak *in trans* binding interaction between Rb^{PL} and Rb pocket. Generally, intermediate exchange is consistent with binding interactions that have dissociation constants on the order of 10-100μM, while fast exchange is consistent with even weaker binding. Together, these two sets of experiments show an *in trans* association between Rb pocket and Rb^{PL} which is strengthened by phosphorylation of Rb^{PL}.

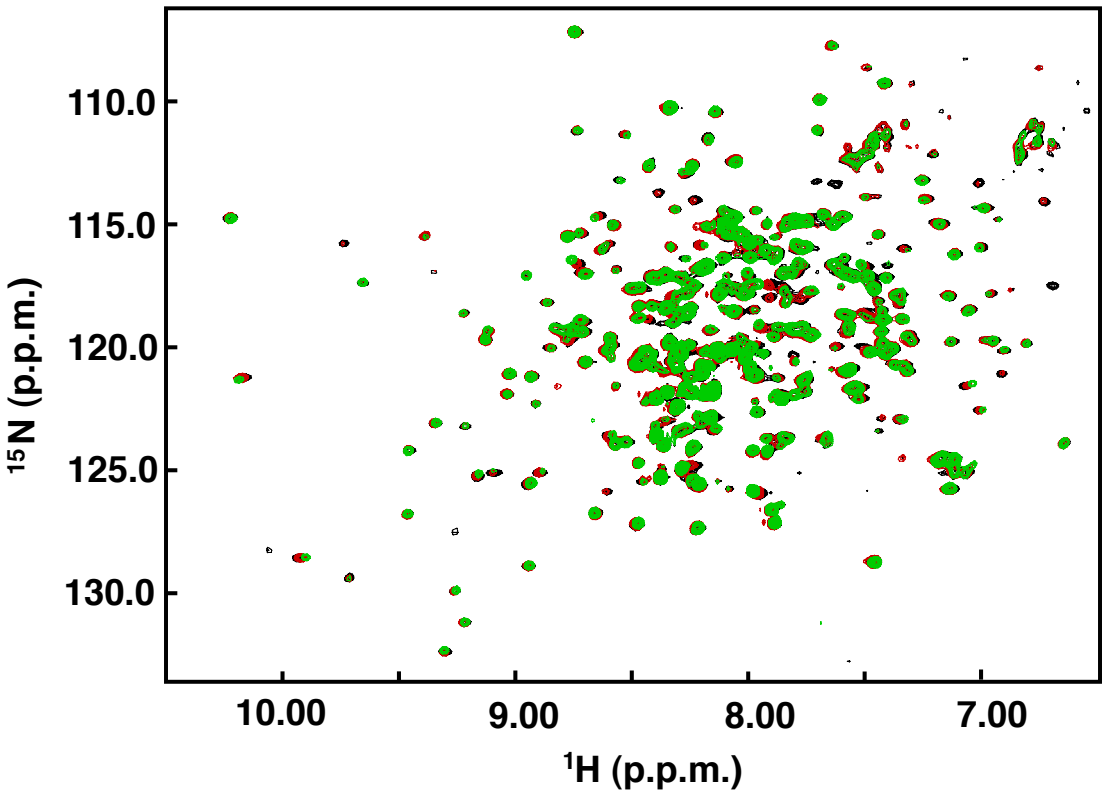

Figure 2.2. Phosphorylated Rb^{PL} binding to Rb pocket *in trans*. ^{1}H-^{15}N HSQC-TROSY of 300 μM ^{2}H-^{15}N-labeled $Rb^{362\text{-}787\Delta PL}$ alone (black) and the presence of unlabeled, phosphorylated $Rb^{PL(592\text{-}624)}$ at 1.5 mM (red) and 4 mM (green).

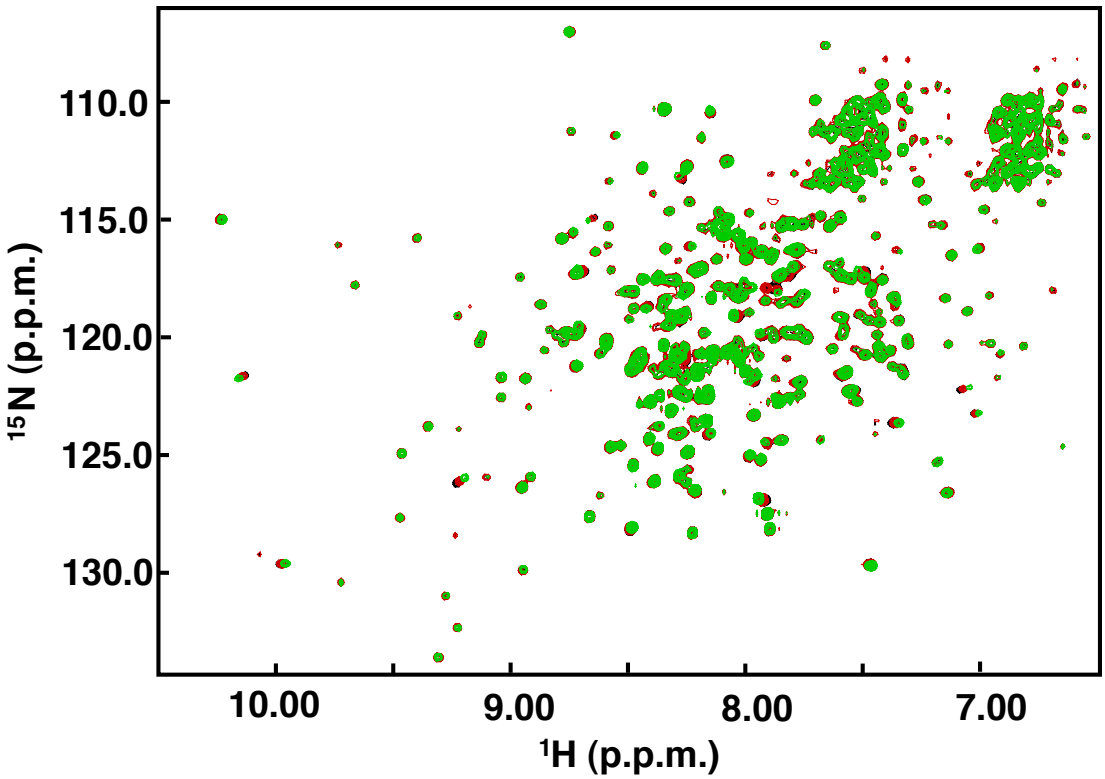

Figure 2.3. Unphosphorylated Rb^{PL} binding to Rb pocket *in trans*. ^{1}H-^{15}N HSQC-TROSY of ^{2}H-^{15}N-labeled 300 μM $Rb^{362\text{-}787\Delta PL}$ alone (black) and the presence of unlabeled, unphosphorylated $Rb^{PL(592\text{-}624)}$ at 1.5mM (red) and 4mM (green).

To determine whether phosphorylated Rb^{PL} binds to Rb pocket in a manner analogous to $E2F1^{TD}$, we added unlabeled $E2F1^{TD}$ to ^{15}N-labeled Rb pocket for the purpose of observing chemical shift changes. In the presence of $E2F1^{TD}$, the number of spectral peaks which undergo chemical shift changes is much greater than the number peaks affected by the binding of phosphorylated Rb^{PL}. However, it is notable that when these spectra are compared directly, the peaks which broaden in the presence of phosphorylated Rb^{PL} represent a subset of the peaks that experience large

chemical shift changes in the presence of E2F1^{TD} (Figure 2.4). This is consistent with a mechanism in which phosphorylated Rb^{PL} inhibits E2F1^{TD} binding to Rb pocket through competitive inhibition.

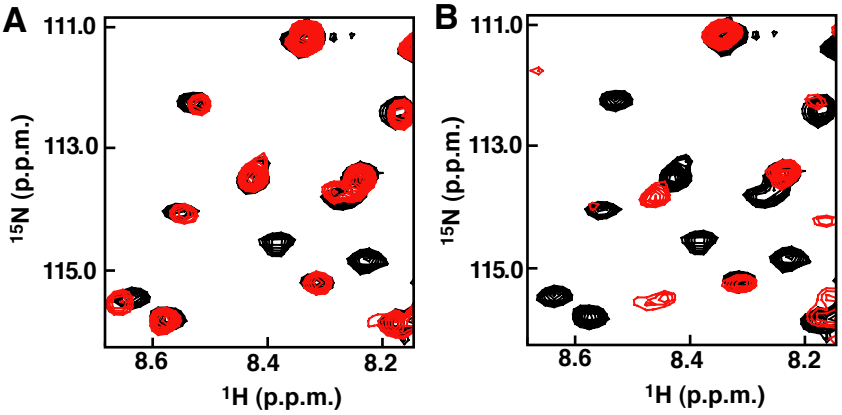

Figure 2.4. ^{1}H-^{15}N HSQC-TROSY detail of Rb pocket bound to phosphorylated Rb^{PL} and E2F1^{TD}. (**A**) ^{1}H-^{15}N HSQC-TROSY of ^{2}H-^{15}N-labeled 300 µM Rb$^{362\text{-}787\Delta PL}$ alone (black) and the presence of 1.5 mM unlabeled, unphosphorylated Rb$^{PL(592\text{-}624)}$ at 1.5 mM (red). (**B**) Rb$^{362\text{-}787\Delta PL}$ alone (black) and in the presence of 2 mM E2F1^{TD} (red). More peaks experience chemical shift perturbations and broaden in the presence of E2F1^{TD} than in the presence of Rb^{PL} (A). Peaks which shift and broaden in the presence of phosphorylated Rb^{PL} represent a subset of peaks which do the same in the presence of E2F^{TD}.

Upon observing the phosphorylation-dependent interaction between Rb^{PL} and Rb pocket through chemical shift changes to Rb pocket, we attempted the reciprocal NMR experiment and sought to observe chemical shift changes to ^{15}N-labeled Rb^{PL} in the presence of unlabeled Rb pocket. Initially, we had two objectives for this experiment. First, we wanted to confirm the phospohrylation-dependent *in-trans* interaction between phosphorylated Rb^{PL} and the Rb pocket domain. Second, we wanted to

assign the ^{1}H-^{15}N HSQC spectrum of Rb^{PL} in order to identify residues potentially involved in binding to Rb pocket. Based on the previous ITC results, we expected we to see selective chemical shift changes to phosphorylated S608, which is essential for $E2F1^{TD}$ binding inhibition (Table 2.1). Likewise we did not expect to see significant chemical shift changes to the amide resonances of phosphorylated S612, which is dispensable for $E2F1^{TD}$ binding inhibition.

To conduct this experiment, we expressed and purified a uniformly ^{15}N-labeled Rb^{PL} construct which contains both S608 and S612 as well as the only sequence of highly-conserved amino acids within Rb^{PL} (residues 595-611). The ^{1}H-^{15}N HSQC spectrum of phosphorylated $Rb^{PL(592-624)}$ shows chemical shift dispersion in the ^{1}H dimension that is consistent with a lack of secondary structure in the pocket linker (Figure 2.5, A). When we combine ^{15}N-labeled, phosphorylated Rb^{PL} with unlabeled $Rb^{380-787}$ (a pocket construct which includes the both the pocket domain and Rb^{PL}), we observe significant peak broadening to six of twenty nine spectral peaks (Figure 2.5, A). When the experiment is repeated using an unlabeled $Rb^{380-787\Delta PL}$, a construct in which Rb^{PL} is deleted, we observe significant peak broadening to eleven of the twenty nine spectral peaks (Figure 2.5, B). A side-by-side comparison of these spectra reveals that a stronger, more specific *in-trans* binding interaction occurs between phosphorylated Rb^{PL} and the Rb pocket domain when Rb^{PL} is excluded from the pocket domain construct.

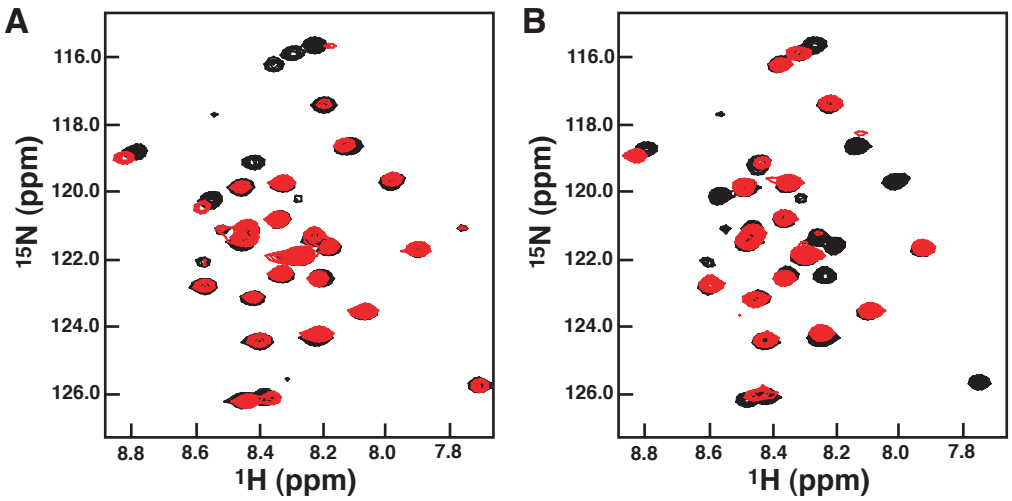

Figure 2.5. ^{1}H-^{15}N HSQC spectra of Rb$^{PL(592-624)}$ binding to Rb pocket *in-trans*. (**A**) 100 µM ^{15}N-labeled, phosphorylated Rb^{PL} alone (black) and with 400 µM unlabeled Rb pocket: Rb$^{380-787}$ (red). In this set of spectra, selective broadening is observed for six of twenty nine peaks. (**B**) Similar to (A) but with 400µM unlabeled Rb pocket excluding Rb^{PL}: Rb$^{380-787/\Delta PL}$ (red). Here selective broadening is observed for eleven of twenty nine peaks. A close comparison of the two sets of spectra reveals that removal of the pocket linker from unlabeled Rb$^{380-787}$ changes the nature of *in-trans* binding between phosphorylated Rb^{PL} and the Rb pocket domain.

Next, we sought to generate a chemical shift map of the peak broadening effects by assigning the observed HSQC peaks to particular residues within Rb^{PL}. The ^{1}H-^{15}N HSQC spectral peaks were assigned to specific amino acids for both the phosphorylated and unphosphorylated Rb^{PL} peptides. For the phosphorylated peptide, the ^{1}H-^{15}N HSQC spectral peak assignments were made using a combination of HNCACB, ^{15}N-filtered HSQC-TOCSY and ^{15}N-filtered HSQC-NOESY experiments. For the unphophorylated peptide, assignments were made from ^{15}N-filtered HSQC-TOCSY and ^{15}N-filtered HSQC-NOESY experiments (Table 2.2).

	phos. Rb^{PL}				unphos. Rb^{PL}	
A.A.	**$^{13}C\alpha$**	**$^{13}C\beta$**	**$^{1}H^{N}$**	**^{15}N**	**$^{1}H^{N}$**	**^{15}N**
L 592	55.1	42.8	8.21	124.4	8.18	124.2
N 593	53.3	38.8	8.31	119.7	8.29	119.5
L 594	53.3	41.9	8.07	123.7	8.05	123.4
P 595	-	-	-	-	-	-
L 596	55.5	42.4	8.26	121.9	8.24	121.64
Q 597	55.8	29.7	8.32	120.8	8.30	120.5
N 598	53.4	38.9	8.43	119.8	8.41	119.5
N 599	53.4	38.9	8.39	119.0	8.37	118.7
H 600	56.1	30.0	-	-	-	-
T 601	62.0	70.4	8.21	115.4	8.17	115.1
A 602	53.1	19.2	8.37	126.3	8.34	126.0
A 603	53.1	19.2	8.20	122.6	8.19	122.3
D 604	54.6	41.1	8.11	118.5	8.09	118.2
M 605	55.8	33.0	7.99	119.6	8.00	119.5
Y 606	58.4	38.8	8.17	121.7	8.07	119.9
L 607	54.3	43.5	7.73	126.4	7.87	123.2
*S 608	56.2	65.2	8.52	120.2	8.12	117.6
P 609	-	-	-	-	-	-
V 610	63.0	32.3	8.23	121.4	8.07	119.9
R 611	55.7	31.5	8.43	126.4	8.34	124.9
*S 612	55.9	65.1	8.75	118.7	8.33	118.4
P 613	63.6	-	-	-	-	-
K 614	56.6	32.6	8.41	121.1	8.33	121.5
K 615	56.3	33.08	8.31	122.5	8.33	123.1
K 616	56.9	33.2	8.40	123.2	8.45	123.8
G 617	45.4	-	8.49	110.6	8.51	110.7
S 618	58.4	64.1	8.28	115.7	-	-
T 619	62.1	69.9	8.19	117.3	8.18	117.0
T 620	62.1	69.9	8.33	116.0	-	-
R 621	56.2	31.1	8.38	124.6	8.37	124.2
V 622	62.8	33.0	8.26	121.9	8.24	121.6
N 623	53.5	39.2	8.54	122.9	8.52	122.5
S 624	60.3	64.7	7.91	121.7	7.88	121.4

Table 2.2. Chemical shift assignments for both phosphorylated and unphosphorylated Rb^{PL}.

Chemical shift mapping experiments were used to determine the specific residues of phosphorylated Rb^{PL} which experience spectral broadening effects in the presence of Rb pocket. Comparison of the assigned spectrum of phosphorylated Rb^{PL} alone to the spectrum of phosphorylated Rb^{PL} in the presence of unlabeled Rb pocket ($Rb^{380\text{-}787/\Delta PL}$), reveals a signal broadening effect for the ^{1}H-^{15}N peaks corresponding to phosphorylated S608 and S612 (Figure 2.6, B). Unexpectedly, we also observe dramatic peak broadening for a sequence of residues corresponding to T601-V610 (Figure 2.6, B-C). Notably, most of these residues are well-conserved in Rb orthologs; an indication these residues are functionally important across a diverse set of species (Figure 2.6, A). In particular, Rb^{PL} residues D604-Y606 are similar to $E2F1^{TD}$ residues D425-F227, and significantly, these $E2F1^{TD}$ residues are critical for $E2F1^{TD}$ to bind Rb pocket (Lee et al. 2002). When this HSQC experiment is repeated using unphosphorylated Rb^{PL}, no spectral changes are observed in the presence of Rb pocket, confirming that the association between Rb^{PL} and Rb pocket is phosphorylation-dependent (Figure 2.6, D).

To assay whether phosphorylated Rb^{PL} and $E2F1^{TD}$ directly compete for binding to the Rb pocket domain, excess $E2F1^{TD}$ was added to the sample containing both ^{15}N-labeled, phosphorylated Rb^{PL} and unlabeled Rb pocket. The resulting spectrum shows reduced peak broadening when compared with the spectrum acquired without $E2F1^{TD}$, which is consistent with excess

E2F1^{TD} displacing phosphorylated Rb^{PL} from the Rb pocket (Figure 2.6, D; compare to B). Together, the NMR and calorimetry data are consistent with a model in which phosphorylation of Rb^{PL} induces an intramolecular association with Rb's pocket domain to inhibit E2F1^{TD} binding.

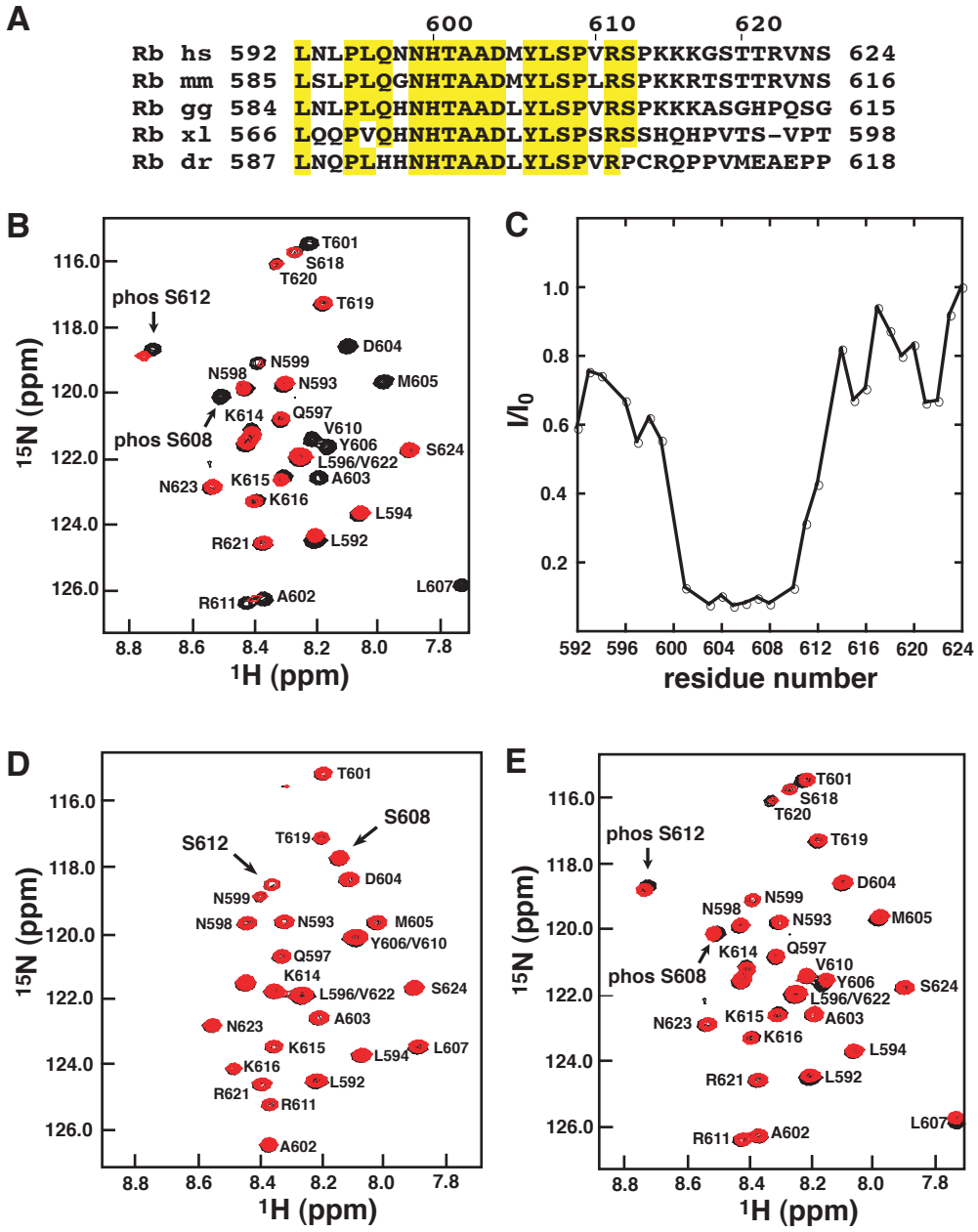

Figure 2.6. Phosphorylated Rb^{PL} associates with Rb pocket and competes with $E2F^{TD}$ for binding. (**A**) Alignment of Rb^{PL} sequences from human (hs), mouse (mm), chicken (gg), frog (xl), and zebrafish (dr) shows that residues 595-611 (human) are highly conserved across these species(yellow). (**B**) HSQC spectra of 100 μM ^{15}N-labeled phosphorylated Rb^{PL} alone (black) and in the presence of 400 μM unlabeled $Rb^{380\text{-}787/\Delta PL}$ (red). Broadening of selective peaks indicates an *in trans* association between the phosphorylated pocket linker and the pocket domain. (**C**) The ratio I/I_0 is defined as the peak intensity of phosphorylated Rb^{PL} in the presence of $Rb^{380\text{-}787/\Delta PL}$ (I) divided by the peak intensity of phosphorylated Rb^{PL} alone (I_0). Spectral peaks from (A) broaden selectively for residues 601-610 in the presence of Rb pocket, indicating that this highly-conserved region of phosphorylated Rb^{PL} binds to Rb pocket. (**D**) HSQC spectra of 100 μM ^{15}N-labeled unphosphorylated Rb^{PL} alone (black) and in the presence of 400 μM unlabeled, unphosphorylated $Rb^{380\text{-}787/\Delta PL}$ (red). No resonance peak broadening is observed for unphosphorylated Rb^{PL} in the presence of Rb pocket, demonstrating that binding is mediated by phosphorylation of Rb^{PL} . (**E**) HSQC spectra of 100 μM ^{15}N-labeled phosphorylated Rb^{PL} alone (black), and with 500 μM unlabeled $Rb^{380\text{-}787/\Delta PL}$ and 2 mM unlabeled $E2F1^{TD}$. In the presence of excess $E2F1^{TD}$, resonance peaks and chemical shifts corresponding to unbound phosphorylated Rb^{PL} reappear, indicating $E2F1^{TD}$ directly competes with phosphorylated Rb^{PL} for binding to Rb pocket.

2.2.3 R467 and F482 of Rb pocket are critical for binding phosphorylated Rb^{PL}

In order to begin to determine the molecular details of the interaction between phosphorylated Rb^{PL} and the Rb pocket domain, we turned to the highly-conserved “D-L-F” sequence that is present in the C-terminus of all E2Fs. As previously noted, this sequence is analogous in physical properties to the conserved Rb^{PL} sequence D604-M605-Y606, which precedes S608. Thus we suspected that these two sequences might form the basis of the competitive binding to Rb pocket that we observe between $E2F^{TD}$ and phosphorylated Rb^{PL}. Crystal structures reveal that the “D-L-F” sequence in

E2F^{TD} makes critical binding contacts to R467 and F482 in the pocket domain of Rb (Lee et al. 2002; Xiao et al. 2003). Specifically, in the structure of E2F2^{TD} bound to Rb pocket, D424 of E2F2^{TD} makes a critical salt bridge with R467 of Rb pocket, while F426 of E2F2^{TD} packs in a hydrophobic groove created by F482 of Rb pocket (Figure 2.7, A). Mutational analysis has shown that a R467A mutation to Rb pocket reduces binding of E2F2^{TD} 7-fold, while a F482A mutation to Rb pocket reduces binding 25-fold (Lee et al, 2002).

To test whether the same point mutations reduce binding between phosphorylated Rb^{PL} and Rb pocket, we observed the peak broadening effects caused by unlabeled pocket mutants: Rb$^{380\text{-}787/\Delta PL/F482A}$ and Rb$^{380\text{-}787/\Delta PL/R467A}$ (Figure 2.7, B-C). By this assay, the Rb pocket mutations F482A and R467A do not induce the same significant peak broadening in the HSQC spectrum of phosphorylated Rb^{PL} that is observed with wild-type Rb pocket (figure 2.7, D). This suggests that the affinity of phosphorylated Rb^{PL} for each Rb pocket mutant is weaker than it is for wild-type Rb pocket. Additionally, these data demonstrate that F482 and R467 are each important for mediating binding between phosphorylated Rb^{PL} and the pocket, and accordingly, that phosphorylated Rb^{PL} and E2F^{TD} binding sites in the pocket domain overlap.

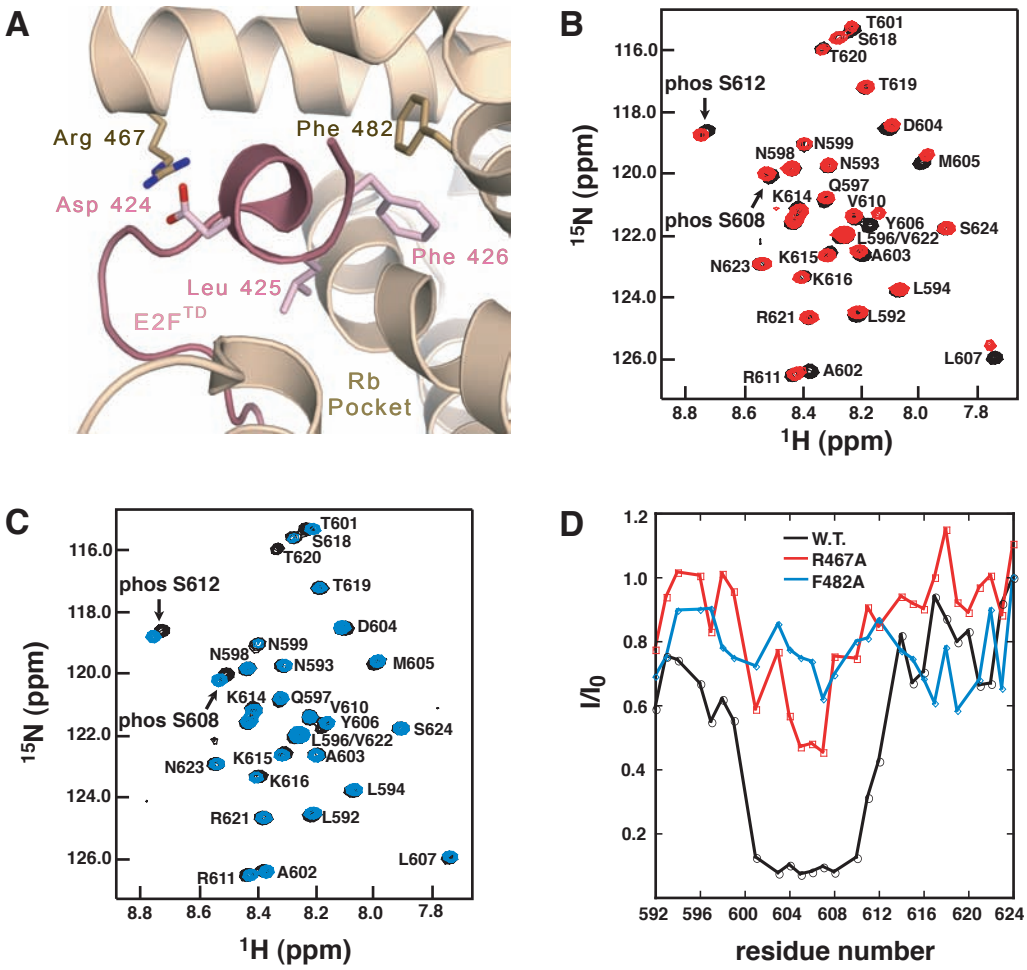

Figure 2.7. Phosphorylated Rb^{PL} binds the Rb pocket domain at the E2F^{TD} binding site. (**A**) The structure of E2F2^{TD} bound to the Rb pocket domain. Critical contacts between D424 and F426 of E2F2^{TD} and F482 of Rb are shown. This figure was generated using Protein Data Bank entry 1N4M. (**B-C**), HSQC spectra of 100 μM ^{15}N-labeled phosphorylated Rb^{PL} alone (black) and in the presence of 500 μM unphosphorylated Rb$^{380\text{-}787/\Delta PL/R467A}$ (red), and 500 μM unlabeled, unphosphorylated Rb$^{380\text{-}787/\Delta PL/F482A}$ (blue), respectively. (**D**) Resonance peak intensity ratios of phosphorylated Rb^{PL} in the presence of Rb$^{380\text{-}787/\Delta PL}$ (black) and mutants Rb$^{380\text{-}787/\Delta PL/R467A}$ (red), and Rb$^{380\text{-}787/\Delta PL/F482A}$ (blue). The ratio I/I_0 is defined as the peak intensity of phosphorylated Rb^{PL} in the presence of Rb$^{380\text{-}787/\Delta PL}$ (I) divided by the intensity of phosphorylated Rb^{PL} alone (I_0). These data demonstrate that R467 and F482 in the pocket domain are important for binding phosphorylated Rb^{PL} as well as E2F^{TD}.

2.2.4. K475 of Rb pocket is dispensable for binding phosphorylated Rb^{PL}

We next sought to design a Rb pocket mutation incapable of binding phosphoserine 608. We expected the correct point mutation might do two things. First, it would abrogate the effect that phosphorylated Rb^{PL} has on reducing the binding affinity between $E2F1^{TD}$ and Rb pocket, as measured by ITC. Second, it would reduce *in trans* binding between phosphorylated Rb^{PL} and Rb pocket as observed by NMR. Lysine and arginine side chains both carry a formal positive charge at physiological pH and are therefore capable of forming salt-bridges to phosphate. Accordingly, there are several examples of lysine and arginine side chains bound to a biologically-important phosphate (Hirsch et al. 2007). We identified K475 as a potential binding site for phosphoserine 608, based both on its high degree of conservation and its close physical proximity to R467 and F482 in Rb pocket. However, when $Rb^{380\text{-}787/K457A}$ is used in an ITC assay to measure the change in binding affinity of $E2F1^{TD}$ upon phosphorylation of Rb pocket, we find that the effect is the same as $Rb^{380\text{-}787}$ (Figure 2.8, A-B). NMR was used to look for direct binding between phosphorylated ^{15}N-labeled Rb^{PL} and unlabeled $Rb^{380\text{-}787/\Delta PL/K475A}$. Here we observe spectral peak broadening that is comparable to that for phosphorylated, ^{15}N-labeled Rb^{PL} in the presence of unlabeled, “wild-type” $Rb^{380\text{-}787/\Delta PL}$; indicating that the K475A mutation does not dramatically inhibit the phosphorylation-dependent association between Rb^{PL} and the Rb pocket domain (Figure 2.8, C-D).

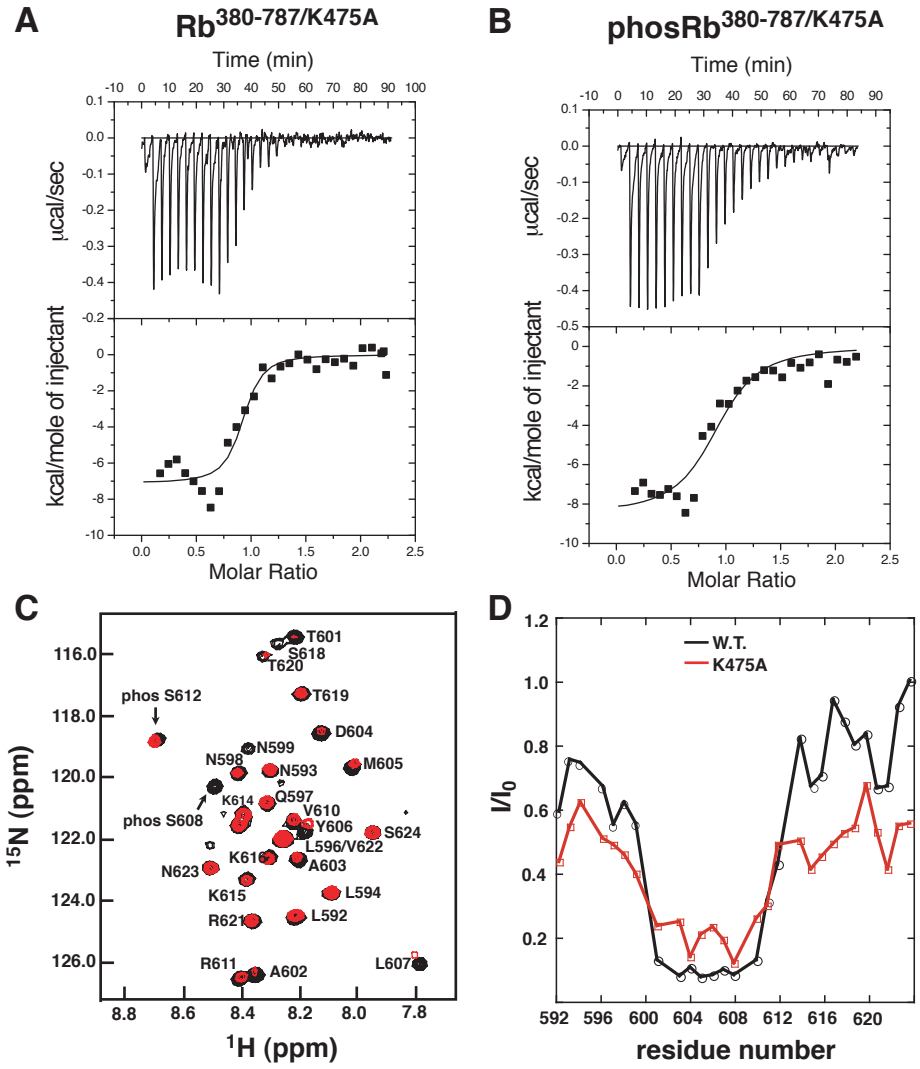

Figure 2.8. K475 is dispensable for phosphorylated Rb^{PL}-Rb pocket binding. (**A**) Unphosphorylated Rb$^{380\text{-}787/K475A}$ binds E2F1^{TD} with an affinity of K_d = 0.178 ± 0.098 µM. (**B**) Phosphorylation of Rb$^{380\text{-}787/K475A}$ reduces binding of E2F1^{TD} to K_d = 0.870 ± 0.338 µM. The difference between E2F1^{TD} binding to unphosphorylated and phosphorylated Rb$^{380\text{-}787/K475A}$ is similar to wild-type (Table 2.1). (**C**) HSQC spectra of 100 µM ^{15}N-labeled phosphorylated Rb^{PL} alone (black) and in the presence of 500 µM unphosphorylated Rb$^{380\text{-}787/\Delta PL/K475A}$ (red). (**D**) The difference in peak intensities of phosphorylated Rb^{PL} in the presence of Rb$^{380\text{-}787/\Delta PL/K475A}$ compared to phosphorylated Rb^{PL} alone (red) is similar to the extent of peak broadening that occurs in the presence of Rb$^{380\text{-}787/\Delta PL}$ (black).

2.2.5. D604, Y606 and L607 are necessary for Rb^{PL} phosphorylatinon to inhibit Rb-$E2F^{TD}$ binding

To further explore the functional importance of Rb^{PL} resides D604 - L607 is in the inhibition of $E2F1^{TD}$ binding, we used ITC to test the affinity of $E2F1^{TD}$ for a series of phosphorylated Rb pocket constructs containing alanine point mutations to this region of the pocket linker. Previously, we determined that $E2F1^{TD}$ binds 15-fold more weakly when $Rb^{380-787}$ is phosphorylated than when it is unphosphorylated (Table 2.1). When we measure the affinity of $E2F1^{TD}$ binding for phosphorylated $Rb^{380-787}$ containing alanine point mutations to D604, Y606, or L607, each individual construct shows a significant decrease in the measured dissociation constant when compared with wild type (Table 2.3, rows 1-5); an indication that each of these highly-conserved residues plays an important role in inhibiting $E2F1^{TD}$ binding by stabilizing the interaction between phosphorylated Rb^{PL} and Rb pocket. In combination, the mutations: D604A/M605A/Y606A completely abrogate the inhibition of $E2F1^{TD}$ binding that occurs upon phosphorylation of Rb^{PL} (Table 2.3, row 6). However, the M605A mutation alone has no significant effect on the inhibition of $E2F1^{TD}$ binding (Table 2.3, row 3). Taken together with the earlier mutational analysis of the pocket linker phosphoacceptor sites, these studies reveal that residues, D604, Y606, L607 and S608, are each important for the phosphorylation-induced inhibition of $E2F^{TD}$ binding to the Rb pocket.

We next conducted an analogous series of experiments to control for whether the previously described alanine mutations to Rb^{PL} change the binding affinity of $E2F^{TD}$ for unphophorylated Rb^{PL}, or alter the ability of Rb^{PL} to be phosphorylated by kinase. When we test each of these unphosphorylated Rb constructs for its ability to bind to $E2F^{TD}$, we find that each has a binding affinity similar to wild-type, an indication that these alanine point mutations only alter the binding affinity of $E2F^{TD}$ for the Rb pocket domain when Rb^{PL} is phosphorylated (Table 2.3). The alanine mutations are adjacent to the CDK-consensus site (S/T-P), therefore we wanted to test whether these mutations still allow for quantitative phosphorylation of Rb^{PL}. Each construct was phosphorylated using an *in vitro* kinase assay (described in materials and methods) then examined for the quantitative incorporation of two phosphates using electrospray ionization mass spectrometry (ESI-MS). With each of these mutation constructs, we are able to observe the correct mass increase, ensures that the changes to binding affinities observed in the alanine scanning mutagenesis experiments are not due to incomplete phosphorylation of Rb (Figure 2.11).

	Rb construct	Phos. Rb-E2F K_d		Unphos. Rb-E2F K_d	
1	$Rb^{380-787}$	0.7 ± 0.4 μM	A	0.05 ± 0.01 μM	A
2	$Rb^{380-787/D604A}$	0.4 ± 0.2 μM	B	0.04 ± 0.02 μM	B
3	$Rb^{380-787/M605A}$	0.9 ± 0.2 μM	C	0.09 ± 0.02 μM	C
4	$Rb^{380-787/Y606A}$	0.2 ± 0.1 μM	D	0.08 ± 0.03 μM	D
5	$Rb^{380-787/L607A}$	0.3 ± 0.2 μM	E	0.09 ± 0.04 μM	E
6	$Rb^{380-787/D604A/M605A/Y606A}$	0.1 ± 0.1 μM	F	0.09 ± 0.02 μM	F

Table 2.3. Residues 604-607 of Rb^{PL} are necessary for the phosphorylation-induced release of $E2F1^{TD}$ from Rb pocket by Rb^{PL}. This table shows the dissociation constants of $E2F1^{TD}$ for each Rb pocket construct. Phosphorylation of $Rb^{380-787}$ reduces the binding affinity of $E2F1^{TD}$ 15-fold (row 1). Point mutations, D604A, M605A, L607A reduce the effect of phosphorylation in weakening $E2F1^{TD}$ binding to Rb, while M605A binds similar to wild-type (rows 3-5). The binding affinity of $E2F1^{TD}$ to a triple mutation construct, $Rb^{380-787/D604A/M605A/Y606A}$, is more similar to unphosphorylated Rb (row 6).

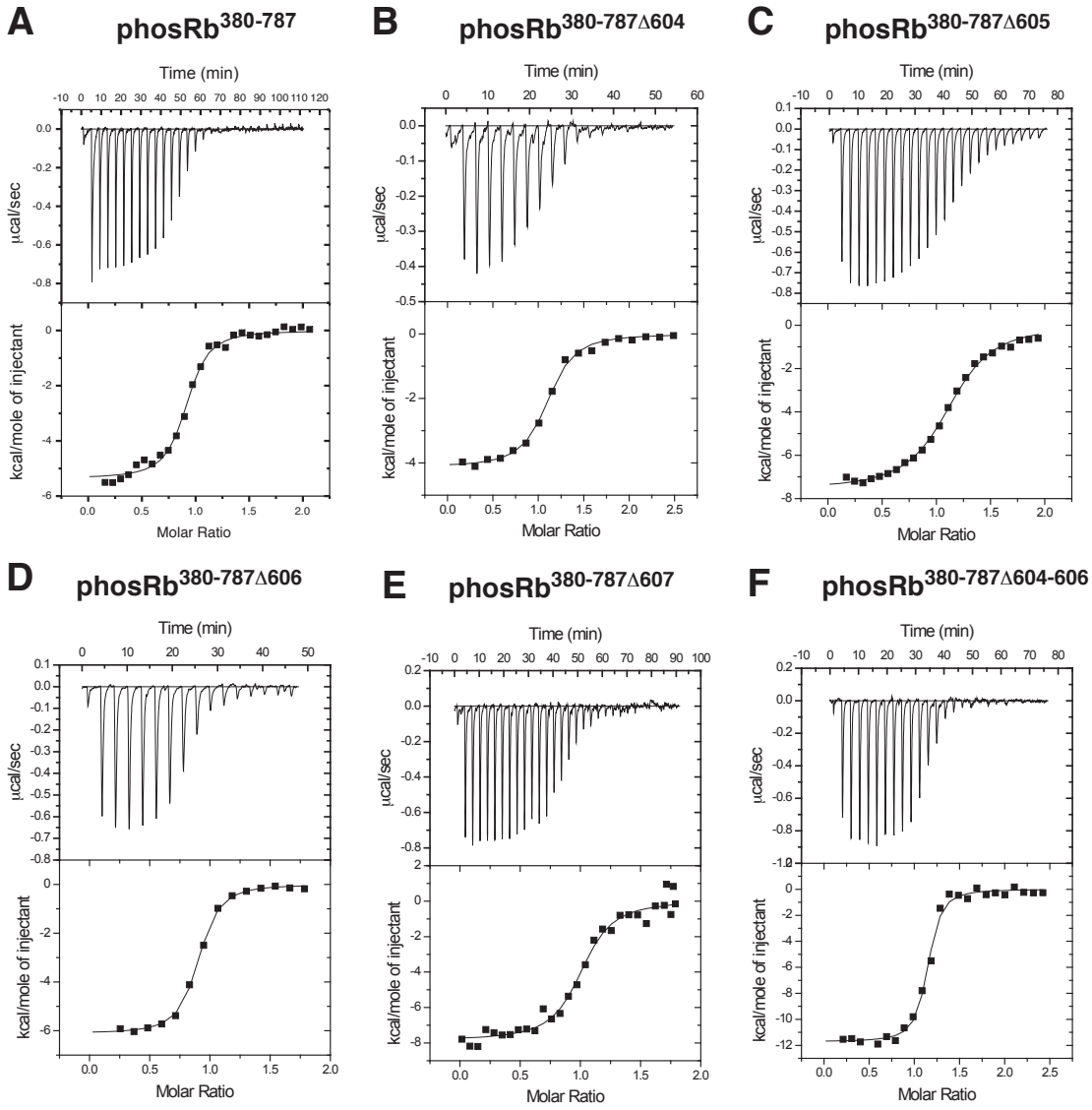

Figure 2.9. Representative ITC binding data for *phosphorylated* Rb and E2F1^{TD} presented in table 2.3.

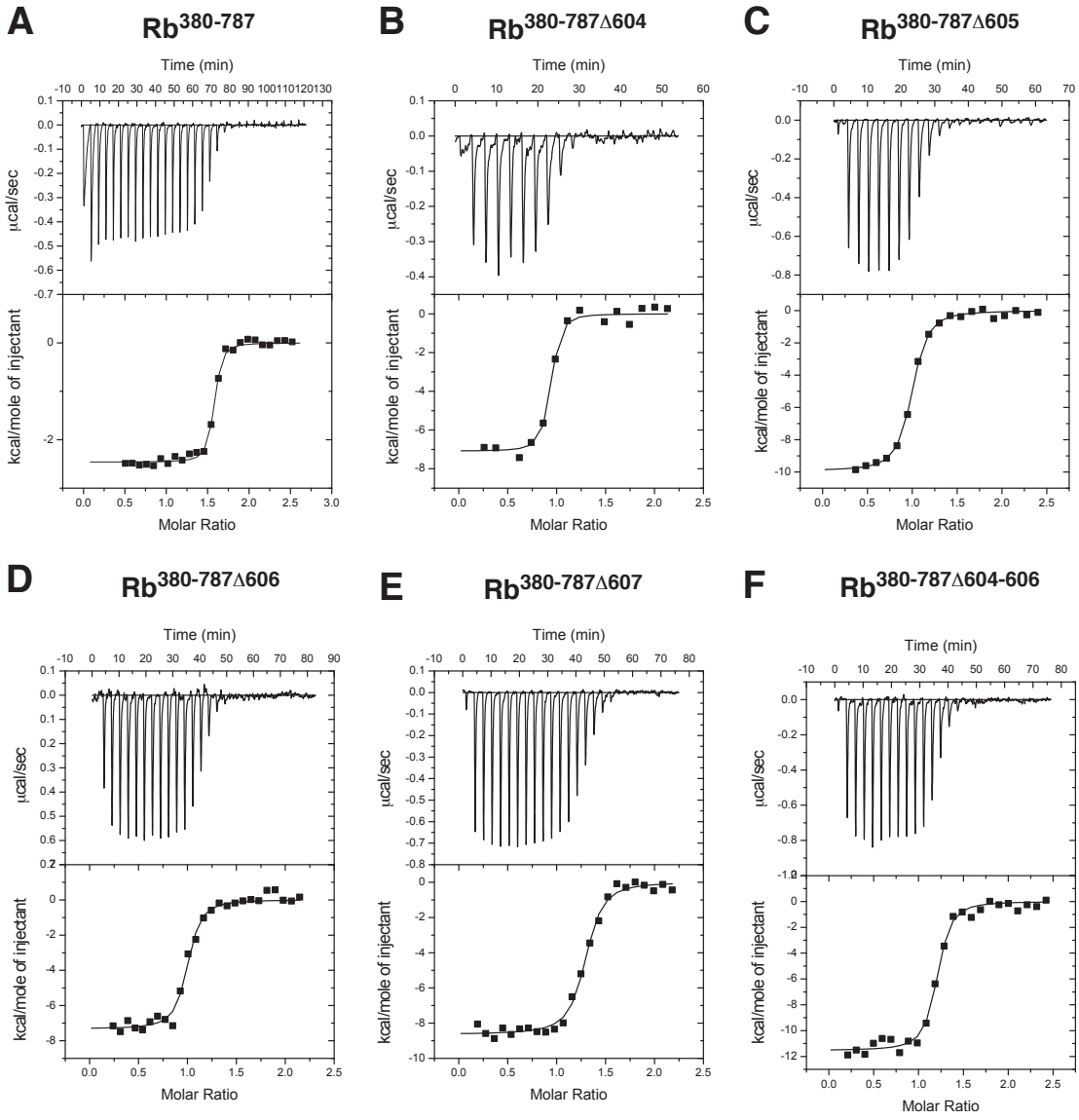

Figure 2.10. Representative ITC binding data for *unphosphorylated* Rb and E2F1^{TD} presented in table 2.3.

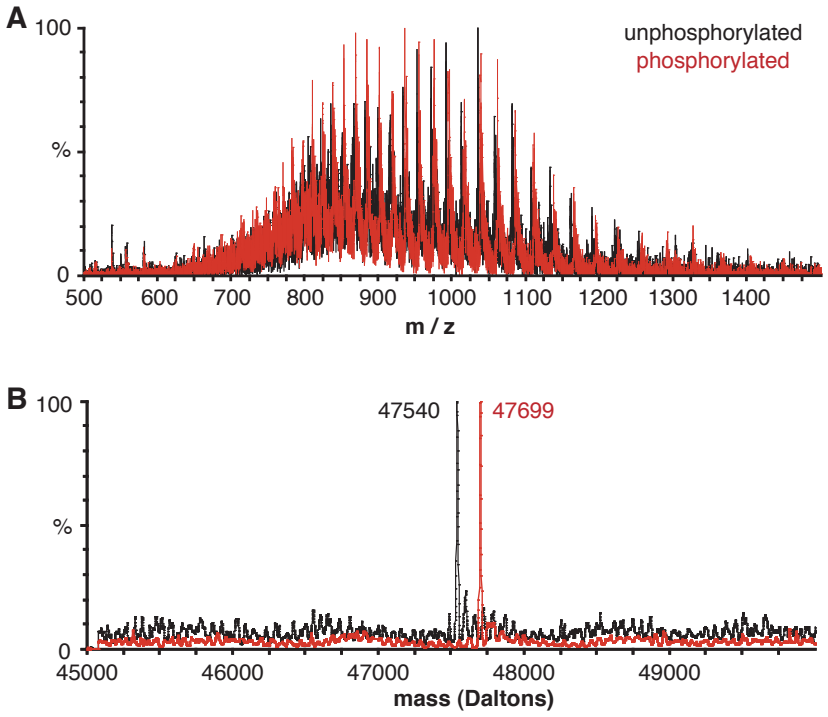

Figure 2.11. ESI-MS analysis of Rb phosphorylation. (**A**) Sample spectrum of $Rb^{380\text{-}787/M605A}$ before and after kinase treatment. (**B**) The overall change in mass after the kinase reaction reflects the addition of two phosphates (+78 A.M.U. each), which is consistent with quantitative phosphorylation for this construct.

2.2.6. Phosphorylated Rb^{PL} partially displaces $E2F2^{TD}$ from Rb pocket.

In the first published structure of Rb bound to $E2F^{TD}$, the authors make a point that $E2F2^{TD}$ binds Rb via the specific interactions of two highly-conserved 6-residue halves of the transactivation domain: an N-terminal segment, consisting of residues 411-416; and a C-terminal segment, consisting of residues 422-427 (Lee et al. 2002). This observation led us to hypothesize that distinct phosphorylation events may selectively displace these buried halves of $E2F^{TD}$ from Rb pocket. Our previous observations

lend support to this hypothesis: NMR-based experiments show that E2F1^{TD} binding causes a large number of chemical shift changes to the HSQC spectrum of Rb pocket, and in contrast, phosphorylated Rb^{PL} causes relatively few observable chemical shift changes (Figure 2.2 and Figure 2.4); ITC-based binding studies reveal a conserved binding motif in Rb^{PL} is similar to the conserved C-terminal segment of all E2F^{TD}s (Figure 2.7).

To test our hypothesis that phosphorylated Rb^{PL} competitively inhibits binding between the C-terminal half of E2F^{TD} and the pocket domain of Rb, we generated a ^{15}N-labeled E2F2^{TD} peptide for use in NMR binding studies. Binding of ^{15}N-labeled E2F2^{TD} to unlabeled, unphosphorylated Rb pocket (Rb$^{380-787}$) results in dramatic signal broadening for all but two peaks of the E2F2^{TD} peptide; this is due to the formation of a stable complex which greatly increases the correlation time of E2F2^{TD} (Figure 2.12, A). In order to assay whether one half of the E2F2^{TD} peptide is released from Rb pocket upon phosphorylation of the Rb^{PL}, we repeat the experiment using phosphorylated Rb$^{380-787}$, which contains S608 and S612, and observe the return of six strong peaks (Figure 2.12, B). This result indicates that a portion of the E2F2^{TD} peptide is selectively competed off of Rb pocket by the phosphorylated pocket linker, thus peak intensity returns for a specific subset of E2F2^{TD} residues due to the increased rotational relaxation rate of these specific nuclei. In comparison, the remaining residues are significantly broadened as to be unobservable in the spectrum, indicating that they remain in complex with

phosphorylated $Rb^{380-787}$. We next attempted to assign the six returning peaks, which have unique chemical shifts and therefore can not be correlated directly to peaks in the spectrum of unbound $E2F2^{TD}$; however, the signal intensity of this sample was too weak for the appropriate assignment experiments, possibly due to the large correlation time of the complex. Because of the lack of peak assignments for these spectra, it was an unfortunate outcome that this assay was not used to definitively conclude which part of $E2F2^{TD}$ binding is affected by the phosphorylation of Rb^{PL}. However, even without assignments, this experiment shows that phosphorylation of Rb^{PL} results in a partial release of the $E2F2^{TD}$ peptide, and not an overall release of the peptide. This result is consistent with a model in which phosphorylation of Rb^{PL} alone selectively disrupts part of the Rb-$E2F^{TD}$ interface, leaving $E2F^{TD}$ partially bound to Rb pocket, albeit with a weaker overall binding affinity (Figure 2.12, C).

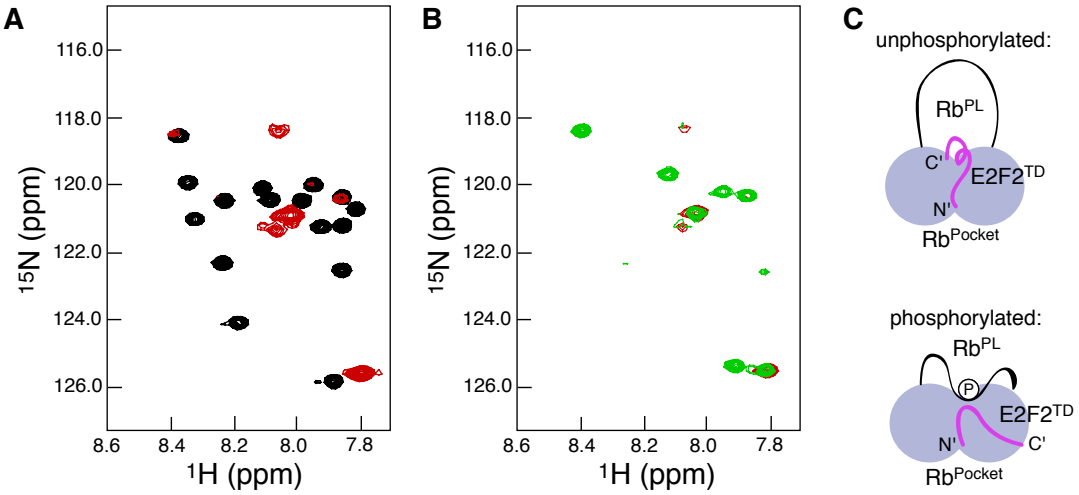

Figure 2.12. Phosphorylation of Rb^{PL} partially displaces E2F^{TD} from Rb pocket. (**A**) HSQC spectra of 50 µM ^{15}N-labeled E2F2$^{410-427}$ alone (black) and in the presence of 100 µM unphosphorylated Rb$^{380-787}$ (red). (**B**) HSQC spectra of 50 µM ^{15}N-labeled E2F2$^{410-427}$ in the presence of 100 µM *unphosphorylated* Rb$^{380-787}$ (red); 50 µM ^{15}N-labeled E2F2$^{410-427}$ in the presence of 100 µM *phosphorylated* Rb$^{380-787}$ (green). (**C**) A model for the role of Rb^{PL} phosphorylation in the disruption of the Rb-E2F^{TD} interface: Rb^{PL} (black) selectively competes off the C-terminal end of E2F^{TD} (pink), thereby weakening the overall affinity of the interaction.

2.2.7 Protein Crystallography reveals details of the Rb^{PL}-Rb pocket interaction

Throughout the course of the above experiments, efforts were made to crystallize the phosphorylation-dependent interaction between Rb^{PL} and the Rb pocket domain. Initially, we used an Rb construct consisting of the pocket domain and the entire pocket linker, Rb$^{380-787}$. Electrospray Ionization mass spectroscopy (ESI-MS) of this construct revealed non-quantitive phosphorylation at the three CDK consensus sites using recombinant CDK2-CyclinA (S608, S612 and S780). Instead, at best, we observe a mixture of masses corresponding to the incorporation of two and three phosphates.

Mutation of S780 to an alanine allows for quantitative incorporation of two phosphates into $Rb^{380\text{-}787/S780A}$; this assuaged our concern that protein heterogeneity might be hampering attempts at crystallization, however, despite this modification, protein crystals of phosphorylated $Rb^{380\text{-}787/S780A}$ could not be obtained.

We next generated a less-flexible Rb protein construct that is therefore more well-suited for crystallography. The design of this construct was based primarily on our NMR study which reveals phosphorylation at S608 induces a binding interaction between residues 600-611 of Rb^{PL} and the Rb pocket domain (Figure 2.6). In this construct, we removed 25 poorly-conserved pocket linker residues (616-642), which are not involved in this interaction and are suspected to be flexibly tethered to the pocket domain. Here we also incorporated a S612A mutation with the goal of readily achieving a more homogeneously phosphorylated protein sample. The resulting protein construct, $Rb^{380\text{-}787\Delta616\text{-}642/S612A/S780A}$, was screened broadly and protein crystals grew in 5 of 672 different initial crystallization conditions. One of these conditions proved to be easily reproducible and was systematically optimized. Repeated optimizations finally resulted in fragile plate-like crystals that would grow in stacks from the bottom and sides of the crystallization well or drop (Figure 2.13, A). Despite exhaustive attempts at further optimization, these crystals consistently diffracted poorly at the synchrotron and often exhibited signs of heavily twinned and anisotropic crystal lattices. Various

other constructs were screened unsuccessfully before we finally incorporated a phosphomimetic glutamate mutation at residue S608 (S608E). This mutation has an important benefit of ensuring protein homogeneity by avoiding the possibility of a protein sample containing small populations of multiple phosphorylation states. The resulting protein construct, $Rb^{380\text{-}787\Delta616\text{-}642/S608E/S612A/S780A}$ (hereafter referred to as $Rb^{PL\text{-}P}$ to denote the Rb^{PL}-Rb pocket domain association), was screened broadly and protein crystals grew in 27 of 400 different initial crystallization conditions. The quality of these protein crystals was good initially (Figure 2.13, B). Each construct that was generated for crystallographic studies was also tested for the ability to inhibit $E2F1^{TD}$ binding by ITC (Figure 2.14).

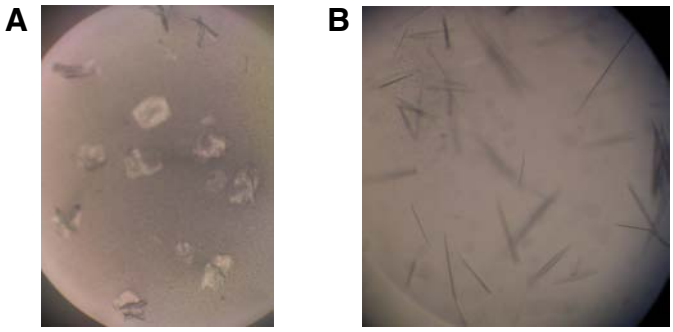

Figure 2.13. Protein crystals Rb^{PL}-Rb pocket. (**A**) Protein crystals of $Rb^{380\text{-}787\Delta616\text{-}642/S612A/S780A}$ grew in stacks and sometimes diffracted to 4Å, but were often heavily twinned. (**B**) Incorporation of S608E into $Rb^{380\text{-}787\Delta616\text{-}642/S612A/S780A}$ produced higher-quality crystals.

Rb constructs	mutations	K_d E2F1^{TD}	Panel
Rb$^{380\text{-}787\Delta 616\text{-}642/S612A/S780A}$	S612A, S780A	0.06 ± 0.03 μM	A
phos. Rb$^{380\text{-}787\Delta 616\text{-}642/S612A/S780A}$	S612A, S780A	0.9 ± 0.1 μM	B
Rb$^{380\text{-}787\Delta 616\text{-}642/S608E/S612A/S780A}$	S612A, S780A, S608E	0.6 ± 0.1 μM	C

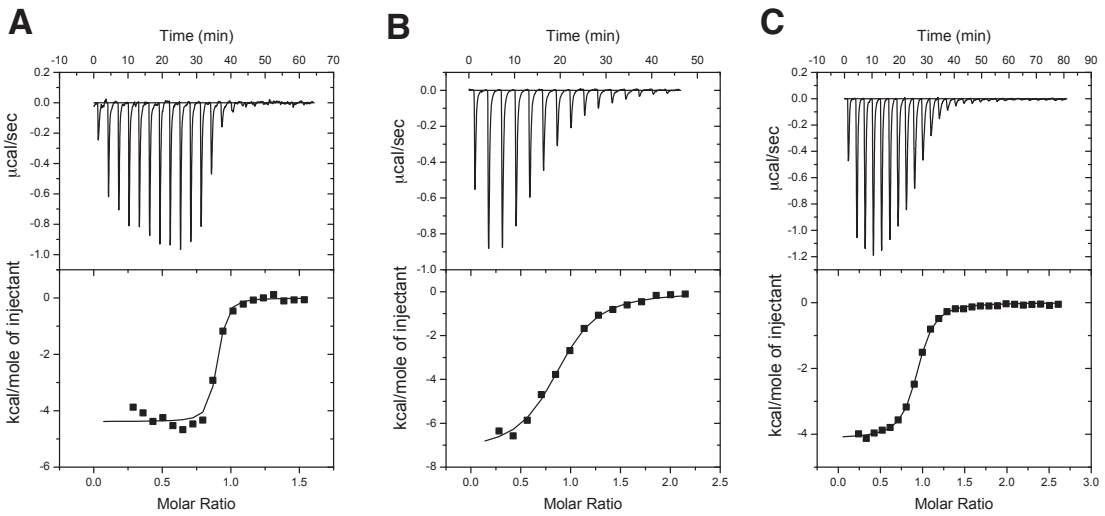

Figure 2.14. ITC of E2F1^{TD} binding between Rb^{PL}-Rb pocket crystal constructs. (**A-B**) Phosphorylation reduces the affinity of E2F1^{TD} for Rb$^{380\text{-}787\Delta 616\text{-}642/S612A/S780A}$ 15-fold, which is consistent with previous experiments using Rb$^{380\text{-}787}$ (Table 2.1). (**C**) Inclusion of S608E in to Rb$^{380\text{-}787\Delta 616\text{-}642/S612A/S780A}$ resulted in a binding affinity of E2F1^{TD} consistent with phosphorylated Rb, suggesting that the S608E mutation functionally mimics phosphorylated S608.

The structure of Rb^{PL} bound to Rb pocket was solved by molecular replacement using a structure of the pocket domain alone as a search model (Balog et al. 2011). The final model was refined to to 2.0Å (Table 2.4). Electron density corresponding to Rb^{PL} was readily observable in the molecular replacement solution prior to building and refinement steps (Figure 2.15). In the final structure, residues 600-610 of Rb^{PL} are ordered and bound

to the pocket at the E2F^{TD}-binding site (Figure 2.16, A). Specifically, residues 602-607 form a short α-helix similar to the α-helix found in the C-terminal half of E2F^{TD} (Lee et al. 2002). The sidechains of two Rb^{PL} residues structurally align with E2F^{TD} sidechains and contact the pocket domain in the same manner: D604 (D424 in E2F2^{TD}) forms a salt bridge with R467, and Y606 (F426 in E2F2^{TD}) makes van der Waals contacts with F482 and I481(Figure 2.16, B). Additionally, the phenolic hydroxyl of Y606 shares a hydrogen bond with the main chain carbonyl of D527. In E2F2^{TD}, residues D424 and F426 are strictly conserved and are critical for tight binding with the Rb pocket (Lee et al. 2002; Xiao et al. 2003); thus it is significant that Rb^{PL} makes analogous interactions to act as a competitive inhibitor of E2Fs.

Previously, we used alanine scanning mutagenesis to determine that the conserved sidechains of D604, Y606 and L607 are each important to stabilize the phosphorylated pocket linker interaction and inhibit E2F^{TD} binding (Table 2.3). The importance of sidechain L607 is now also evident from the structure: it is buried within a hydrophobic pocket composed of N472, L476 and the aliphatic portion of K475. Additionally, the quaternary amine of K475 forms a hydrogen bond with the backbone carbonyl of L607. Although K475 is highly conserved and appears to make important contacts to phosphorylated Rb^{PL}, it is important to note that the mutation of this residue to an alanine did not significantly affect phosphorylation-induced binding between Rb^{PL} and Rb pocket, or reduce the inhibition of E2F^{TD} binding that

occurs upon Rb^{PL} phosphorylation (Figure 2.8). One additional contact observed in the structure that may be important to stabilize the Rb^{PL} - Rb pocket interface is a hydrogen bond between conserved residues T601 in Rb^{PL} and E464 in the Rb pocket domain (Figure 2.16, B).

Data collection	
Beamline	7.1 SLAC
Space group	H3
Cell dimensions: a, b, c (Å)	249.66, 249.66, 35.11
Cell dimensions: α, β, γ (°)	90, 90, 120
Resolution (Å)	36 - 2.0
R_{pim}	4.2 (33.1)
I / σ^I	14.4 (2.7)
Completeness (%)	99.9 (100.0)
Redundancy	6.0 (5.9)
Refinement	
Resolution (Å)	36 - 2.0
No. reflections	57103
R_{work} / R_{free}	19.3 / 23.6
No. atoms: protein	5606
No. atoms: water	355
R.M.S.D. bond lengths (Å)	0.008
R.M.S.D. bond angles (°)	1.0
Average B-factor: protein ($Å^2$)	39.5
Ramachandran analysis (%)	
Preferred	97.7
Allowed	2.3
Outliers	0.0

Table 2.4. **Statistics from X-ray crystallography data and refinement**.

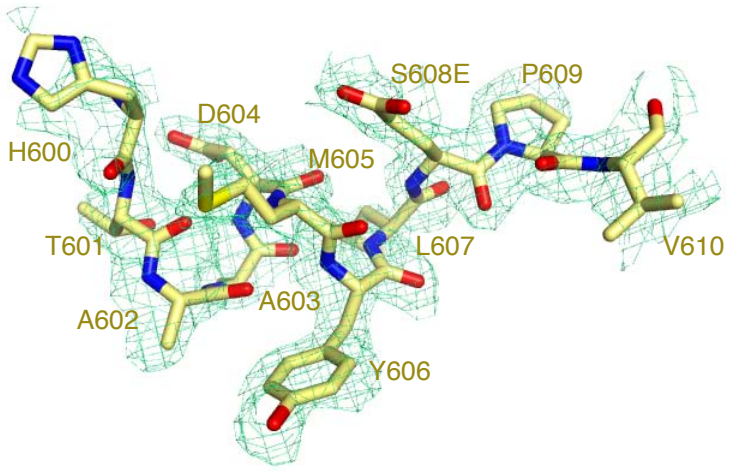

Figure 2.15. Electron density map for Rb^{PL}. The mesh corresponds to a 1.5σ mf_o–Df_c map, generated from the initial molecular replacement solution (without Rb^{PL}) and before building and refinement steps. The final Rb^{PL} solution (yellow sticks) fits well within this initial electron density map.

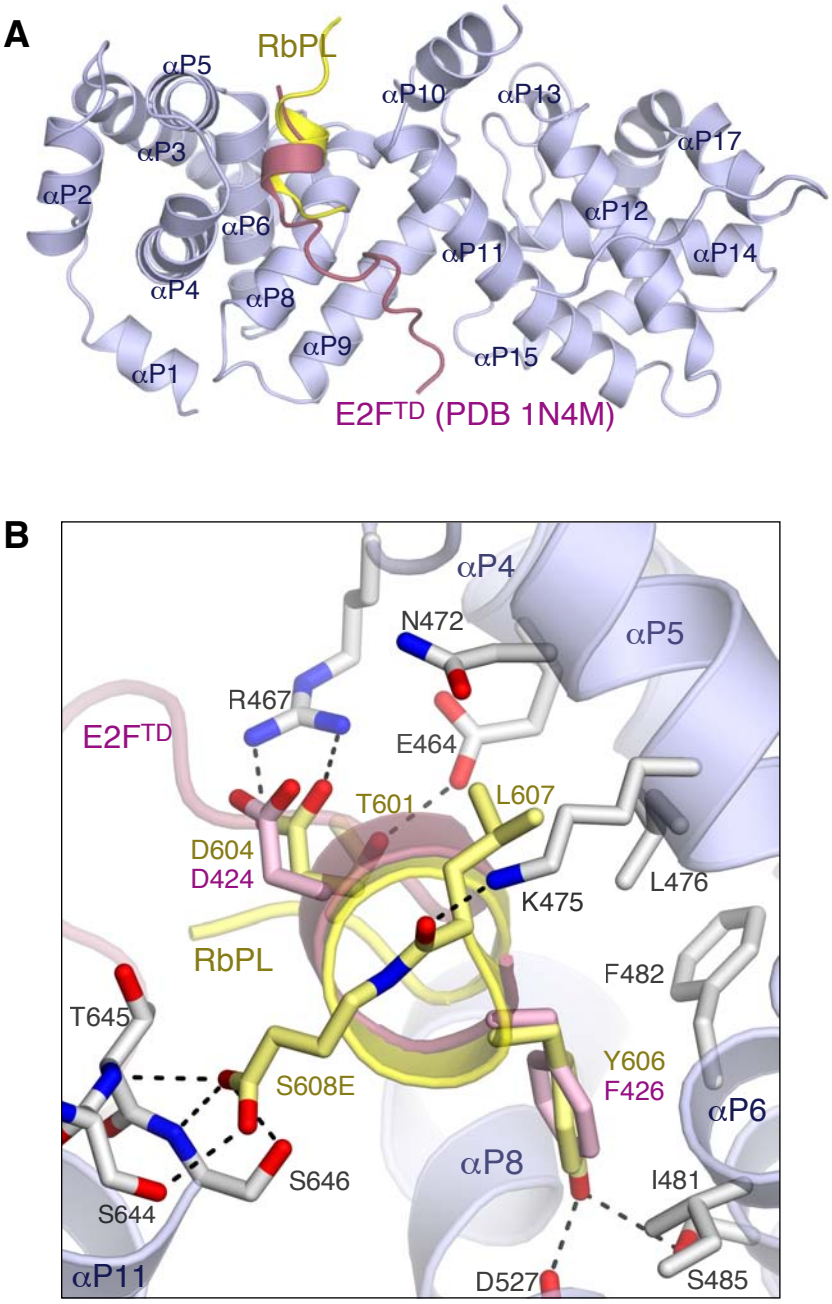

Figure 2.16. Structure of the Rb pocket domain bound by Rb^{PL}. (**A**) Rb^{PL} (yellow) binds at the interface between the A and B subdomains of Rb pocket (blue) and partially occludes E2F^{TD}-binding at it's C-terminal end (E2F2 (pink) is rendered from PDB: 1N4M). (**B**) Detailed interactions stabilizing the Rb^{PL}–pocket interface, and comparison with the E2F^{TD}–Rb pocket interface. This Rb$^{PL\text{-}P}$ structure is available from the PDB as 4ELL.

The phosphoserine-mimetic, S608E, binds the N-terminus of helix αP11 where it stabilizes the positive helix dipole and acts as a hydrogen bond acceptor for the amide protons of residues S644 and T645 as well as the hydroxyl sidechains of S644 and S646 (Figure 2.16, B). Prior to solving this structure, we did not consider the N-terminus of an alpha helix as a potential binding site for phosphorylated S608; however, several structural examples exist of phosphorylated amino acids functionally bound to the N-terminus of alpha helices (Hirsch et al. 2007).

To directly observe the nature of the binding interaction between the phosphate of S608 and the N-terminus of helix αP11, we used COOT to construct a model of this interaction based on the position of S608E in the structure. Through this model, we find that phosphorylated S608 can form a greater number of hydrogen bond contacts than the glutamate side chain seen in the structure (Figure 2.17). Additionally, the phosphate is positioned so that two oxygens adopt an ideal geometry for hydrogen bonding with the amide protons S644 and T645. This type of phosphate binding mode, in which a phosphate molecule forms two strong, in-plane hydrogen bonds with the amide protons of the two most N-terminal amino acids of an alpha helix, has been observed in several structures of phosphate bound at the N-terminus of alpha helices, and is a common feature of the “p-loop” binding motif as well as the “phosphate binding cup” (Hirsch et al. 2007). As further

validation that S608E is indeed a suitable mimic for phosphorylated S608, we see the same type helix-capping interaction with phosphorylated T373 in our structure of $Rb^{N\text{-}P}$ (Chapter 3).

The binding interaction between Rb^{PL} and the Rb pocket domain is structurally similar to a previously characterized interaction between adenovirus E1A protein and the Rb pocket domain (Liu and Marmorstein 2007). Functionally, the E1A protein is known to bind and dissociate Rb-E2F complexes, and thereby cause the up-regulation of E2F-regulated S-phase genes (Liu et al. 2006). A structural comparison of E1A and Rb^{PL} reveals that both inhibit $E2F^{TD}$ through a competitive binding mechanism that involves sidechain interactions analogous to E2F's F426 (Figure 2.18). Additionally, E1A also uses an aspartic acid to cap the N-terminus of helix αP11 of Rb pocket; an interaction similar to 608E in the $Rb^{PL\text{-}P}$ structure and distinct from $E2F^{TD}$ (Figure 2.18). The mechanistic significance of this unique binding site is perhaps that it acts as a charge-mediated docking site for Rb^{PL} and E1A, and also allows Rb^{PL} and E1A to partially bind Rb pocket in the presence of $E2F^{TD}$ in order to prime for competitive binding to the $E2F^{TD}$ binding-cleft. When taken together, the E1A structure is further validation that the S608E mutation is functionally and structurally analogous to the interaction between phosphorylated S608 and Rb pocket. Furthermore, it is remarkable that the adenovirus has created a molecular mimic of Rb's own mechanism for inhibiting $E2F^{TD}$ binding and promoting S-phase entry

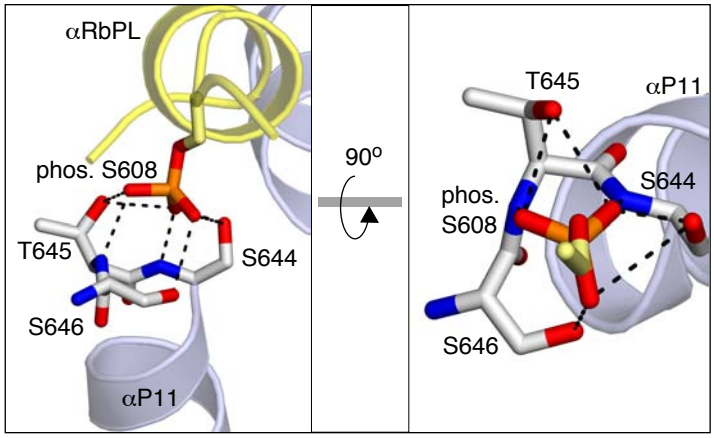

Figure 2.17. **Phosphoserine model at S608E**. A phosphoserine modeled in for S608E forms several additional stabilizing interactions with helix αP11.

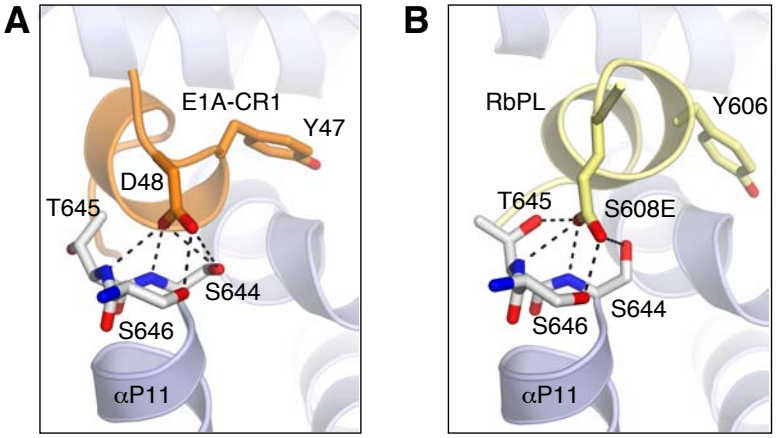

Figure 2.18. Rb^{PL} is structurally similar to E1A. (**A)** The adenovirus E1A conserved region 1 (CR1) bound to Rb pocket and structurally aligned to Rb^{PL} (rendered from PDB: 2R7G). (**B**) Rb^{PL} bound to Rb pocket for comparison (PDB: 4ELL).

Finally, in light of this structure, we revisited the effort to construct a loss-of-function mutant that would compromise the putative phosphate binding site within the pocket domain. For this study, a S644A/S646A double-

mutant was designed to abrogate the hydrogen bond interactions between phosphorylated S608 and the sidechains of S644 and S646 ($Rb^{380\text{-}787/644A/S646A}$). When we test this construct by ITC we see no significant change in $E2F1^{TD}$ binding inhibition upon phosphorylation, compared with wild-type (Figure 2.19). This result indicates that these sidechain interactions play only a minor role stabilizing phosphorylated S608 binding to helix αP11; therefore, phosphate binding is stabilized primarily though the helix dipole interaction and amide proton hydrogen bonds formed with T645 and S644. A different mutation to Rb pocket was designed to eliminate amide proton hydrogen bonding (S644P); however, this construct unexpectedly showed highly reduced $E2F1^{TD}$ binding to unphosphorylated Rb, perhaps indicating a structural change to the pocket domain and thus making it unsuitable for further studies. Next we generated a Rb pocket construct designed to electrostaticly repel phosphorylated S608 from S644/S646 (S644E/S646E); however, this construct did not bind $E2F^{TD}$.

Rb construct	mutations	Kd E2F1^{TD}
Rb$^{380\text{-}787/S644A/S646A}$	S644A/S646A	0.08 ± 0.02 μM
phos. Rb$^{380\text{-}787/S644A/S646A}$	S644A/S646A	0.6 ± 0.1 μM

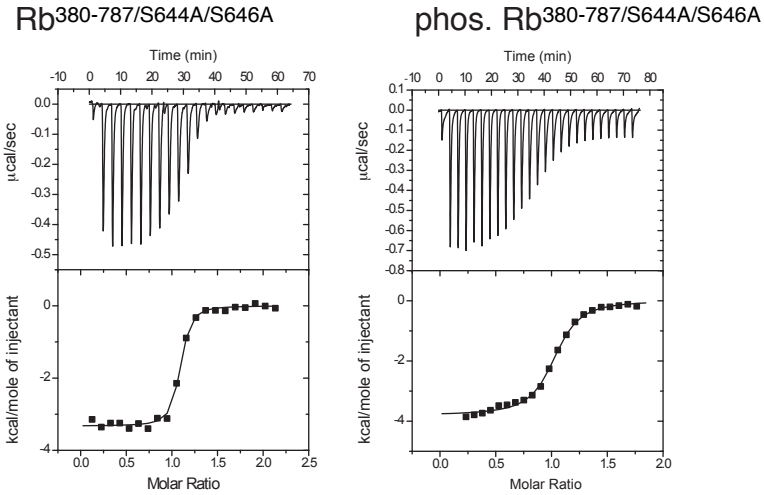

Figure 2.19. Phosphate-binding pocket mutations to Rb. Alanine mutations to S644 and S646 did not abrogate the effect of phosphorylation-induced E2F^{TD} inhibition. The measured affinities of unphosphorylated and phosphorylated Rb$^{380\text{-}787/S644A/S646A}$ for E2F1^{TD} are similar to wild-type (Table 2.1).

In conclusion, the crystal structure solution presented here confirms the molecular determinants for phosphorylation-dependent binding between Rb^{PL} and the Rb pocket domain, which are further supported through a combination of ITC and NMR studies. This structure also confirms the nature of E2F^{TD} inhibition to be competitive, as it can be seen that several key sidechains of Rb^{PL} structurally align with key sidechains of E2F^{TD} (Figure 2.16 B). Furthermore, the structure reveals the phosphomimetic mutation, S608E, forms an N-terminal capping interaction at helix αP11. We believe this to be a

legitimate structural representation of the binding mode for phosphorylated 608 based on modeling studies, similar structures of phosphate bound to the N-terminus of alpha helices (including our Rb^{N-P} structure presented in Chapter 3), and the structure of E1A bound to Rb pocket, which reveals an important biological role for helix αP11 in $E2F^{TD}$-binding inhibition.

2.3 Discussion

2.3.1. S608/S612 phosphorylation in cell-based studies

The work presented within this chapter suggests an important role for S608 phosphorylation in the regulation of the Rb-$E2F^{TD}$ complexes. Several independent studies have used transcriptional reporter assays and cellular growth assays to investigate the cellular roles of different phosphorylation events. The first and only study to suggest that Rb^{PL} itself has a critical role in the phosphorylation-induced dissociation of Rb-$E2F^{TD}$ complexes also surmised that the structured N-terminal domain is important for this effect (Knudsen and Wang 1997). However, the structural and biochemical data presented here clearly indicate that this is not the case. More likely, this original study was observing the effect of phosphorylation at the inter-domain linker (Rb^{IDL}, T356/T373), which we confirm requires the presence of the N-terminal domain to dissociate Rb-$E2F^{TD}$ complexes (Chapter 3). Significantly, several later studies which investigated the roles of different phosphorylation sites arrived at the opposite conclusion of Knudsen and Wang, regarding the

importance of S608/S612. Brown et al. (1999) used full-length mouse Rb with S608A/S612A mutations and found that this construct is basically indistinguishable from wild-type Rb in its ability to restore E2F activity upon phosphorylation; indicating that S608 and S612 phosphorylation is not necessary to fully restore E2F activity. Similar work has shown that phosphorylation of S612 alone or in combination with S608 is not sufficient to rescue significant E2F reporter activity in the context of full-length Rb (Gorges et al. 2008; Lents et al. 2006). However, it is an interesting distinction that when S608 is phosphorylated in addition to S795 and T821, there is significantly greater E2F reporter activity than when only S795 and T821 are present (Lents et al. 2006). Similarly, in a cyclin E reporter assay, the presence of S612 in addition to S795 and T821 produces greater activity than S795 and T821 alone (Gorges et al. 2008). Therefore, although we see a definitive effect of phosphorylating S608 alone in our *in vitro* assays, it seems that in the context of the cell, S608/S612 phosphorylation may be part of a larger cooperative mechanism necessary to fully disassemble Rb-E2F^{TD} complexes. Many of our results actually support this idea. First, full-length Rb weakens E2F1^{TD} binding 200-fold upon phosphorylation, while S608 phosphorylation alone weakens binding only 15-fold. Second, our crystal structure solution identifies a clear mechanism of competitive inhibition; however, this only accounts for the C-terminal half of the transactivation domain interaction, and our NMR data suggest that the N-terminal half of the

transactivation domain may remain bound to Rb pocket even in the presence of S608/S612 phosphorylation. The cell-based work suggests that S795 and T821 phosphorylation may contribute to dissociation of $E2F^{TD}$ from Rb pocket. In the context of our work it makes sense that this may happen through release of the N-terminal half of $E2F^{TD}$. Therefore, the mechanistic details we have discovered are a good compliment to the cell-based work which suggests that Rb^{PL} phosphorylation alone is insufficient to either release or activate E2F.

Although we find the effect of S612 phosphorylation alone to be minimal in our assay (3-fold inhibition of Rb-$E2F^{TD}$ binding), it is tempting to speculate that within the context of the whole protein and additional phosphorylation events, S612 may have a more important role. The protein construct we used for the crystal structure includes a S612A point mutation, which raises the possibility that we missed crystallizing a minor, yet important, phosphorylated S612-Rb pocket interaction. However, examination of the crystal structure solution reveals no additional phosphate binding sites proximal to the S608 site; this includes either a potential helix-capping interaction or salt bridge. Therefore, it is likely that S612 phosphorylation probably behaves the same as S608 phosphorylation: capping helix a11 in the absence of phosphorylation of S608, albeit less optimally. This would explain why S612 phosphorylation alone has a minor effect, but there is not an additive effect of both S608 and S612 phosphorylation in our assay (Table

2.1). Furthermore, this may explain why S612 phosphorylation has a more important role in the context of other phosphorylation events (Gorges et al. 2008). Overall, when our findings are considered in the context of the previously published cell-based assays, it seems that S608/S612 phosphorylation may be part of a larger cooperative mechanism necessary to fully disassemble Rb-E2F^{TD} complexes, and within this mechanism, S608 and S612 may play different roles in the context of different phosphorylation events.

2.3.2. The Rb^{PL} mechanism in p107 and p130

Rb has two pocket protein homologues, p107 and p130, which are known to bind and regulate E2F's. A sequence alignment of pocket protein orthologs reveals that p107 and p130 also contain pocket loops with the highly-conserved, D/ExYxSP motif that is necessary for S608 phosphorylation to perturb Rb-E2F^{TD} binding (Figure 2.20). Additionally, p107 has several highly conserved hydrophobic residues preceding the S650 phosphorylation site. These are distinct from Rb's conserved alanine residues, which may be an indication that p107's pocket linker binds uniquely to the pocket domain upon phosphorylation of S650. However, based on the turn needed to accommodate binding of the D/ExYxSP motif in Rb, it is likely this sequence also forms some sort of helix in p107 and p130. This sequence similarity may indicate a conserved mechanism between Rb and it's pocket protein

homologues; it is known that p107 and p130 are phosphorylated in a cell cycle-dependent manner, and phosphorylation results in E2F dissociation (Cobrink, D. 2005).

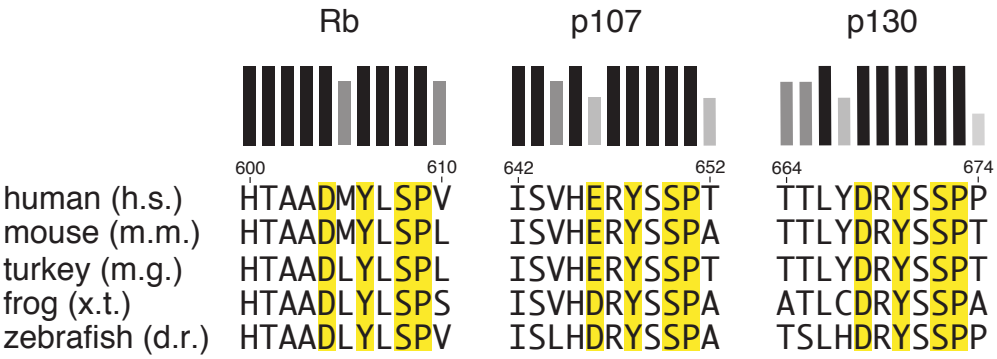

Figure 2.20. Rb^{PL} consensus sequences in Rb homologues. Alignment of Rb^{PL} sequences from human (hs), mouse (mm), chicken (gg), frog (xl), and zebrafish (dr). The sequence, D/ExYxSP is conserved in Rb, p107 and p130.

2.3.3. Non-specific binding at the LxCxE site in the Rb^{PL-P} structure

Finally, a notable feature of the Rb^{PL-P} structure may be of interest from a purely structural point-of-view. Upon solving the structure, we noticed one of the two molecules in each asymmetric unit forms a crystal contact between the "LxCxE" binding cleft and an unbound portion of Rb^{PL} from a symmetry-related molecule. This feature is notable because similar non-specific contacts are observed in the structures of E1A bound to Rb pocket and $E2F2^{TD}$ bound to Rb pocket. In these structures, there are also two molecules in the asymmetric unit, only one of which is involved in LxCxE binding to an extra peptide molecule (Lee et al. 2002; Liu and Marmorstein 2007). Thus it seems that occupancy of the "LxCxE" binding cleft can be

important determinant for how well a particular Rb pocket construct crystallizes. Interestingly, a comparison of all three structures further reveals that the hydrophobic leucine pocket of the "LxCxE" binding cleft is occupied in each case by a structurally superimposable leucine: L586 of Rb; L416 of E2F2^{TD}; L46 of E1A. This observation strongly suggests leucine may be the most stringent requirement of the so-called "LxCxE-binding motif", while the cystine and glutamate positions may tolerate functional analogues.

2.4 Methods

2.4.1 Protein expression and purification

All Rb constructs used in this study were expressed overnight at room temperature in *Escherichia coli*, and as fusions with glutathione S-transferase. Proteins were lysed at 4°C in buffer containing: 25 mM Tris-HCL pH 8, 100 mM NaCl, 1 mM DTT and 1 mM PMSF. The cell lysate was centrifuged at 15,000 r.p.m. for 20-30 minutes the supernatant was loaded directly on to GS4B resin and then purified by glutathione affinity chromatography, followed by ion-exchange chromatography. Rb pocket constructs were cleaved with GST-TEV, diluted to 50 mM NaCl and subsequently purified over heparin sulfate. RbPL$^{592\text{-}624}$ and E2F2^{TD} were similarly diluted, purified over source Q and then cleaved from GST with GST-TEV before they were re-purified over GS4B resin. E2F1^{TD} (residues 372-437) was expressed as a His6 fusion protein in *Escherichia coli*. Cells were induced for 2–4 hours at 37°C, and

proteins were purified by Ni^{2+} nitrilotriacetic acid affinity and anion exchange chromatography.

For NMR studies, proteins were expressed and purified as described except, upon induction, *E. coli* were spun down and switched to M9 minimal medium including ^{15}N-ammonium chloride, ^{13}C-glucose, and D_2O as necessary. Cells were then gently resuspended and allowed to recover for 1 hour at 37°C with shaking prior to induction with 1 mM IPTG. D_2O was saved and distilled for reuse.

2.4.2 Protein phosphorylation

Rb protein constructs were concentrated to 4 mg/ml following purification and then phosphorylated in a reaction containing 10 mM $MgCl_2$, 10 mM ATP (freshly dissolved and adjusted to pH 7), 100 mM NaCl, 25 mM Tris-HCL pH 8.0, and up to 10% Cdk2-CycA (percentage of mass of the total substrate in the reaction). Reactions were incubated at room temperature for 1 hour, and/or at 4C overnight.

Electrospray ionization mass spectrometry (ESI-MS) was used to quantify the phosphate incorporation after each kinase reaction. 2-5 mg of kinase-treated and untreated protein was desalted and purified by reverse phase HPLC prior to mass spec.

2.4.3 Nuclear Magnetic Resonance procedures, data acquisition and analysis

Purified Rb protein constructs were dialyzed in an NMR buffer containing 50 mM sodium phosphate (pH 6.1), 5 mM DTT. Samples were concentrated and mixed with 10% D_2O. For binding experiments involving labeled $Rb^{PL(592–624)}$, HSQC spectra were recorded at the UCSC NMR facility on a Varian INOVA 600-MHz spectrometer equipped with an HCN 5-mm cryoprobe. Experiments observing labeled Rb pocket and experiments to assign $RbPL^{592–624}$ were conducted with an Avance II 900-MHz spectrometer (Bruker-Biospin, Boston, MA) at the Central California 900-MHz NMR facility (Berkeley, CA). Amide resonances for $RbPL^{592–624}$ were assigned via two-dimensional ^{1}H-^{15}N HSQC-TOCSY (100-ms mixing time) and two-dimensional ^{1}H-^{15}N HSQC-NOESY (350-ms mixing time) experiments and via $^{13}C\alpha\beta$ (i, i-1) and $^{13}C\beta$ (i, i-1) linkages observed in a three-dimensional HNCACB experiment (Muhandiram et al. 1994; Norwood et al. 1990; Wittekind et al. 1993). NMR spectra were processed with NMRPipe and analyzed with NMRViewJ (Delagio et al. 1995; Johnson et al. 1994).

2.4.4 Isothermal Titration Calorimetery

ITC experiments were conducted with a MicroCal VP-ITC calorimeter. Typically, 0.5–1 mM $E2F^{TD}$ and 25–50 μM Rb were used in each experiment. Proteins were dialyzed overnight prior to the assay in a buffer containing 100 mM NaCl, 1 mM dithiothreitol, and 25 mM Tris-HCL (pH 8.0). Sometimes 1

mM BME was substituted for DTT, but it was observed that BME adds readily to exposed cystine residues (+78 A.M.U.); therefore, BME was used only for experiments in which the peptide and protein do not contain an important cystine at the known binding interface. Otherwise experiments were often repeated alternatively using BME and DTT. Fast stirring speeds can cause Rb to aggregate and introduce noise into the data, therefore, experiments were routinely conducted with the stirring speed set to 155. Data were analyzed with the Origin calorimetry software package assuming a one-site binding model. Each experiment was repeated 2–4 times, and the reported error is the standard deviation of each set of measurements.

2.4.5 Crystallization, X-ray data collection, structure determination, model refinement

Proteins were prepared for crystallization by elution from a Superdex 200 column in a buffer containing 25 mM Tris-HCL pH 8, 200 mM NaCl, and 5 mM DTT. Proteins were crystallized by sitting drop vapor diffusion at 4°C. $Rb^{PL–P}$ crystals grew best after 1 wk in a solution containing 100 mM sodium citrate, 1 M LiCl, and 18% PEG 8K (pH 5.5). These crystals were frozen in the same solution with 30% ethylene glycol.

Data was collected on Beamline 7.1 at the Stanford Synchrotron Radiation Lightsource. Reflections were integrated with Mosflm (Leslie 2006) and scaled with SCALE-IT (Howell and Smith 1992). Phases were solved by molecular replacement using PHASER (Mccoy et al. 2007), using the Rb

pocket as a search model (PDB: 3POM). The initial model of the structure was rebuilt with COOT (Emsley and Cowtan 2004) and was refined with Phenix (Adams et al. 2010). Several rounds of position refinement with simulated annealing and individual temperature factor refinement with default restraints were applied. Coordinates and structure factors for $Rb^{PL\text{-}P}$ have been deposited in the Protein Data Bank under the accession code 4ELL.

2.5 References

Adams PD, Afonine PV, Bunkoczi G, Chen VB, Davis IW, Echols N, Headd JJ, Hung LW, Kapral GJ, Grosse-Kunstleve RW, McCoy AJ, Moriarty NW, Oeffner R, Read RJ, Richardson DC, Richardson JS, Terwilliger TC, Zwart PH. "PHENIX: A comprehensive Python-based system for macromolecular structure solution."
Acta Crystallogr D Biol Crystallogr. 66, 213–221. (2010)

Balog ER, Burke JR, Hura GL, Rubin SM. Crystal structure of the unliganded retinoblastoma protein pocket domain." *Proteins.* 79(6), 2010-4. (2011)

Brown VD, Phillips RA, Gallie BL. "Cumulative effect of phosphorylation of pRB on regulation of E2F activity."
Mol Cell Biol. 19(5), 3246-56. (1999)

Burke JR, Deshong AJ, Pelton JG, Rubin SM. "Phosphorylation-induced conformational changes in the retinoblastoma protein inhibit E2F transactivation domain binding."
J Biol Chem 285(21):16286-93. (2010)

Burke JR, Hura GL, Rubin SM. "Structures of inactive retinoblastoma protein reveal multiple mechanisms for cell cycle control."
Genes Dev. 26(11):1156-66. (2012)

Cobrinik D. "Pocket proteins and cell cycle control."
Oncogene 24(17), 2796-809. (2005)

Delaglio, F., Grzesiek, S., Vuister, G. W., Zhu, G., Pfeifer, J., and Bax, A. "NMRPipe: a multidimensional spectral processing system based on UNIX pipes." *J. Biomol. NMR* 6, 277–293. (1995)

Emsley P, Cowtan K. 2004. "Coot: Model-building tools for molecular graphics." *Acta Crystallogr D Biol Crystallogr.* 60, 2126–2132. (2004)

Gorges LL, Lents NH, Baldassare JJ. "The extreme COOH terminus of the retinoblastoma tumor suppressor protein pRb is required for phosphorylation on Thr-373 and activation of E2F. " *Am J Physiol Cell Physiol.* 295(5), 1151-60. (2008)

Hirsch AK, Fischer FR, Diederich F. "Phosphate recognition in structural biology." *Angew Chem Int Ed Engl.* 46(3), 338-52. (2007)

Howell PL, Smith GD. "Identification of heavy-atom derivatives by normal probability methods." *J Appl Crystallogr* 25, 81–86. (1992)

Johnson BA. "Using NMRView to visualize and analyze the NMR spectra of macromolecules." *Methods Mol Biol.* 278, 313-52. (2004)

Knudsen ES, Wang JY. "Dual mechanisms for the inhibition of E2F binding to RB by cyclin-dependent kinase-mediated RB phosphorylation." *Mol Cell Biol.* 17(10), 5771-83. (1997)

Lee C, Chang JH, Lee HS, Cho Y. "Structural basis for the recognition of the E2F transactivation domain by the retinoblastoma tumor suppressor." *Genes Dev.* 16(24), 3199-212. (2002)

Lents NH, Gorges LL, Baldassare JJ. "Reverse mutational analysis reveals threonine-373 as a potentially sufficient phosphorylation site for inactivation of the retinoblastoma tumor suppressor protein (pRB)." *Cell Cycle* 5(15),1699-707. (2006)

Leslie AG. "The integration of macromolecular diffraction data." *Acta Crystallogr D Biol Crystallogr* 62, 48–57. (2006)

Liu X, Clements A, Zhao K, Marmorstein R. "Structure of the human Papillomavirus E7 oncoprotein and its mechanism for inactivation of the retinoblastoma tumor suppressor." *J Biol Chem.* 281(1), 578-86. (2006)

Liu X, Marmorstein R. “Structure of the retinoblastoma protein bound to adenovirus E1A reveals the molecular basis for viral oncoprotein inactivation of a tumor suppressor.” *Genes Dev.* 21(21), 2711-6. (2007)

Mccoy AJ, Grosse-Kunstleve RW, Adams PD, Winn MD, Storoni LC, Read RJ. “Phaser crystallographic software.” *J Appl Crystallogr* 40, 658–674. (2007)

Muhandiram DR and Kay LE. *J. Magn. Reson. B* 103, 203–216. (1994)

Norwood TJ, Boyd J, Heritage JE, Soffe N, Campbell ID. *J. Magn. Reson.* 87, 488 –501. (1990)

Pettersen EF, Goddard TD, Huang CC, Couch GS, Greenblatt DM, Meng EC, Ferrin TE. “UCSF Chimera- a visualization system for exploratory research and analysis.” *J Comput Chem* 25, 1605–1612. (2004)

Wittekind M, and Mueller L. *J. Magn. Reson. B* 101, 201–205. (1993)

Xiao B, Spencer J, Clements A, Ali-Khan N, Mittnacht S, Broceño C, Burghammer M, Perrakis A, Marmorstein R, Gamblin SJ. “Crystal structure of the retinoblastoma tumor suppressor protein bound to E2F and the molecular basis of its regulation.” *Proc Natl Acad Sci* 100(5), 2363-8. (2003)

Chapter 3: Phosphorylation of Rb^{IDL} (T373) promotes Rb pocket-RbN binding and displaces $E2F^{TD}$ from Rb pocket.

3.1. Introduction

While Rb's pocket domain has been well-studied, several factors have contributed to the relative obscurity of Rb's N-terminal domain (RbN): Early investigations into Rb's function revealed that the pocket domain and C-terminus are together sufficient for E2F binding and growth suppression (Qin et al. 1992); unlike Rb's other domains, RbN is not a targeted binding site for viral proteins (Felsani et al. 2006); structural studies of Rb's domains indicated that the pocket and N-terminus resemble beads on a string and are therefore distinct in their functions (Hensey et al. 1994). For these reasons, a majority of the early studies which sought to characterize Rb's role in the cell also used constructs which lacked the N-terminal domain. The first indication that RbN has an important and distinct function came from work by Knudsen and Wang (1997), who suggested it is a critical component of Rb's E2F release mechanism. Specifically, they proposed that the presence of RbN is required for phosphorylation at S608/S612 to release E2F from Rb. Our work has revised this model to replace S608/S612 with T373, but to their credit, Knudsen and Wang did propose a large phosphorylation-induced

conformational change to potentially explain a role for the structured N-terminal domain in modulating E2F binding.

A recent crystal structure solution of the isolated N-terminal domain has shed some new light on this old problem. The solution reveals that RbN is structurally similar to the pocket domain: it consists of two tandem cyclin folds and a flexible 25-residue loop which harbors two closely-spaced phosphorylation sites (Hassler et al. 2007). In order to crystalize the N-terminal domain, the loop is proteolytically removed; this is also similar to Rb pocket (Lee et al. 1998; Hassler et al. 2007). In seeking out the function of this domain, the authors seemed to overlook the work of Knudsen and Wang and instead found that EID-1 (EP300 Inhibitor of Differentiation 1: a transcription factor) binds Rb via a bipartite mechanism involving both the LxCxE cleft on the pocket domain and the N-terminal loop. Additionally they show that phosphorylation of this loop releases EID-1 from Rb. Consistent with this theory, multiple studies have indicated that phosphorylation of the N-terminal loop alone (S249/T252) is neither necessary, nor sufficient, for the release of E2F (Brown et al. 1999; Gorges et al. 2008, Knudsen and Wang 1997; Lents et al. 2006).

A second critical finding of Hassler et al, (2007), is that the pocket domain and the N-terminal domain interact directly. Pull-down assays show that only the structured pocket domain is required for this interaction. Hassler et al. also used FRET experiments probe the importance of phosphorylation

for this effect and found that association of the two domains is independent of the phosphorylation state of either. However, in these experiments, the pocket construct lacks the phosphorylation site: T373. Finally, Hassler et al, find that they can inhibit the binding interaction between Rb pocket and RbN in a pull-down assay by adding a large molar excess of the LxCxE peptide from EID-1.

Studies conducted in our lab indicate a role for the structured N-terminal domain that is consistent with regulation of E2F. In the process of narrowing down the phosphorylation requirements for E2F regulation, E2F binding experiments were conducted using Rb constructs that contain either phosphorylation site mutations or domain truncations. Evaluation of these constructs by ITC assays reveals an Rb construct which contains both structured domains but harbors alanine mutations to T356/T373 and S608/S612, completely looses its ability to inhibit $E2F^{TD}$ binding (Table 3.1, row 1-3). Similarly, these two set of sites (T356/T373 and S608/S612) also contribute individually to $E2F^{TD}$ inhibition, as both are needed for full inhibition of $E2F^{TD}$ (Table 3.1, rows 4-6). A construct which lacks only the N-terminal loop sites, but retains T356/T373 and S608/S612, is still able to fully inhibit $E2F^{TD}$ binding upon phosphorylation (Table 3.1, row 6). However, a construct which contains these same phosphorylation sites but lacks the structured N-terminal domain is far less effective at inhibiting $E2F^{TD}$ binding (Table 3.1, row 7); this was our first indication that the structured N-terminal

domain has an important role in mediating inhibition of $E2F^{TD}$. The partial binding inhibition that occurs in the absence of the N-terminal domain is comparable to a similar construct lacking T356/T373 (Table 3.1, row 8). This suggests that T356/T373 phosphorylation is not able to contribute to the inhibition of $E2F^{TD}$ binding if the structured N-terminal domain is absent. The requirement of the structured N-terminal domain, coupled with the knowledge that Rb's pocket domain and RbN exist similar to "beads on a string", is suggestive of a mechanism in which phosphorylation of T356/T373 induces the domains to interact in such a way as to block $E2F^{TD}$ binding to Rb pocket.

	Rb construct	phosphorylation sites	K_d $E2F1^{TD}$
1	unphos. Rb^{55-787}	-	0.3 ± 0.2 μM
2	phos. Rb^{53-787}	S249, T252, T356, T373, S608, S612, S780	13 ± 3 μM
3	phos. $Rb^{53-787\Delta T356/T373/S608/S612}$	S249, T252, S780	0.33 ± 0.02 μM
4	phos. $Rb^{53-787\Delta S249/T252/T356/T373}$	S608, S612, S780	2.7 ± 0.6 μM
5	phos. $Rb^{53-787\Delta S249/T252/S608/S612}$	T356, T373, S780	2.9 ± 0.1 μM
6	phos. $Rb^{53-787\Delta S249/T252}$	T356, T373, S608, S612, S780	25 ± 1 μM
7	phos. $Rb^{252-787\Delta RbN}$	T356, T373, S608, S612, S780	0.97 ± 0.03 μM
8	phos $Rb^{380-787}$	S608, S612, S780	0.7 ± 0.4 μM

Table 3.1. ITC results of Rb mutation/truncation studies.

Initially, we set out to look for a phosphorylation-induced inter-domain binding mechanism using NMR. Our previous success using NMR to explore the intramolecular binding between a phosphorylated Rb^{PL} peptide and Rb pocket led us to believe we could reuse this method to obtain similarly insightful clues to this new puzzle. While we were able to obtain some useful information from these NMR studies, it is really only insightful in the context of what we discovered through subsequent SAXS, ITC and protein crystallography experiments. Our first major windfall in studying this system came when we turned to SAXS to identify a large-scale conformational change that occurs as a result of phosphorylation at T373. As an accompaniment to the SAXS data, ITC was used to reveal this conformational change correlates with a dramatic weakening of $E2F^{TD}$ binding to Rb pocket. Finally, we were lucky enough to solve the crystal structure of Rb phosphorylated at T356/T373 to 2.7 angstroms. To our surprise, this structure reveals an allosteric mechanism for $E2F^{TD}$ dissociation. The allosteric mechanism is supported through additional ITC and mutagenesis experiments.

3.2. Results

3.2.1. NMR studies of binding between phosphorylated Rb^{IDL} and Rb pocket

Our first attempt to use NMR to study this system did not yield definitive answers. This study was underway at the same time as the ITC

studies described in the introduction to this chapter (Table 3.1); therefore, we had only a partial understanding of the system when we endeavored to use NMR to explain it. Specifically, at the time of these experiments, we did not yet know that the structured N-terminal domain is a requirement for T356/ T373 phosphorylation to inhibit $E2F^{TD}$ binding. This first section therefore describes a set of experiments which sought to identify a phosphorylation-dependent interaction between a peptide of Rb's phosphorylated inter-domain linker (Rb^{IDL}) and the pocket domain. Importantly, this study does characterize an less-important, but relevant, interaction between phosphorylated Rb^{IDL} and the pocket domain. We began this study with a ^{1}H-^{15}N HSQC-TROSY experiment (described in detail in chapter 2.2.2), which is designed to look for chemical shift changes to labeled Rb pocket in the presence of unlabeled, phosphorylated Rb^{IDL}. Using 5 molar excess of phosphorylated $Rb^{IDL(338\text{-}377)}$, we observe very minimal chemical shift perturbations to the spectrum of Rb pocket; this indicates a minor *in-trans* binding interaction (Figure 3.1).

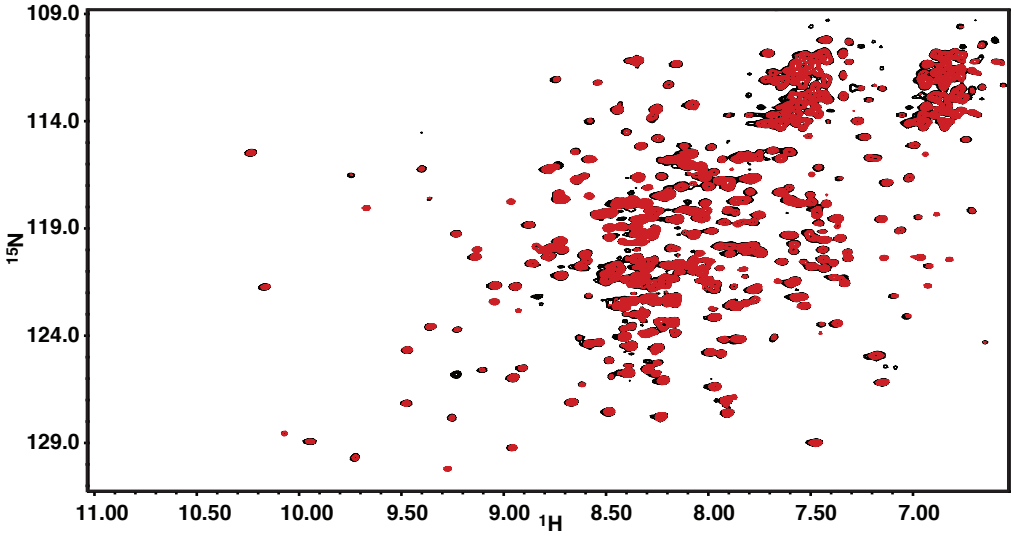

Figure 3.1. Phosphorylated Rb^{IDL} binding to ^{15}N-labeled Rb pocket *in trans*. ^{1}H-^{15}N HSQC-TROSY of 300 µM ^{2}H-^{15}N-labeled Rb$^{362\text{-}787\Delta578\text{-}642}$ alone (black), and the presence of 1.5mM unlabeled, phosphorylated Rb$^{IDL(338\text{-}377)}$ (red).

Next, we performed the reciprocal set of experiments in which we looked for chemical shift changes to a ^{1}H-^{15}N HSQC spectra of ^{15}N-labeled phosphorylated Rb^{IDL} in the presence of unlabeled Rb pocket. The HSQC spectrum for this Rb^{IDL} peptide was assigned using a combination of triple and double-labeled experiments (Table 3.2). Upon binding of unlabeled Rb pocket to ^{15}N-labeled phosphorylated Rb^{IDL}, we see dramatic chemical shift broadening that corresponds primarily to residues 343-355 (Figure 3.2, A-B). Notably, this interaction is not entirely dependent on phosphorylation, but it can be competed off by adding excess E2F^{TD} peptide (Figure 3.2, C-D).

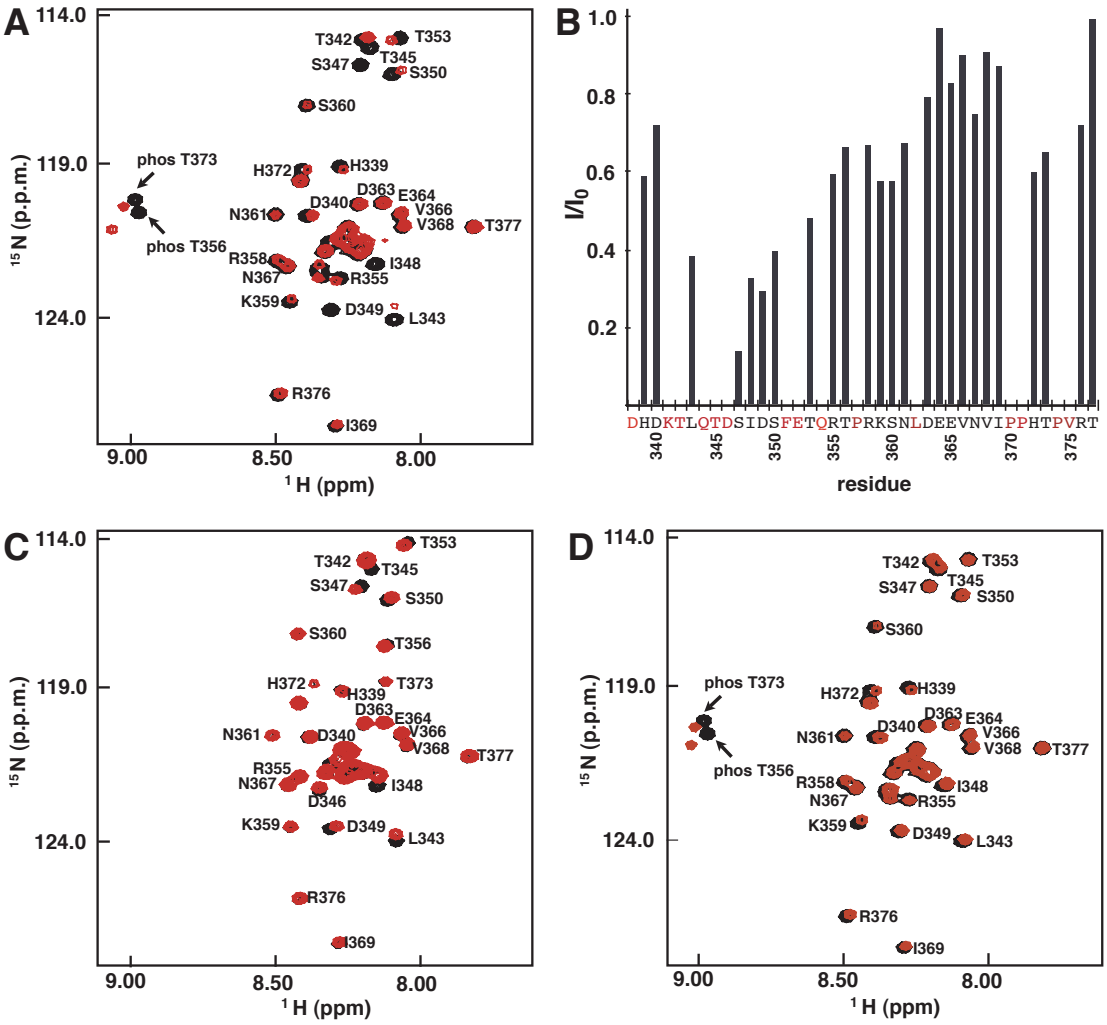

Figure 3.2. Phosphorylated Rb^{IDL} associates with the Rb pocket domain and competes with E2F^{TD} binding. (**A**) ^{1}H-^{15}N HSQC spectra of 100 µM ^{15}N-labeled phosphorylated Rb$^{IDL(338-377)}$ alone (black) and in the presence of 600 µM unlabeled Rb$^{380-787\Delta PL}$ (red). Broadening of selective peaks indicates binding between phosphorylated Rb^{IDL} and the pocket. (**B**) The ratio I/I$_0$ is defined as the peak intensity of phosphorylated Rb^{IDL} in the presence of Rb$^{380-787\Delta PL}$ (I) divided by the peak intensity of phosphorylated Rb^{IDL} alone (I$_0$). (**C**) HSQC of 100 µM ^{15}N-labeled unphosphorylated Rb^{IDL} alone (black) and in the presence of 650 µM unlabeled Rb$^{380-787\Delta PL}$ (red). Less peak broadening is observed in this spectrum than (A), demonstrating that binding is mediated by phosphorylation of Rb^{IDL}. (**D**) HSQC of 100 µM ^{15}N-labeled phosphorylated Rb^{IDL} alone (black), and with 600 µM unlabeled Rb$^{380-787\Delta PL}$ and 1 mM unlabeled E2F4^{TD}. In the presence of excess E2F4^{TD}, Rb^{IDL} resonance peaks

and chemical shifts corresponding to unbound phosphorylated Rb^{IDL} return, indicating that $E2F4^{TD}$ competes with phosphorylated Rb^{IDL} for binding to the Rb pocket domain.

	phos. RbIDL				unphos. RbIDL			
A.A.	**$^{13}C\alpha$**	**$^{13}C\beta$**	**$^{1}H^{N}$**	**^{15}N**	**$^{13}C\alpha$**	**$^{13}C\beta$**	**$^{1}H^{N}$**	**^{15}N**
D 338					54.81	41.44	8.39	120.5
H 339	56.31	29.66	8.28	119.3	56.6	29.91	8.27	119
D 340	54.96	41.11	8.4	120.8	55.19	41.34	8.2	120.1
K 341	56.88	32.82			33.01	57.2		
T 342	62.88	69.83	8.21	115	63.21	70.04	8.2	114.8
L 343	55.38	42.45	8.14	120.4	55.72	42.65	8.08	123.9
Q 344	55.91	29.47			56.17	29.72		
T 345	62.03	69.97	8.18	115.3	62.28	70.15	8.16	115.1
D 346	54.64	41.35			41.55	54.89	8.34	122.3
S 347	58.38	64.01	8.22	115.9	58.66	64.27	8.21	115.6
I 348	61.59	38.98	8.16	122.4	61.9	39.18	8.15	122.1
D 349	54.62	41.39	8.32	123.9	54.85	41.6	8.31	123.5
S 350	58.56	63.93	8.1	116.2	59.01	64.12	8.11	116.1
F 351	58.31	39.56			58.79	39.64	8.28	119
E 352	54.61				57.59	30.47		
T 353	62.4	69.91	8.08	115	63.15	30.48	8.05	114.2
Q 354	55.9	29.44				32.52		
R 355	56.01	31.28	8.29	122.9	56.54	31.38	8.41	121.8
T 356	60.77	72.79	9.02	120.8	60.37	70.08	8.11	117.5
P 357								

	phos. RbIDL				unphos. RbIDL			
A.A.	**13Cα**	**13Cβ**	**1HN**	**15N**	**13Cα**	**13Cβ**	**1HN**	**15N**
R 358	56.38	31	8.52	122.2	68.03	31.38		
K 359	56.46	33.29	8.46	123.6	56.83	33.63	7.84	121.2
S 360		64.2	8.4	117.2	58.6	64.65	8.43	117.2
N 361	53.55	38.82	8.52	120.8	53.86	39	8.51	120.5
L 362	55.76	42.33			56.03	42.56		
D 363	54.94	41.12	8.22	120.5	55.12	41.36	8.42	119.4
E 364	56.82	30.66	8.14	120.4	57.12	30.93	8.13	120.1
E 365	56.83	30.41			57.15	30.58		
V 366	62.51	32.88	8.08	120.8	62.87	33.12	8.07	120.5
N 367	53.35	39.28	8.47	122.5	56.33	31.38	8.45	122.1
V 368			8.07	121.1	53.5	39.5	8.05	120.8
I 369	58.5	38.55	8.3	127.6	58.76	38.8	8.29	127.3
P 370								
P 371								
H 372	56.66	29.9	8.41	119.3	56.2	30.34	8.38	118.8
T 373	60.43	73.01	9.02	120.4	60.3	70.19	8.12	118.7
P 374								
V 375	62.88	32.58			33.12	62.95		
R 376	56.14	31.12	8.5	126.6	56.33	31.38	8.42	125.8
T 377		70.78	7.82	121.2	63.58	70.98	7.84	121.2

Table 3.2. Chemical shift assignments for $Rb^{IDL(338-377)}$.

3.2.2. NMR studies of phosphorylation-dependent binding between Rb pocket and RbN

As the ITC experiments caught up to the NMR work, we realized that the presence of the structured N-terminal domain is necessary for T356/T373 phosphorylation to inhibit $E2F^{TD}$ binding. Therefore in an attempt to learn something more about this complicated mechanism, we next investigated a potential role of T356/T373 phosphorylation in promoting binding between the pocket and N-terminal domains *in-trans,* by NMR. We explored two theoretical modes by which phosphorylation of Rb^{IDL} promotes such an inter-domain association: Rb^{IDL} phosphorylation might create a binding interface for Rb pocket on the surface of RbN, so to facilitate a direct association between the domains; conversely, Rb^{IDL} phosphorylation might create a binding interface for RbN on the surface of Rb pocket. Before we could test these models, we had to generate a construct of the N-terminal domain which is suitable for NMR studies. At 35KDa, the N-terminal domain is on the large side for NMR, we therefore used the same preparations that were used for the pocket domain to acquire ^{1}H-^{15}N HSQC-TROSY spectra (Chapter 2.2.2). Upon initial examination of the N-terminal domain spectra, we also decided it pertinent to remove the N-terminus loop (Rb^{NL}) from this construct. For this task we employed a proteolytic digestion procedure similar to that described by Hassler et al, (2007). Comparison of the RbN spectra with and without

Rb^{NL} indicates that this linker, like Rb^{PL}, is highly dynamic and alters the correlation time of the molecule (Figure 3.3).

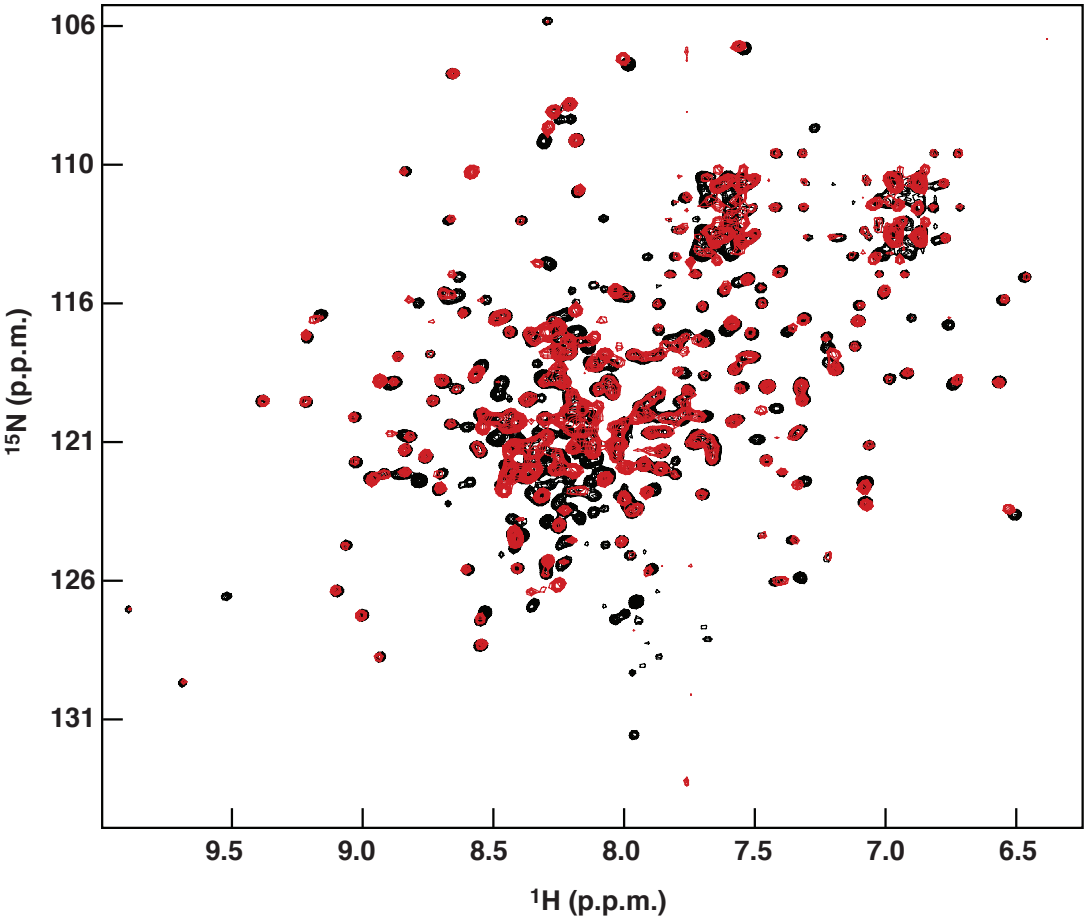

Figure 3.3. ^{1}H-^{15}N HSQC-TROSY spectra of $RbN^{53\text{-}345/\Delta NL}$ with no loop(black) and $RbN^{53\text{-}345}$ with loop (red). Proteolytic cleavage of the n-terminus domain loop (NL, residues 244-264) improves the quality of the spectrum.

To test our two models of how phosphorylation of Rb^{IDL} promotes inter-domain binding between RbN and Rb pocket, we used protein constructs with one of the two structured domains covalently linked to Rb^{IDL} and looked for *in trans* binding of the other structured domain. We then compared the extent of

spectral signal broadening between phosphorylated and unphosphorylated samples. In the first experiment, we wanted to test if Rb^{IDL} phosphorylation creates a binding interface for Rb pocket on the surface of RbN. For this experiment we observe chemical shift perturbations to the HSQC-TROSY spectrum of labeled Rb pocket in the presence of unphosphorylated or phosphorylated RbN^{IDL}; RbN^{IDL} includes both RbN and Rb^{IDL}, residues: 53-377 (Figure 3.4, A). To quantitate the extent of signal broadening in the different spectra of Rb pocket, a change in signal intensity is determined for each spectral peak, and binned in a histogram to convey the extent of overall peak broadening of the pocket spectra. For this experiment, we find that the addition of either unphosphorylated or phosphorylated RbN^{IDL} broadens the Rb pocket spectrum in a similar fashion (Figure 3.4, B); indicating that Rb^{IDL} phosphorylation in this context does not change the way in which the two domains interact. To test our second model (does Rb^{IDL} phosphorylation create a binding interface for RbN on the surface of Rb pocket?), we acquire the spectra of RbN in the presence of phosphorylated or unphosphorylated Rb $pocket^{IDL}$. In these spectra we see more extensive signal broadening to the RbN spectrum when Rb $pocket^{IDL}$ is phosphorylated (Figure 3.4, C). The difference in signal broadening between these two spectra is represented in the histogram, which shows extensive signal broadening to the RbN spectrum in the presence of phosphorylated Rb $pocket^{IDL}$ but not unphosphorylated Rb $pocket^{IDL(352\text{-}787)}$ (Figure 3.4, D). This signal broadening effect reflects a

substantial increase in the overall size of the observed RbN molecule. Therefore, this result suggests that phosphorylation of Rb^{IDL} creates a binding surface for RbN on Rb pocket and not the other way around.

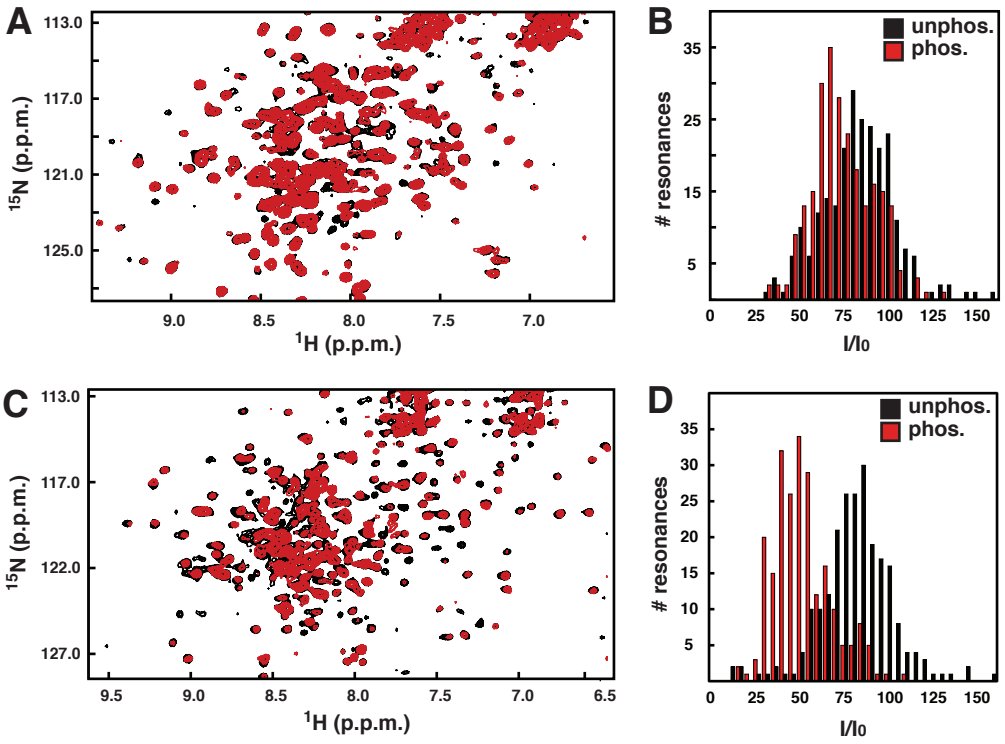

Figure 3.4. Phosphorylation-dependent binding between Rb pocket and RbN. (**A**) Detail of ^{1}H-^{15}N HSQC-TROSY spectra of 300 µM ^{2}H-^{15}N-labeled Rb pocket$^{362\text{-}787\Delta PL}$ in the presence of 400 µM unlabeled, unphosphorylated RbN$^{IDL(53\text{-}377)}$ (black), or in the presence of 400 µM unlabeled, phosphorylated RbN$^{IDL(53\text{-}377)}$ (red). (**B**) Histogram of differences in signal broadening to the HSQC-TROSY spectrum of Rb$^{362\text{-}787\Delta PL}$ between the two experiments shown in (A). The ratio I/I_0 is defined as the peak intensity of Rb pocket in the presence of RbN^{IDL} (I) divided by the peak intensity of Rb pocket alone (I_0). A direct comparison of spectral broadening effects indicate that phosphorylation of RbN^{IDL} does not change the extent of spectral broadening, indicating that phosphorylation of RbN^{IDL} does not change the way in which the two domains interact. (**C**) Detail of ^{1}H-^{15}N HSQC-TROSY spectra of 250 µM ^{2}H-^{15}N-labeled RbN$^{53\text{-}345/\Delta NL}$ in the presence of 540 µM unlabeled, unphosphorylated Rb pocket$^{IDL(352\text{-}787)}$ (black), or in the presence of 540 µM unlabeled, phosphorylated Rb pocket$^{IDL(352\text{-}787)}$(red). (**D**) Comparison of the signal

broadening effects between the experiments shown in (C), reveals that $RbN^{53\text{-}345/\Delta NL}$ binds better to phosphorylated Rb $pocket^{IDL}$.

3.2.3. SAXS: Phosphorylation of T373 causes a large conformational change in $Rb^{53\text{-}787}$

Small Angle X-ray Scattering (SAXS) is a low-resolution, low-stress alternative to protein X-ray crystallography. However, data obtained from a SAXS experiment can supply only a few important biophysical parameters to the investigation of a purified protein (or protein complex): SAXS is particularly useful for determining the approximate size of a molecule, its radius of gyration, and is dispersion state in solution (it is easy to detect aggregation). Furthermore, an *ab initio* model of a well-behaved protein can provide a low-resolution envelope, which includes the rough size, shape and gross contours of the protein; although the accuracy of such details is questionable. Molecular modeling studies can be used in conjunction with SAXS data to predict conformational states, dynamics, or the details of assemblage of multi-protein complexes. An accessible and thorough review of SAXS can be a great help to anyone trying to get a handle on this technique (Putnam et al, 2007).

To further our investigation of the inter-domain binding interaction that occurs upon the phosphorylation of Rb at T356/T373, we generated an Rb construct to study with SAXS. Notably, because SAXS is sensitive to the size and shape of a molecule, a protein which contains large, flexible loops, linkers or tails can average out the scattering signal of the structured portion of the

molecule. Therefore both the N-terminal and pocket linker loops were cloned out of Rb to generate a construct which consists only of the structured N-terminal domain, pocket domain and the 24-residue inter-domain linker ($Rb^{53\text{-}787/\Delta NL/\Delta PL}$). The X-ray scattering data for the unphosphorylated protein and phosphorylated protein is noticeably distinct (Figure 3.5, A). When the protein is unphosphorylated, the scattering curve shows an linear decay of log (I) along the scattering angle (q), until the signal intensity dies off sharply at about 5 angstroms. In contrast, the scattering data for the phosphorylated sample contains “mid resolution” curves that automatically distinguish it from the unphosphorylated sample; however, the important distinctions in this curve come from the smallest scattering angles. A Guinier plot for this narrow range of data ($qR_G<1.3$ for a compact molecule, $qR_G<0.8$ for elongated), should show a linear dependence of ln(I) vs q^2. If the Guinier plot can not be fit to a straight line, this is a key indication that the protein sample is aggregated. Notably, both the phosphorylated and unphosphorylated samples do not show this sign of aggregation (Figure 3.5, B). From the Guinier plot, a linear regression can be used to derive the radius of gyration (R_G) of the molecule, which is simply proportional to the slope. The radius of gyration is defined as the square root of the average distance of each scatterer from the particle center (Putnam et al. 2007). The R_G values for unphosphorylated and phosphorylated $Rb^{53\text{-}787/\Delta NL/\Delta PL}$ are 37Å and 31Å, respectively; indicating that the molecule becomes more compact upon

phosphorylation (Table 3.3). By comparison, the theoretical R_G value for a completely globular molecule of this size is 27 Å. A second useful parameter is D_{max}, which is defined as the maximum linear dimension in the scattering particle. D_{max} can be obtained from the pair distribution function, P(r), which is a Fourier transform of the scattering curve. The pair distribution functions for phosphorylated and unphosphorylated Rb are distinct in that phosphorylated Rb has more of a Gaussian distribution and is therefore more globular or "sphere-like". In comparison, unphosphorylated Rb has a more bimodal distribution and is therefore more similar to two beads on a sting (Figure 3.5, inlay). The D_{max} value is generally considered approximate as its exact value can be difficult to determine from the pair distribution function (Putnam et al. 2007). For the unphosphorylated sample D_{max} is 134Å, for the phosphorylated sample D_{max} is 110Å (Table 3.3). Again these parameters are an indication that the phosphorylated sample is more compact, or in a conformationally closed state, while the unphosphorylated sample is more elongated in a conformationally open state. Finally the program GASBOR was used to generate *ab initio* model envelopes of the phosphorylated and unphosphorylated proteins. Qualitatively, these models visually represent the parameters derived from analysis of the Guinier and P(r) plots (Figure 3.5, C). By staring too hard at the GASBOR results, the next obvious question becomes clear: *how* do the domains come together to inhibit $E2F^{TD}$ binding? Unbiased attempts to answer this question were made using the program

BUNCH (Petoukhov and Svergun 2005). BUNCH incorporates the known domain structures with the linker sequence to sample orientations and generate theoretical scattering data to fit the experimental scattering data; however, a consistent, well-scored solution could not be obtained.

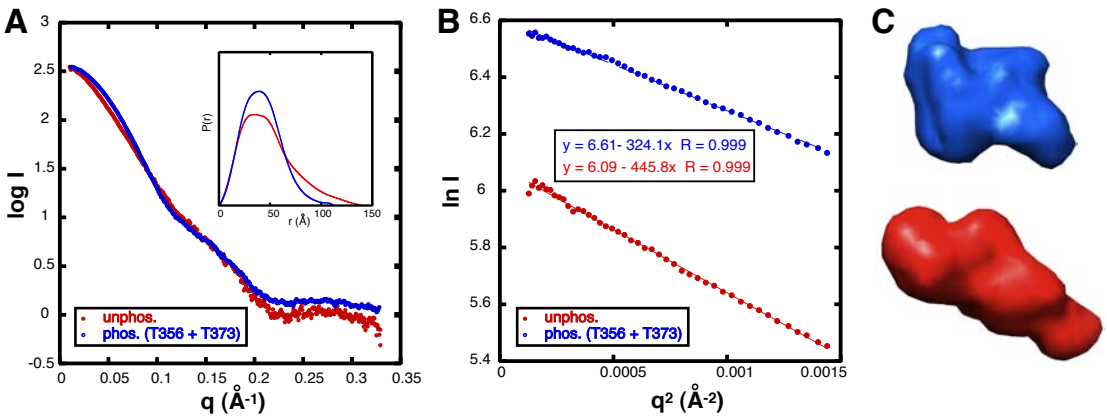

Figure 3.5. SAXS of phosphorylated vs. unphosphorylated Rb$^{53\text{-}787\Delta NL\Delta PL}$. (**A**) X-ray scattering curve and pair distribution plots for phosphorylated (blue) and unphosphorylated (red) Rb$^{53\text{-}787/\Delta NL/\Delta PL}$. The differences between these plots suggest the phosphorylated protein is more compact. (**B**) The Guinier plot is extracted from the X-ray scattering curve and indicates these proteins are not aggregated in solution. (**C**) Protein envelopes for phosphorylated Rb (blue) and unphosphorylated Rb (red), generated from GASBOR.

In leu of a detailed structural answer for *how* the domains interact, we next asked a question more suitable for SAXS: Is phosphorylation of either T356 or T373 responsible for the conformational change? For these experiments, two Rb constructs were generated, each of which contains a single phosphorylation site. Quantitive phosphate incorporation was confirmed for each construct using mass spec (data not shown). SAXS

analysis revealed that Rb which is phosphorylated only at T373 has an R_G of 31Å and a D_{max} of 108Å. When unphosphorylated, this construct has an R_G of 37Å and a D_{max} of 140Å (Figure 3.6; Table 3.3) Overall, this is very similar to the change in R_G and D_{max} observed when both T356 and T373 are present, indicating that T373 phosphorylation alone is sufficient to produce the conformational change to a “closed state”. Accordingly, SAXS analysis of the construct that contains only T356 reveals that when this protein is phosphorylated, it has an R_G of 37Å and a D_{max} of 130Å. This is almost identical to the unphosphorylated construct which has an R_G of 37Å and a D_{max} of 137Å (Figure 3.6; Table 3.3). Overall, the parameters obtained from this set of experiments indicate that phosphorylation at T356 is neither sufficient nor necessary to induce the conformational change to the “closed state”, while T373 phosphorylation is both necessary and sufficient for this effect.

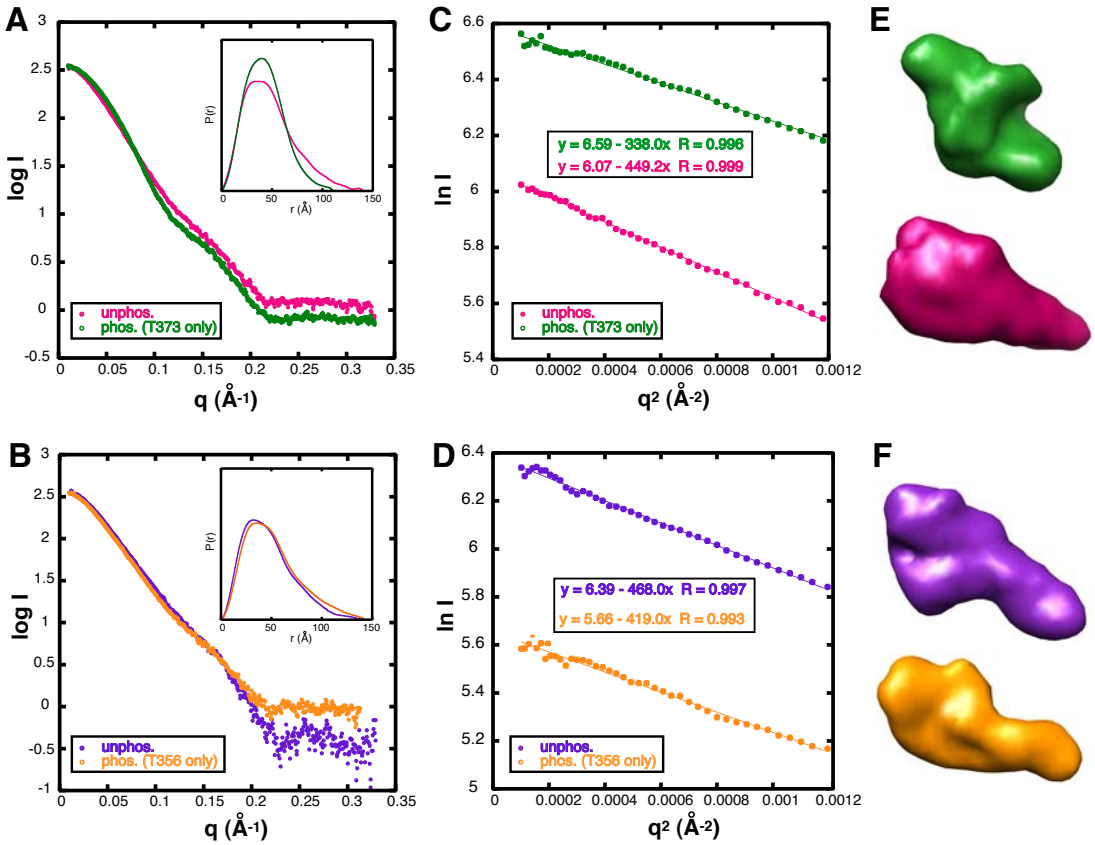

Figure 3.6. SAXS: T356 vs. T373. Each of these Rb constructs contain only a single phosphorylation site: T356 or T373. (**A-B**) X-ray scattering curve and pair distribution plot (inlay) for phosphorylated and unphosphorylated Rb. The differences in these plots suggest T373 phosphorylation causes a conformational change while T356 phosphorylation does not (compare green with orange). (**C-D**) Guinier plot analysis all proteins reveals no aggregation in the samples. (**E-F**) Protein envelopes generated from GASBOR: Rb phosphorylated at T373 (green), Rb phosphorylated at T356 (orange), and unphosphorylated Rb (magenta, purple).

Rb construct	Sites phosphorylated	R_G	D_{max}
unphos. $Rb^{53\text{-}787/\Delta NL/\Delta PL}$	-	37 Å	134 Å
phos. $Rb^{53\text{-}787/\Delta NL/\Delta PL/S780A}$	T356 T373	31 Å	110 Å
unphos. $Rb^{53\text{-}787/\Delta NL/\Delta PL/S780A/T373A}$	-	36 Å	137 Å
phos. $Rb^{53\text{-}787/\Delta NL/\Delta PL/S780A/T373A}$	T356	37 Å	130 Å
unphos. $Rb^{53\text{-}787/\Delta NL/\Delta PL/S780A/T356A}$	-	37 Å	140 Å
phos. $Rb^{53\text{-}787/\Delta NL/\Delta PL/S780A/T356A}$	T373	32 Å	108 Å

Table 3.3. SAXS parameters, R_G and D_{max} for each protein.

Prior to SAXS analysis, each singly-phosphorylated protein was purified over a SD200 and we observe that the phosphorylated proteins elute at different retention times: the protein with only T356 phosphorylated elutes faster, while the protein with T373 phosphorylated elutes slower (Figure 3.11). This difference in elution speed is a further indication that each protein has a distinct hydrodynamic radius: Specifically, Rb phosphorylated at T356 is more extended and elutes similar to unphosphorylated Rb, while Rb phosphorylated at T373 is more compact. Unlike the SAXS analysis, this is not a rigorous demonstration of the conformational change brought about by T373 phosphorylation; however, this assay is easy to perform and therefore may be useful for monitoring the effects of various drugs or peptides on the conformational state of phosphorylated Rb.

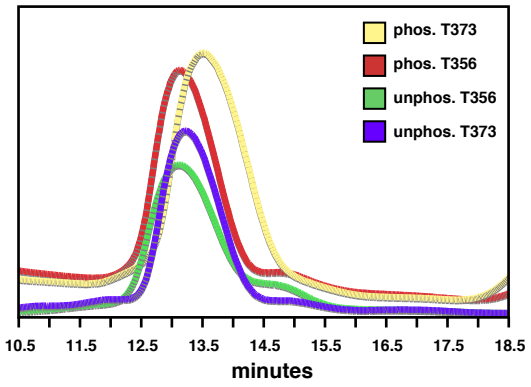

Figure 3.7. Gel-filtration analysis of SAXS proteins. Phosphorylation of Rb at T373 significantly increases its retention time when compared to unphosphorylated Rb or Rb phosphorylated at only T356.

3.2.4. Phosphorylation of Rb^{IDL} inhibits $E2F^{TD}$ binding to Rb by ITC

To confirm that the conformational change we observe upon T373 phosphorylation correlates to $E2F^{TD}$ binding inhibition, we tested the same proteins used in the SAXS experiments for $E2F^{TD}$ binding. By ITC, phosphorylation of both T356 and T373 reduces $E2F1^{TD}$ binding from K_d = 0.15 ± 0.06 µM to K_d = 6.01 ± 0.57 µM (Table 3.4, row 1-2; Figure 3.8, A-B). Rb phosphorylated at only T356 binds $E2F1^{TD}$ with a K_d = 0.32 ± 0.06 µM, while Rb phosphorylated at T373 binds $E2F1^{TD}$ with an affinity of K_d = 1.97 ± 0.99 µM (Table 3.4, row 4-5; Figure 3.8, D-E). This data indicates that phosphorylation at T373 is responsible for most of the $E2F1^{TD}$ binding inhibition caused by phosphorylation of Rb^{IDL}, while T356 alone is less significant. Analysis of this difference in terms of Gibbs free energy (ΔG) shows that T373 phosphorylation reduces the binding energy of $E2F1^{TD}$ by

approximately 1.6 Kcal/mol, while T356 phosphorylation reduces binding energy by approximately 0.4 Kcal/mol. Phosphorylation of both T356/T373 reduces the binding energy of $E2F1^{TD}$ by 2.2 Kcal/mol, indicating that both T356 and T373 contribute significantly to full inhibition of $E2F1^{TD}$ binding caused by phosphorylation of Rb^{IDL}. Interestingly, T356 inhibition of $E2F1^{TD}$ binding does not require T373 phosphorylation, therefore this independent but additive mechanism probably involves direct phosphorylated Rb^{IDL} binding at the $E2F1^{TD}$ site, as is suggested by NMR (Figure 3.2).

Five different E2F proteins have transactivation domains which bind Rb, and three of these are thought to be regulated by phosphorylation events in the cell. While structural studies have indicated the $E2F1^{TD}$-Rb pocket interaction is conserved among E2F's, nothing is known about how they might be differentially regulated by phosphorylation. We therefore tested the ability of $Rb^{53\text{-}787/\Delta NL/\Delta PL}$ phosphorylation to inhibit binding of $E2F2^{TD}$. We find that $E2F2^{TD}$ binds unphosphoryated Rb with a $K_d = 0.05 \pm 0.02$ μM; this is 3-fold tighter than $E2F1^{TD}$ binding to the same Rb construct (table 3.4, row 1&6; figure 3.8, A&F). When Rb is phosphorylated at T356/T373, $E2F2^{TD}$ binds with an affinity $K_d = 0.28 \pm 0.03$ μM, a 5-fold difference, and difference in ΔG of 1Kcal/mol (table 3.4, row 7; figure 3.8, G). Therefore, T356/T373 phosphorylation is less efficient at inhibiting $E2F2^{TD}$ binding than $E2F1^{TD}$ binding. Interestingly, this result hints that there may be key differences in the

way different E2F transactivation domains are regulated by different phosphorylation events.

	Rb construct	mutations	K_d E2F1^{TD}	panel
1	unphos. Rb$^{53\text{-}787/\ \Delta Loops}$	-	0.15 ± 0.06 μM	A
2	phos. Rb$^{53\text{-}787/\ \Delta Loops}$	-	6.01 ± 0.57 μM	B
3	phos. Rb$^{53\text{-}787/\ \Delta Loops/S780A}$	S780A	6.74 ± 1.11 μM	C
4	phos. Rb$^{53\text{-}787/\ \Delta Loops/S780A/373A}$	S780A, T373A	0.32 ± 0.06 μM	D
5	phos. Rb$^{53\text{-}787/\ \Delta Loops/S780A/356A}$	S780A, T356A	1.97 ± 0.99 μM	E
	Rb construct	mutations	K_d E2F2^{TD}	panel
6	unphos. Rb$^{53\text{-}787/\ \Delta Loops}$	-	0.05 ± 0.02 μM	F
7	phos. Rb$^{53\text{-}787/\ \Delta Loops}$	-	0.28 ± 0.03 μM	G

Table 3.4. ITC analysis of single-site Rb^{IDL} phosphorylation.

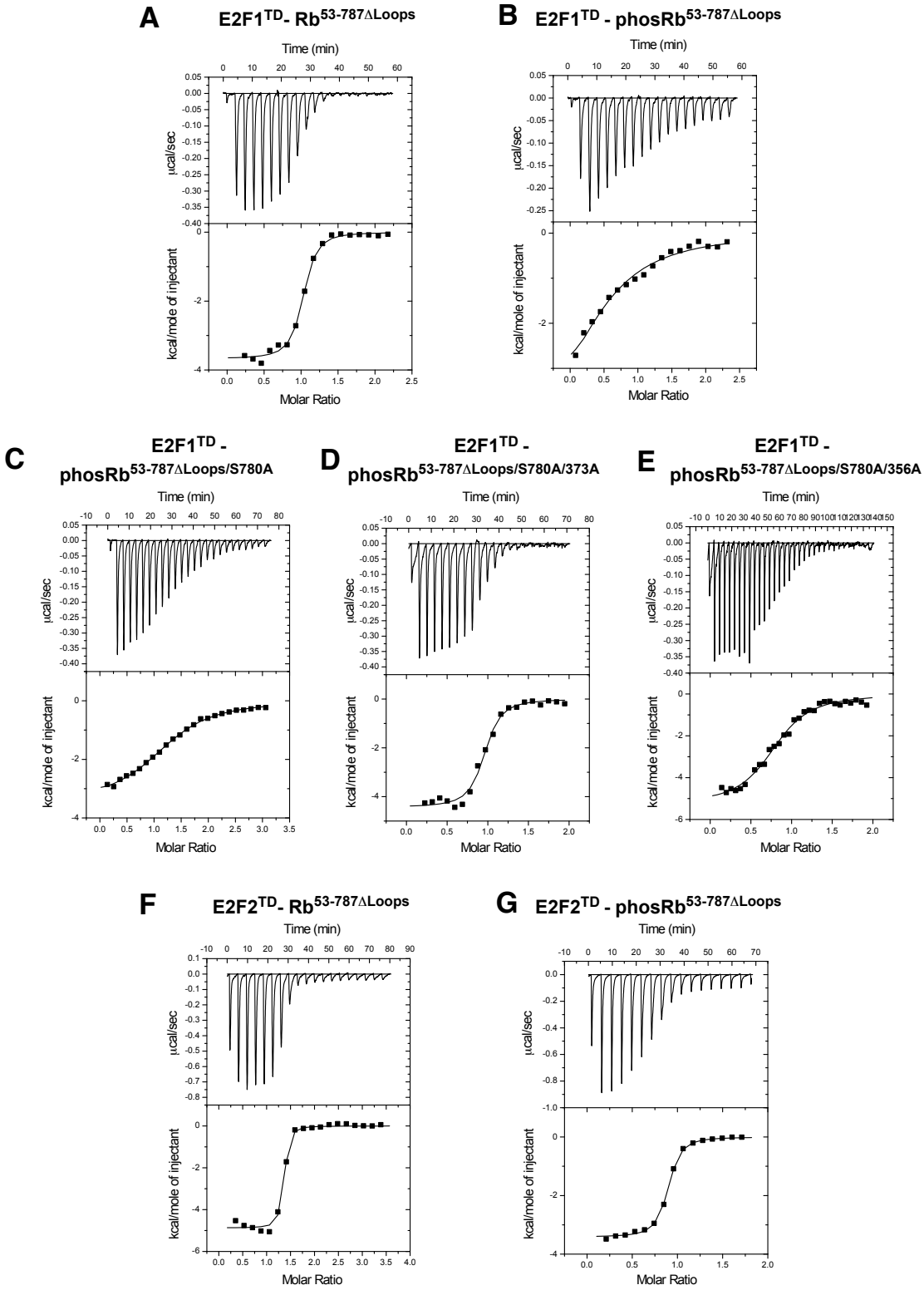

Figure 3.8. Representative ITC data presented in table 3.3.

3.2.5. 2.7 Å Crystal Structure of Rb phosphorylated at T356/T373

The ultimate goal of this research has been to crystallize Rb in its conformationally closed state. Initially we attempted to crystallize a phosphorylated SAXS protein construct ($Rb^{53\text{-}787\Delta NL/\Delta PL/S780A}$), which lacks both the Rb pocket and RbN loops; however repeated attempts to crystallize this construct proved unsuccessful. Next, we returned to the glutamate mimmic strategy and introduced T356E and T373E mutations into Rb. SAXS analysis of this glutamate mutant reveals its solution conformation is more similar to unphosphorylated Rb, and by ITC, $E2F1^{TD}$ binds with an affinity between unphosphorylated and phosphorylated wild type Rb (Figure 3.9, A-B). Therefore, unlike the crystal construct with the S608E mutation, glutamate mutations to Rb^{IDL} are semi-functional and non-crystallizable.

For our next crystallography strategy, we turned to blind luck. In an separate attempt to characterize the phosphorylation-induced domain interaction, we introduced two point mutations to a conserved surface of RbN: K289A and Y292A. While these point mutations did not have the intended effect of disrupting the phosphorylation-induced conformational change or reducing the inhibition of $E2F1^{TD}$ binding, strangely, they allowed the protein to crystallize (figure 3.9, C-D). Through the subsequent optimization of these crystallization conditions, we were able to obtain good-quality crystals of phosphorylated $Rb^{53\text{-}787\Delta NL/\Delta PL/K289A/Y292A/S780A}$, hereafter denoted as $Rb^{N\text{-}}$

P(Figure 3.10). The structure was solved to 2.7 angstroms using both the pocket domain and N-terminal domain structures as molecular replacement search models (Balog et al. 2010; Hassler et al. 2007)

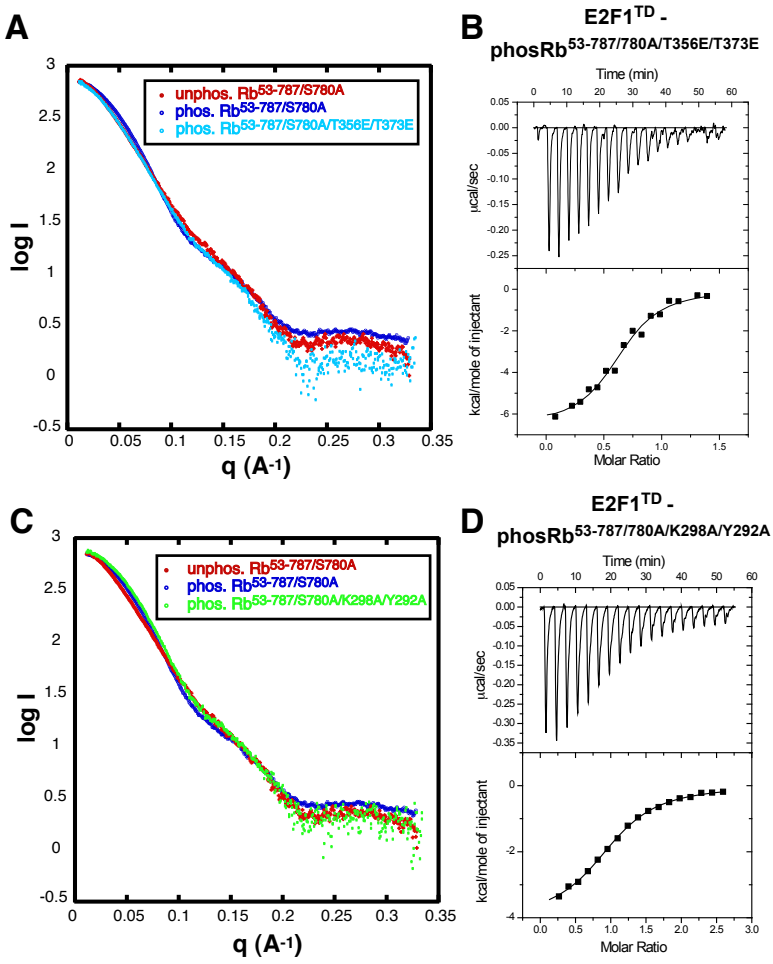

Figure 3.9. Functional characterization of Rb pocket-RbN crystallography constructs. (A) The X-ray scattering curve for $Rb^{53\text{-}787\Delta NL/\Delta PL/T356E/T373E/S780A}$ is more linear in its initial slope and signal intensity decay features to unphosphorylated $Rb^{53\text{-}787\Delta NL/\Delta PL/S780A}$. (**B**) $E2F1^{TD}$ binds $Rb^{53\text{-}787\Delta NL/\Delta PL/T356E/T373E/S780A}$ with an affinity of $K_d = 0.82 \pm 0.22$ µM. (**C**) SAXS analysis of phosphorylated $Rb^{53\text{-}787\Delta NL/\Delta PL/K289A/Y292A/S780A}$ reveals a similar conformation in solution to phosphorylated $Rb^{53\text{-}787\Delta NL/\Delta PL/S780A}$. (**D**) $E2F1^{TD}$ binds to phosphorylated $Rb^{53\text{-}787\Delta NL/\Delta PL/K289A/Y292A/S780A}$ with an affinity of $K_d = 0.6 \pm 0.1$ µM, which is similar to phosphorylated $Rb^{53\text{-}787\Delta NL/\Delta PL/S780A}$.

Figure 3.10. Crystals of phosphorylated $Rb^{N\text{-}P}$.

Data collection	
Beamline	APS 23-ID-B
Space group	$P2_12_12_1$
Cell dimensions: a, b, c (Å)	51.62, 129.51, 135.04
Cell dimensions: α, β, γ (°)	90, 90, 90
Resolution (Å)	58 - 2.7
R_{pim}	5.9 (31.0)
I / σ^I	8.2 (2.3)
Completeness (%)	92.3 (90.0)
Redundancy	4.9 (5.0)
Refinement	
Resolution (Å)	58 - 2.7
No. reflections	23354
R_{work} / R_{free}	21.2 / 26.6
No. atoms: protein	4851
No. atoms: water	57
R.M.S.D. bond lengths (Å)	0.004
R.M.S.D. bond angles (°)	0.9
Average B-factor: protein ($Å^2$)	62.1
Ramachandran analysis (%)	
Preferred	95.0
Allowed	4.7
Outliers	0.3

Table 3.5. Data collection and refinement statistics.

The crystal structure of Rb^{N-P}, phosphorylated at T356 and T373, reveals a "closed" conformation and two distinct inter-domain binding interfaces between the pocket and N-terminal domains (Figure 3.11, A). The overall structures of the individual domains are similar to their structures observed in isolation; both contain two subdomains composed primarily of helical cyclin folds (Lee et al. 1998; Hassler et al. 2007). The larger binding interface is between subdomain B of the N-terminal domain (RbN) and subdomain A of pocket domain, and buries 2277$Å^2$ of surface area. At this interface, helix αP1 of the pocket domain adopts two extra turns at its N-terminus relative to other pocket structures; this bridges the RbN and pocket domains (figure 3.12). The phosphate group at T373 stabilizes this conformation of helix αP1 through an N-terminal capping interaction, in which phosphate oxygens O2 and O3 serve as in-plane h-bond acceptors to backbone amide protons from R376 and V375, respectively (Figure 3.11, B). In addition, O2 at phosphate T373 forms an inter-domain hydrogen bond with sidechain K164 (αN6). Helix αP1 is also amphipathic and forms a hydrophobic interface that spans both the RbN and pocket domains (Figure 3.11, B). As part of this interface, the sidechains of residues V375 and M379 of helix αP1 pack within a groove formed by residues L212, V213 and F216 of RbN helix αN8, and residue L161 of RbN helix αN6. This highly-conserved patch of hydrophobic residues was previously suggested to constitute a protein interaction surface in RbN (Hassler et al. 2007). The C-terminal half

of the aP1 helix packs against the pocket domain via a hydrophobic interface that consists of residues I382 and L385 of helix αP1, which pack against V494, T497, and Y498 of pocket helix αP8. Additional stabilizing features of helix αP1 are the sidechain-mainchain hydrogen bonds formed between the sidechain of Q383 (αP1) and the mainchain carbonyl of E282 (RbN), and T381 (αP1) and the mainchain carbonyl of T497 (αP6). Additional hydrogen bond and polar contacts exist at this interface that don't involve helix αP1, but contribute to the overall buried surface area. In sum, T373 phosphorylation lengthens helix αP1 two turns and positions it to form an interface with RbN, holding both domains in the docked conformation.

A second interdomain interface is between pocket subdomain B and RbN subdomain A (Figure 3.11, C). This smaller interface (387Å^2 buried surface area) is formed exclusively by polar contacts from highly-conserved residues. Q736 from the pocket makes a side chain hydrogen bond with D145; the latter reaches the interface from the N-terminal end of the RbN-bridging helix aN6. K740 makes a hydrogen bond with the backbone carbonyl T140 and a salt bridge with D139 in RbN. Notably, K740 is 3.7 angstroms from D139 in the structure, but seems well placed to make a salt bridge with either D139 or D145, depending on its rotation. K740 is part of the previously identified ‘‘lysine patch,’’ a set of conserved lysine residues in pocket subdomain B thought to play a role in binding phosphorylated RbC (Brown et al. 2002; Harbour et al. 1999; Rubin et al. 2005; Singh et al. 2005).

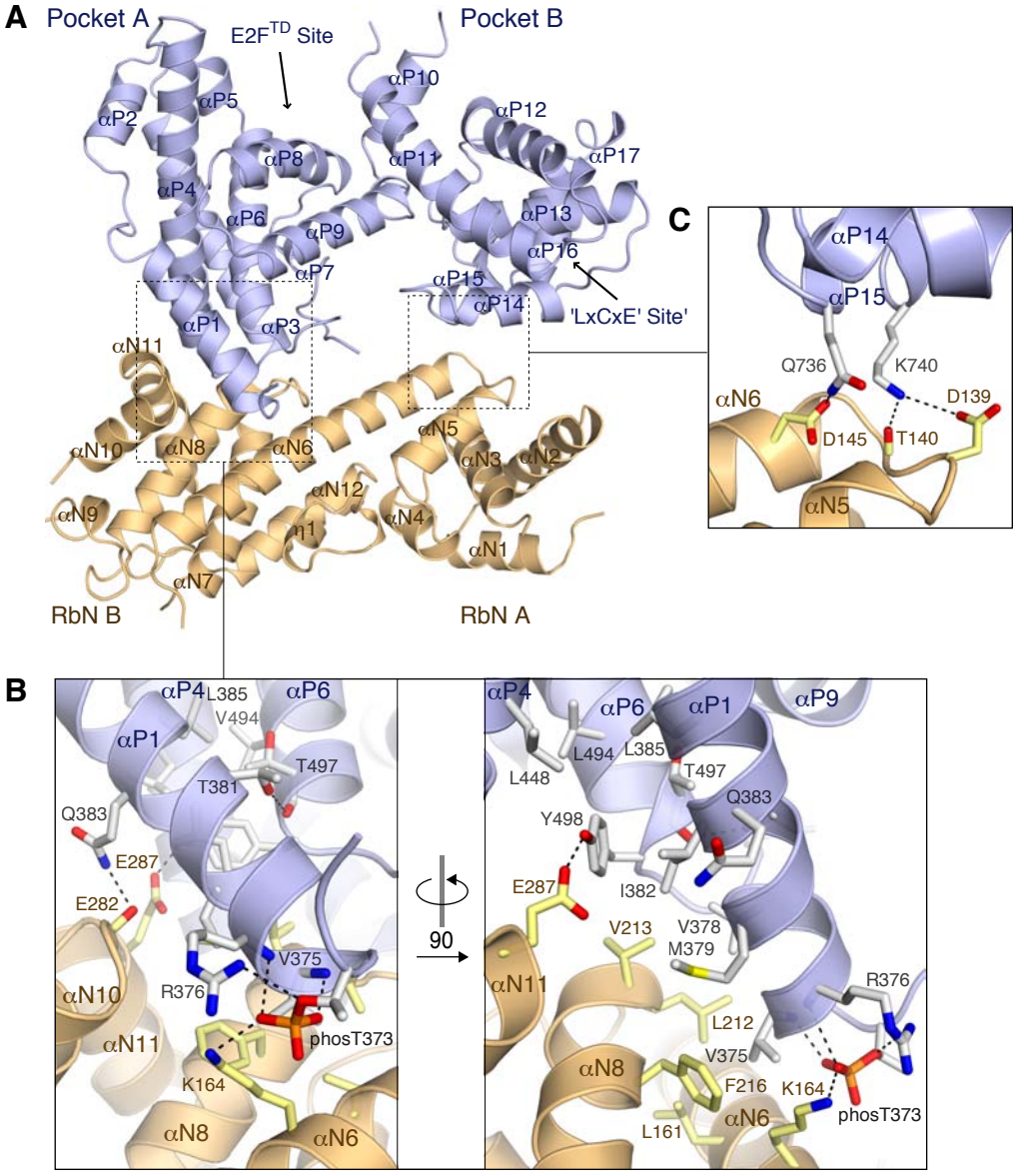

Figure 3.11. Structure of the phosphorylated RbN–pocket complex. (**A**) Overall structure of $Rb^{N–P}$. RbN and the pocket domain are colored gold and blue, respectively. (**B**) The larger interface between pocket subdomain A and RbN subdomain B is mediated by T373 phosphorylation. Phosphothreonine 373 directly contacts K164 and orders the two N-terminal turns of helix αP1, which form a hydrophobic interface with RbN. (**C**) The smaller interface between pocket subdomain B and RbN subdomain A is mediated by pocket residues Q736 and K740.

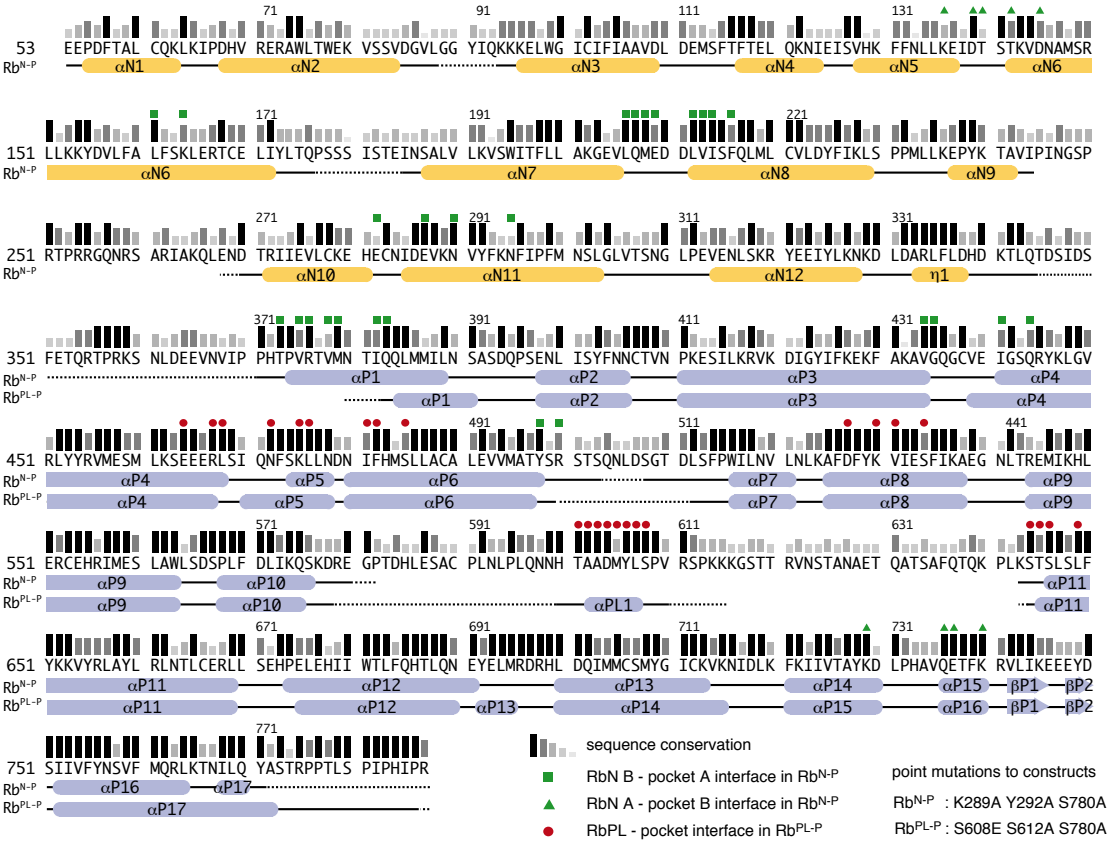

Figure 3.12. Summary of Rb crystal structures and inter-domain interactions. Rb sequence conservation (grey bars) and secondary structure analysis are shown. The bottom secondary structure markings are assigned from the Rb^{PL-P} structure (chapter 2), and the top markings are assigned from the Rb^{N-P} structure. Residues that make inter-domain contacts in each crystal structure are indicated. The degree of sequence conservation is based on alignment of the human, mouse, chicken, frog, and zebrafish sequences.

Electron density corresponding to phosphorylated T356 is not present in the Rb^{N-P} crystal structure solution. Additionally, helix αN13, which is formed by residues 347-354 in the structure of the N-terminal domain alone, is not present here (Figure 3.12; Hassler et al. 2007). One possible explanation for the disordering of helix αN13 is that phosphorylation at T356

has a destabilizing effect at its negative, C-terminal dipole, similar to the way in which phosphorylation at T373 stabilizes the positive dipole at the N-terminus of helix αP1. Indeed, studies have shown that post-translational phosphorylation does have a general stabilizing effect a the N-terminus of an alpha helix and a destabilizing effect at the C-terminus of an alpha helix (Andrew et al. 2002). Additionally, many examples of phosphorylation-induced order to disorder transitions in proteins have been characterized (Wright and Dyson 2009). The functional importance of such a transition for T356 is not crystal clear; however, one might speculate that it is allows for the extended flexibility in Rb^{IDL} so it may directly inhibit binding at the $E2F^{TD}$ site. Accordingly, our NMR studies confirm that a peptide of phosphorylated $Rb^{IDL(338-377)}$ binds to Rb pocket in a phosphorylation-dependent manner that overlaps with $E2F^{TD}$ binding (Figure 3.2). Significantly, T356 phosphorylation alone inhibits $E2F1^{TD}$ binding by ITC, albeit minimally (Table 3.4, rows 1&4). Therefore it is possible that destabilization of helix αN13 by T356 phosphorylation is part of a mechanism that contributes to inhibition of $E2F^{TD}$ binding to Rb pocket. On the other hand, there are several features of helix αN13 in the original N-terminal domain structure that bring in to question its legitimacy (Hassler et al. 2007). Notably, helix αN13 is extensively involved in crystal contacts; it has significantly higher b-factors than the rest of the protein; and the fit of helix αN13 into the electron density map provided to the PDB is questionable. Therefore it is possible that helix αN13 is a

crystallography artifact in the original structure, which is why we don't see electron density for it in the Rb^{N-P} structure.

One final nagging detail of the Rb^{N-P} structure is: why are the K289A/Y292A mutations necessary for crystallization? The practice of making point mutations to surface residues is not an uncommon strategy for obtaining protein crystals or improving crystal hits. In fact, studies have shown that specifically replacing a key flexible lysine with an alanine can itself be an effective strategy for producing hits (Dale et al. 2003). Analysis of the crystal contacts in the Rb^{N-P} structure reveals a symmetry mate that is close to-but not directly contacting-the surface created by the alanines, 289 and 292. This symmetry mate has a near-by lysine-rich loop (residues 713-722) that may feel the effects of electrostatic repulsion from wild-type K289, which suggests the presence of wild-type K289 may prevent the formation of this critical crystal contact.

3.2.6. Phosphorylation at T373 inhibits $E2F1^{TD}$ binding through a unique allosteric mechanism

Upon observing the initial molecular replacement solution for the Rb^{N-P} structure, we were alarmed to find that RbN and $E2F^{TD}$ each bind an opposite face of Rb pocket (Figure 3.11, A). This immediately ruled out the possibility we had been entertaining all along: that RbN directly competes with $E2F^{TD}$ for binding. To explore the new possibility of an allosteric mechanism, we used

the program “DynDom” to compare the pocket domain in the $Rb^{N\text{-}P}$ structure to the pocket domain in the structure of Rb bound to $E2F^{TD}$ (Hayward and Berendsen 1998). Through DynDom, we find a relative 9.6° rotation of the pocket A and B subdomains about a central axis. To better visualize how this structural change is inconsistent with tight $E2F1^{TD}$ binding, we aligned the A subdomains of $Rb^{N–P}$ and the pocket–$E2F^{TD}$ structure (Figure 3.13, A). In this alignment, contacts between $E2F^{TD}$ and residues in the pocket A subdomain of $Rb^{N–P}$ can be maintained; however, distances to key residues in the B subdomain are too far for proper binding. We chose this example of $E2F^{TD}$ binding to illustrate our point because $E2F^{TD}$ makes extensive contacts to the A subdomain, but relatively few contacts to the B subdomain (Lee et al. 2002). Therefore upon changing the relative orientation of the subdomains, it makes sense that $E2F^{TD}$ would maintain its contacts with the A subdomain and break its contacts with the B subdomain. The most prominent change in this model of how $E2F^{TD}$ might interact more weakly with $Rb^{N–P}$, is that the alpha carbon of K652 is translated 2.5 angstroms away from its position in the pocket–$E2F^{TD}$ structure; therefore, K652 is too distant to make the salt bridge with E417 of $E2F^{TD}$ (Figure 3.13, B). Significantly, mutation of K652 to a glutamine, which is charge neutral, reduces binding of $E2F1^{TD}$ 20-fold (Figure 3.13, C). This mutation corresponds to an approximate 2 Kcal/mol change in the binding energy (ΔG) between Rb and $E2F1^{TD}$, which is similar to the reduction in binding energy that is observed by phosphorylating T373 alone

(1.6 Kcal/mol). Therefore this work suggests that the allosteric mechanism brought about by T373 phosphorylation ultimately disrupts a single critical salt bridge to profoundly weaken binding between E2F1^{TD} and Rb pocket.

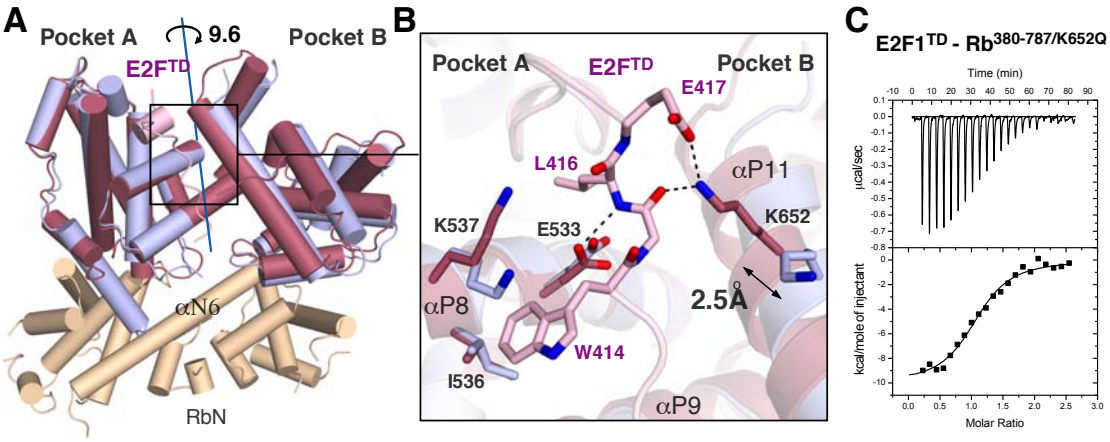

Figure 3.13. Structural change in the pocket domain induced by RbN binding and its effect on the E2F^{TD} binding site. (**A**) Structural comparison of Rb$^{N–P}$ (gold and blue) with the E2F^{TD}-bound pocket domain (red, PDB: 1N4M), generated by aligning the pocket subdomain A of each structure. The pocket subdomain B of Rb$^{N–P}$ is rotated by 9.6° about a central axis (blue)relative to the E2F^{TD}–pocket subdomain B. (**B**) Close-up of the E2F^{TD}-binding cleft in the same structural alignment as in A. The subdomain orientation induced by RbN docking is incompatible with optimal E2F^{TD} binding. For example, in this alignment, pocket A residues (E533, I536, and K537) can contact E2F^{TD}, but the position of K652 in subdomain B of Rb$^{N–P}$ is too distant. (**C**) E2F1^{TD} binds to Rb$^{380-787/K652Q}$ with a K_d = 1.94 ± 0.81 µM. This is comparable to the binding affinity between E2F1^{TD} and Rb singly-phosphorylated at T373 (K_d = 1.97 ± 0.99 µM).

The Rb$^{N–P}$ structure reveals additional important features that are critical for the observed rotation of the pocket subdomains and the allosteric inhibition of E2F^{TD} binding. First, RbN subdomains are in a fixed orientation relative to one another due to the presence of a rigid domain-spanning helix, αN6 (Figure 3.13, A). By comparison, there are no obvious structural barriers

to subdomain rotation in the pocket domain, other than when it is bound to RbN (Figure 3.11; Hassler et al. 2007). A second structural feature critical for this mechanism is the presence of highly-conserved residues on each end of the bridging RbN helix; these RbN residues make distinct, simultaneous contacts with each pocket subdomain in order to form the two interfaces that serve to constrain the pocket subdomain geometry and thereby "open" the $E2F^{TD}$ binding cleft. To add experimental support to this proposed allosteric mechanism, we rationalized that it would be easiest to disrupt the minimal contacts at the smaller interface between pocket subdomain B and RbN subdomain A by making a point mutation to the single salt bridge at this interface. In the presence of this mutation, we expect that T373 phosphorylation will still promote domain docking to form the large interface; however, without the small interface intact, the subdomains of the pocket are free to rotate, thus the pocket can bind $E2F^{TD}$ with an affinity similar to unphosphorylated Rb (Figure 3.14, A). When we test this theory using an Rb construct with two mutations to the small interface (K740A/Q736A), we find that T356/T373 phosphorylation only weakly inhibits $E2F^{TD}$ binding to Rb; proportional to the effect of phosphorylating T356 alone (Figure 3.14, B-C; compare to Table 3.4, row 4). Importantly, mass spec was used to confirm full phosphorylation of this construct (Figure 3.14, D). This set of experiments indicates that K740/Q736 are necessary to maintain the small interface, although, they may not be sufficient for this role; there are additional inter-

domain hydrogen bonds, polar contacts and charge-dipole interactions at this interface that are undoubtably important to stabilize it beyond just one salt bridge and hydrogen bond. In summary, these experiments confirm that both interfaces are necessary for the inhibition of $E2F^{TD}$ binding that results from T373 phosphorylation. Furthermore, these experiments add much-needed support to our proposed allosteric mechanism.

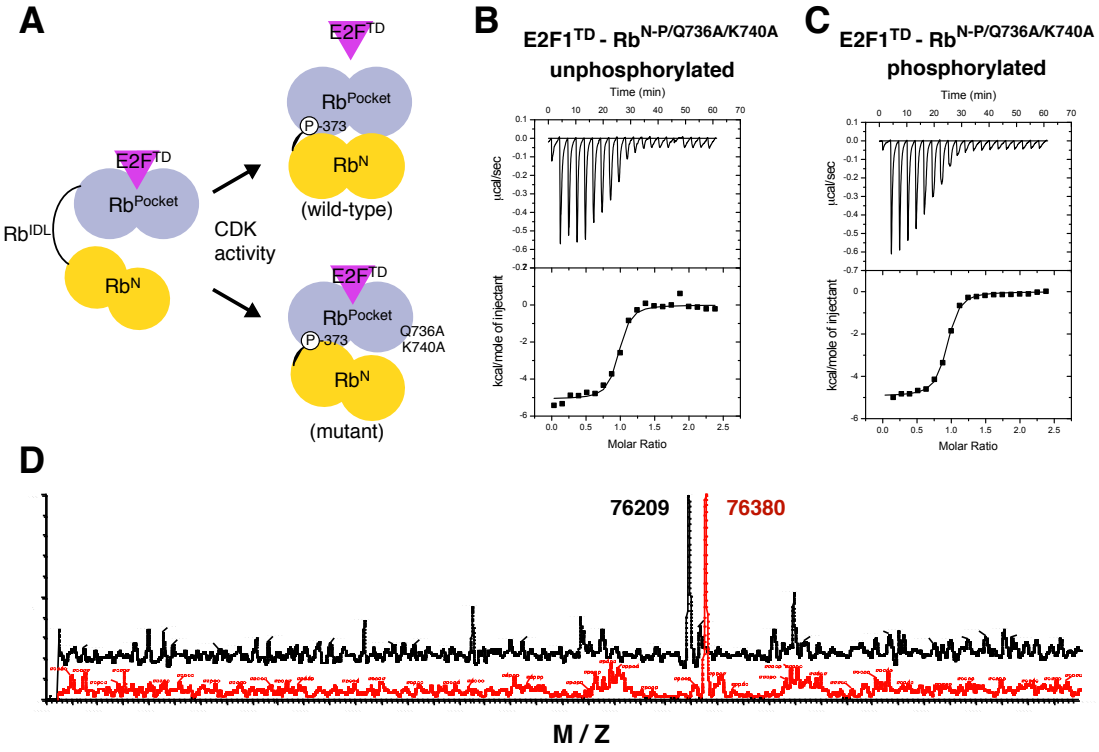

Figure 3.14. Mutations to the small interface abrogate the effect of T373 phosphorylation. (**A**) Model of the effect of Q736A/K740A mutations on $E2F^{TD}$ binding to Rb phosphorylated at T356/T373. (**B**) $E2F1^{TD}$ binding to unphosphorylated $Rb^{53\text{-}787/\Delta NL/\Delta PL/Q736A/K740A/S780A}$: $K_d = 0.15 \pm 0.81$ µM. (**C**) $E2F1^{TD}$ binding to phosphorylated $Rb^{53\text{-}787/\Delta NL/\Delta PL/Q736A/K740A/S780A}$: $K_d = 0.29 \pm 0.10$ µM (for comparison, $E2F1^{TD}$ binding to phosphorylated $Rb^{N\text{-}P}$: $K_d = 6.01 \pm 0.57$ µM; $E2F1^{TD}$ binding to phosphorylated $Rb^{53\text{-}787/\ \Delta Loops/S780A/373A}$: $K_d = 0.32 \pm 0.06$ µM). (**D**) Mass spectrometry of unphosphorylated (black) and

phosphorylated (red) $Rb^{53\text{-}787/\Delta NL/\Delta PL/Q736A/K740A/S780A}$. A change in the mass of approximately 160 A.M.U. is proportional to the addition of two phosphates.

3.2.7. LxCxE binding is modulated by phosphorylation of T373

The structure of $Rb^{N\text{-}P}$ reveals that the smaller interface between RbN and Rb pocket is proximal to the "LxCxE-binding site". We therefore wondered whether phosphorylation of Rb disrupts binding of a peptide containing a LxCxE sequence. For this assay we used the E7 peptide from HPV-18. This peptide was also used in the first crystal structure of Rb pocket (Lee et al, 1998). $E7^{LxCxE}$ binds to unphosphorylated $Rb^{53\text{-}787/\Delta NL/\Delta PL/S780A}$ with a K_d = 120 ± 60 nM; this is consistent with a previously-reported affinity of $E7^{LxCxE}$ for the pocket domain alone (Figure 3.15, A; Lee et al. 1998). When Rb $Rb^{53\text{-}787/\Delta NL/\Delta PL/S780A}$ is phosphorylated, we find $E7^{LxCxE}$ binds with an 8-fold weaker affinity of K_d = 860 ± 200 nM (Figure 3.15, B). This moderate change in affinity indicates the conformational change that is driven by T373 phosphorylation does somehow occlude a portion of the $E7^{LxCxE}$ binding site, although its not clear from the structure of $Rb^{N\text{-}P}$ exactly how this happens. Notably, a conserved "lysine patch" sits right next to the "LxCxE-binding site"; this is also important for viral peptide binding, as many LxCxE sequences are adjacent to a string of conserved glutamates (Brown et al. 2002; Felsani et al. 2006). This lysine patch is clearly regulated by T373 phosphorylation, and includes many conserved lysine residues at, and around, the small inter-domain interface. However, the 8-residue LxCxE peptide we used in our

study does not contain the glutamate sequence; therefore, its likely that our assay is missing a more significant regulation of viral peptide binding to this lysine patch.

Rb is deregulation through hyperphosphorylation is a common feature of cancer, and drug discovery efforts to target this pathway generally focus on small molecule inhibitors of cyclin dependent kinases. Our study in to the role of T373 phosphorylation indicates a new way in which hyperphosphorylated Rb itself may be targeted to re-gain its critical $E2F^{TD}$-binding function. Previously, we were able to show that simple mutations to the small inter-domain interface allow Rb to re-bind $E2F^{TD}$ even though its phosphorylated at T373. Additionally, binding of an LxCxE peptide to Rb is disrupted by the formation of this same small inter-domain interface. Therefore, we reasoned that an LxCxE peptide can disrupt this interface when Rb is phosphorylated at T373, so to cause Rb to re-bind $E2F^{TD}$ (Figure 3.15, D). To explore this hypothesis, we measure the binding affinity of $E2F1^{TD}$ for phosphorylated $Rb^{53\text{-}787\Delta NL/\Delta PL/S780A}$-already bound to $E7^{LxCxE}$- and find that $E2F1^{TD}$ binds with a K_d = 700 ± 200 nM (figure 3.15, C). This binding affinity is about 8-fold stronger than the affinity we measure between $E2F1^{TD}$ and phosphorylated $Rb^{53\text{-}787\Delta NL/\Delta PL/S780A}$, and 5-fold weaker than the affinity we measure between $E2F1^{TD}$ and unphosphorylated $Rb^{53\text{-}787\Delta NL/\Delta PL/S780A}$. Clearly, there is room to improve the $E7^{LxCxE}$ peptide so to better disrupt the small inter-domain interface and therefore cause $E2F^{TD}$ to bind phosphorylated Rb more

efficiently. One obvious strategy is to use a longer version of the $E7^{LxCxE}$ peptide that includes conserved glutamic acid residues to bind the “lysine patch”. Accordingly, K740 is part of this group of conserved lysine residues and is also a necessary element for the inter-domain binding interaction that contributes to the release of $E2F^{TD}$; therefore a $E7^{LxCxE}$ peptide that interacts strongly with K740 would probably be highly effective in causing phosphorylated Rb to re-bind $E2F^{TD}$. Finally, it is notable that this potential “drug” singly targets T373 phosphorylation out of the many phosphorylation events that potentially contribute to the regulation of Rb. Studies have shown that phosphorylation of T373 alone is both necessary and sufficient to fully activate E2F in cells (Lents et al. 2006). Additionally, it has been suggested that T373 phosphorylation is sort of a “master switch” for E2F regulation and cell cycle progression (Gorges et al. 2008). Therefore, targeting the effect of T373 phosphorylation might be sufficient to slow or stop the growth of cancers which exploit hyperphosphorylated Rb.

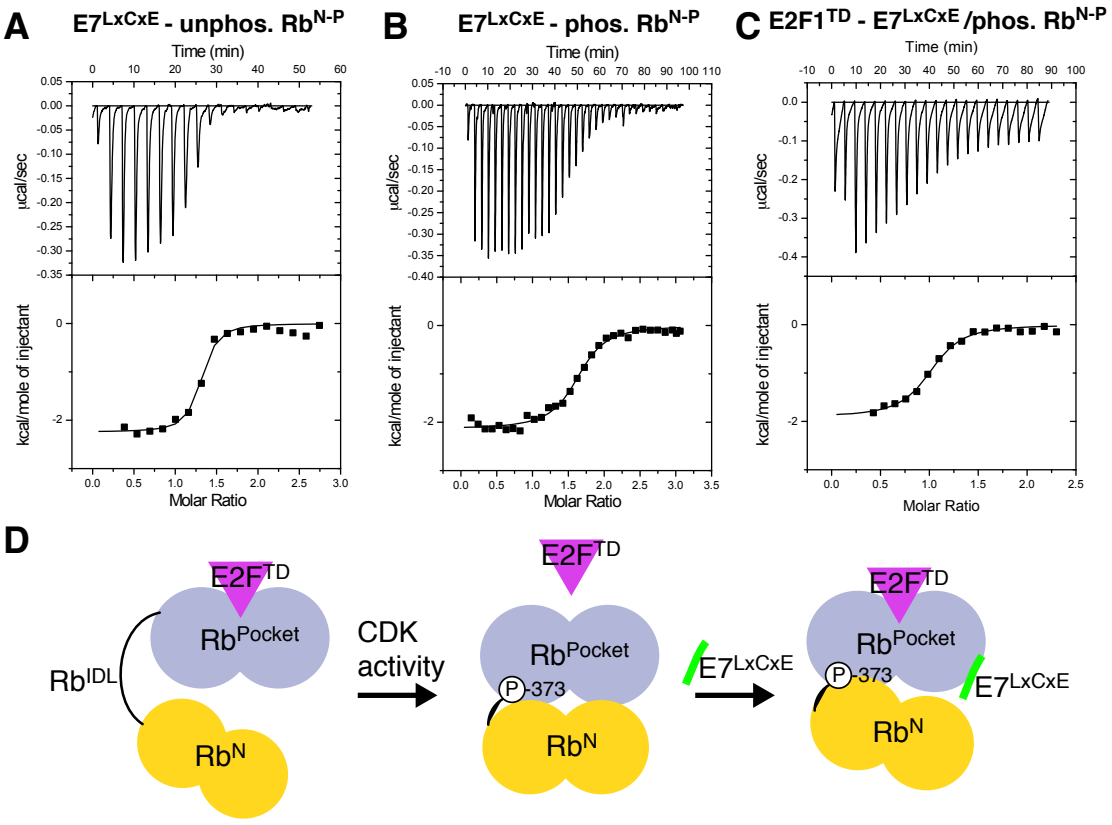

Figure 3.15. LxCxE binding is inhibited by phosphorylation of Rb^{N-P}. (**A**) $E7^{LxCxE}$ binds to unphosphorylated $Rb^{53\text{-}787\Delta NL/\Delta PL/S780A}$ with an affinity of K_d = 0.12 ± 0.06 µM. (**B**) $E7^{LxCxE}$ binds to phosphorylated $Rb^{53\text{-}787\Delta NL/\Delta PL/S780A}$ with an affinity of K_d = 0.8 ± 0.2 µM. (**C**) Phosphorylated $Rb^{53\text{-}787\Delta NL/\Delta PL/S780A}$ pre-bound to three molar equivalents of $E7^{LxCxE}$, binds $E2F1^{TD}$ with an affinity of K_d = 0.7 ± 0.2 µM, which is 9-fold tighter than when $E7^{LxCxE}$ is absent. (**D**) Model of how $E7^{LxCxE}$ inhibits the allosteric mechanism promoted by T373, through the disruption of the small Rb pocket-RbN interface.

3.2.8. Crystallography of phosphorylated RbN

The role of RbN in $E2F^{TD}$ binding regulation may seem definitive, however, additional roles for this structured domain have been suggested. Several independent research papers have proposed a variety of proteins, many of which are involved in transcription, directly bind to the N-terminal

domain (Hassler et al. 2007). On RbN, one conserved surface was previously identified which we now know is not involved in Rb pocket binding (Hassler et al. 2007). This surface consists of highly-conserved residues 332-343, and sits a cleft between the RbN subdomains. While phosphorylation of Rb^{NL} (S249/T252) has never been suggested to regulate an interaction at this surface, the many structural similarities between RbN and Rb pocket make it seem like a possibility. From NMR studies, we know that Rb^{NL} is a flexible loop when it is unphosphorylated (Figure 3.3). When we use SAXS to look for a conformational change upon phosphorylation, we find that phosphorylated RbN is more compact, indicating an association between phosphorylated Rb^{NL} and RbN (Figure 3.16, A). We next endeavored to crystallize the phosphorylated version of this protein and were able to obtain an initial hit, although it has been difficult to reproduce these crystals outside of the original broad screen (Figure 3.16, B-C). One possible reason for this is that RbN is relatively difficult to phosphorylate quantitatively (Figure 3.16, D). It is also possible there is something peculiar about the reagents in the broad screen condition that make it difficult to accurately reproduce. Optimization around the original hit has produced a similar hit condition, but this has also been difficult to reproduce (Figure 3.16, E).

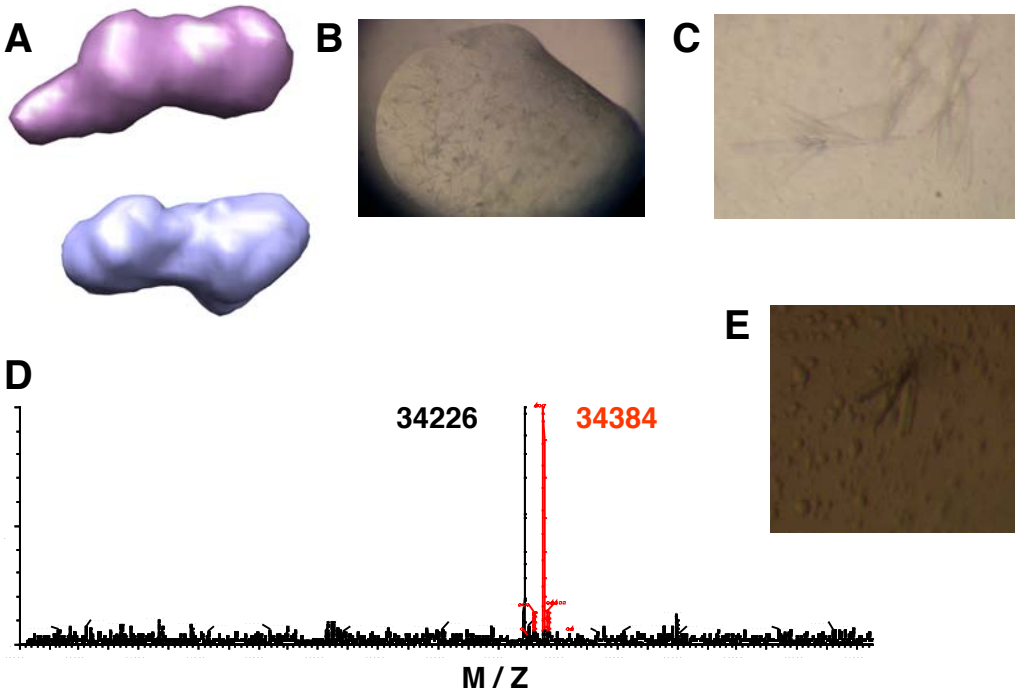

Figure 3.16. Structural studies of phosphorylated RbN. (**A**) GASBOR envelopes generated from SAXS data on unphosphorylated RbN^{53-345} (purple) and phosphorylated RbN^{53-345} (blue). (**B**). Crystals of phosphorylated RbN^{53-345} grow in 1 week in 20% PEG3350 and 0.2M AmI (**C**) Close up of crystals grown in the same condition. (**D**) Phosphorylation of N12 using K2A results in a mass that suggests the incorporation of of two phosphates. (**E**) Crystals which grew after 1 month in a similar condition to the original hit: 18% PEG2000 and 0.2M AmI.

3.3. Discussion

The results presented in this chapter reveal that Rb, phosphorylated at T373, dramatically inhibits $E2F^{TD}$ binding to Rb pocket through a large-scale conformational change which brings together the pocket and RbN domains. Despite this extensive inter-domain binding interface, the nature of $E2F^{TD}$ binding inhibition turns out to be allosteric. This chapter also describes how T356 phosphorylation has a small but distinct role in regulating $E2F^{TD}$ binding

to Rb pocket, although the molecular details of this interaction remain unknown.

3.3.1. T356/T373 phosphorylation in cell-based studies

Our results correlate well with several cell-based studies. T356 phosphorylation alone can promote partial E2F activity in a transcription reporter assay (Gorges et al. 2008). T373 phosphorylation is both necessary and sufficient to activate E2F transcription and progress cells from G_1 to S phase (Lents et al. 2006). Separate cell-based work suggests that T356 and T373 phosphorylation are both targets of CDK4-cyclinD, which indicates they are probably early phosphorylation events in Rb's cascade of deactivating phosphorylations (Gorges et al. 2008; Zarkowska et al. 1997). In support of this theory, removal of a cyclinD binding motif from RbC results in impaired phosphorylation of T373 (Gorges et al. 2008; Grafstrom et al. 2001).

Uniquely, we find that the allosteric mechanism resulting from T373 phosphorylation requires docking of RbN to the conserved "lysine patch" on Rb pocket subdomain B. This lysine patch has been suggested to be critical for HDAC binding, and alternatively, dispensable for HDAC binding (Brown et al. 2002; Dick et al. 2000; Harbour and Dean 1999; Signh et al. 2005). The lysine patch has also been suggested to be important for the phosphorylation-dependent RbC interaction at the LxCxE binding site (Harbour and Dean 1999; Lee et al. 1998; Rubin et al. 2005). While this seems probable, the

requirement of these lysine residues for this specific interaction has not been demonstrated. In light of our findings, we propose that several of these lysine residues are highly-conserved because they are important for the RbN-Rb pocket small interface. Specifically, K740 is involved in a salt-bridge that is critical for the integrity of this interface. Additionally, both K729 and K722 are positioned closely to the small interface so to promote charge stabilization, inter-domain docking and coordinate hydrogen bonding across the interface. An electron density feature corresponding to two or three water molecules is visible at the smaller RbN–pocket interface in Rb^{N-P}. While we had difficulty refining water at this site, perhaps due to heterogeneity in the precise water geometry throughout the crystal, it is apparent that ordered solvent is also an important feature of this interface. One study used cell-based methods to probe the role of the lysine patch in binding and regulating E2F. In this study, 5 highly-conserved lysine residues were mutated to alanine residues in murine Rb. These mutations correspond to the human residues: K720, K722, K729, K740 and K765. While this Rb construct is able to bind E2F similar to wild-type, when it is phosphorylated it is deficient for E2F release and activation in a reporter assay. At the time of this study, the authors clearly had no knowledge of our proposed T373-mediated allosteric mechanism for $E2F^{TD}$ release, therefore, they attributed this lack of E2F activity to the failure of the phosphorylated RbC (T821/T826) - pocket interaction to displace E2F. While this explanation makes sense, T373 is clearly more important for E2F release

and therefore would better explain the potent effect of these lysine mutations. However, since this study did use 5 lysine to alanine mutations, it is unfortunately impossible to know exactly which mutations were responsible for the effect. In summary, this study is an indication that our proposed allosteric mechanism is valid within the context of the living cell.

3.3.2. The interplay of different phosphorylation sites

As we begin to understand the details of how phosphorylation regulates Rb-E2F complexes, it is interesting to consider the functional interplay between different phosphorylation events. In this chapter, we show that T373 alone has a major role in dissociating Rb-E2F complexes, while T356 alone has a relatively minor role. Our ITC studies indicate that these roles seem to be independent but additive for inhibiting Rb-E2F^{TD} complexes. In chapter 2, we describe the roles of S608 and S612 phosphorylation in dissociating Rb-E2F^{TD} complexes. In that case, we find that these closely-spaced events seem exclusive in regulating Rb-E2F^{TD}, such that phosphorylation of S608 has a much greater effect than phosphorylation of S612, and together there is no added effect. Thus, when taken together we can say that both S612 and T356 each have minor effects, while S608 and T373 each have major effects. Work in our lab also shows that these sets of sites (T356/T373 and S608/S612) together have an additive effect in inhibiting Rb-E2F1^{TD}. Using ITC, we find that Rb$^{55\text{-}787}$ with either T356/T373

or S608/S612 inhibits E2F1^{TD} binding about 10-fold (Burke et al. 2010). When both sets of sites are present, inhibition of E2F1^{TD} is 8-fold greater than with either set alone. Structurally, how do these sites work together? Examination of the structures together reveals that the mechanisms promoted by T373 and S608 phosphorylation seem incompatible. In the S608 mechanism, Rb^{PL} binds to the cleft between the A and B subdomains and makes critical contacts with each subdomain. The subdomain geometry in the Rb^{PL-P} structure is nearly identical to the subdomain geometry in the structure of Rb pocket bound to E2F2^{TD} (Lee et al. 2002). In the Rb^{N-P} structure, the subdomain geometry is different such that the backbone amides of helix αP11, which are likely critical for S608E binding, are over 5 angstroms away from S608E in a structural alignment. Therefore in comparing the structures it seems like mechanism associated with S608 phosphorylation is incompatible with T373 phosphorylation. However, T373 phosphorylation is probably compatible with S612 phosphorylation, and several observations support this idea. First, S612 would be in a better structural position to bind helix αP11 in the presence of T373 phosphorylation, while maintaining the Rb^{PL} contacts with the A subdomain that are analogous to E2F^{TD} contacts. Second, S608 and S612 do not have an additive effect, indicating an “either, or” type of binding situation to helix αP11. Third, the energy of Rb-E2F^{TD} binding inhibition by S612 alone (ΔG = 0.9 Kcal/mol) accounts for the extra inhibition of E2F^{TD} binding when both sets of sites are present (compared to

T356/T373 alone; ΔG = 1.2 Kcal/mol). Therefore it is a strong possibility that S612 phosphorylation and T373 phosphorylation together have an additive effect, although this idea needs some experimental support. Within the scope of this idea, it is interesting to consider that S612 phosphorylation is one of the only events considered to be specific for CDK2-cyclinE (Zarkowska et al. 1997). Thus it seems that the addition of a weak phosphorylation event to a previous strong event (T373) may serve to increase the potency of Rb phosphorylation late in G1.

3.3.3. T373 phosphorylation regulates the "LxCxE-binding site"

Another major finding presented in this chapter is that T373 phosphorylation regulates the "LxCxE-binding site". This finding is comparable to a finding by Hassler et al. (2007), which shows that an IED-1^{LxCxE} peptide can inhibit the association of the Rb pocket and RbN domains in a pull-down assay. One interesting distinction between these two results is that the proteins used by Hassler et al., were not phosphorylated. Our SAXS studies suggest there is some transient binding between the domains in the unphosphorylated state. Thus when considered together, these findings indicate that this transient interaction is probably at the small interface, which is affected by LxCxE-binding and not mediated directly by phosphorylation.

Another significant finding presented here is that LxCxE binding is capable of partially inhibiting the small interface; this allows Rb phosphorylated at T356/T373 to bind $E2F^{TD}$ more tightly when $E7^{LxCxE}$ is present. The notion that the LxCxE peptide-the most famous oncogenic epitope of HPV-may itself be a good drug, can seem counterintuitive. However, without the rest of the E7 or E1A protein, the LxCxE peptide alone is not sufficient to disrupt Rb-E2F complexes (Liu et al. 2006; Huang et al. 1993; Phelps et al. 1992). Importantly, there are already obvious avenues to improve this potential anti-cancer drug. A thorough biochemical characterization of the Rb-LxCxE interaction has revealed several important binding determinants that significantly enhance the affinity of this interaction, these include: an acidic residue directly preceding the L, a hydrophobic residue two places after the E, and the addition of glutamic acid residues to the C-terminal end of the peptide, which may have the added effect of interfering with the lysine patch at the small interface (Signh et al. 2005). Generally, peptides are not considered to be good drugs because they are quickly proteolysed within the cell. Therefore it is notable that a recent drug discovery effort has identified a class of compounds that specifically inhibit the LxCxE interaction (Fera et al. 2012). While this study did not take in to account the potential of these compounds to act as therapeutics against hyperphosphorylated Rb by blocking the small interface, it is conceivable they can be modified to include the functionalities of any good peptide inhibitor.

3.3.4. Precedence for phosphorylation-driven conformational changes

Post-translational phosphorylation is thought to structurally regulate proteins through one of two general mechanisms: allosteric changes to protein structure, or bulk electrostatic effects. Our studies demonstrate that Rb is regulated by the former, and whether or not this is the exception or the rule for the majority of CDK substrates is not entirely clear; although, a recent, large-scale proteomic analysis of CDK substrates indicates bulk electrostatic effects may be more common (Holt et al. 2009). Nevertheless, there are examples of phosphorylation regulating disorder to order transitions to either enhance or inhibit a functional binding interaction (Wright and Dyson 2009). Interestingly, some of these disorder to order transitions seem to require the presence of specific binding partners while others do not (Dyson and Wright 2002). Despite a handful of structural examples, the vast majority of cases in which phosphorylation regulates protein-protein interactions are not yet structurally characterized. In the case of Rb, we see that the pocket linker becomes ordered upon phosphorylation at S608 and the phosphate mimetic interacts specifically at the N-terminus of an alpha helix. Similarly, T373 phosphorylation promotes the extension of an alpha helix and stabilizes that helix through a capping interaction at it's N-terminus. Together these examples may indicate a common structural mechanism for how phosphorylation drives disorder to order transitions: through the stabilization

of alpha helices. A few similar examples of phosphoproteins have been reported (Andrew et al. 2002), and there are many structural examples of phosphate binding to the N-terminus of an alpha helix, however, these are not related to known disorder to order structural transitions (Hirsch et al. 2007). On the other hand, there are no well-studied examples of phosphorylation causing large-scale order to disorder transitions. An increasing majority of mapped phosphorylation sites exist within unstructured regions of proteins, further emphasizing how rare this type of structural transition might be. Our work which suggest that T356 phosphorylation causes the destabilization of helix αN13 may therefore be an exceedingly unusual example. However, given the functional importance of T356 phosphorylation in E2F binding assays, it is likely part of a structured interaction with the pocket domain when it is phosphorylated, and may be an example of a helix to coil (or strand) rearrangement driven by phosphorylation.

3.4. Methods

ITC and NMR experiments were performed as described in chapters 2.2.3 and 2.2.4.

3.4.1. Protein Expression and Purification

Rb SAXS constructs, crystallography constructs and the Rb^{IDL} peptide were all expressed in *Escherichia coli* as fusions with glutathione S-

transferase. Cells were induced overnight at room temperature with 1 mM IPTG. The proteins were purified by glutathione affinity chromatography, followed by ion exchange chromatography on a source Q column, cleaved with GST-TEV, and subsequently re-purified over GS4B resin to remove cleaved GST and GST-TEV. The proteins were later further purified over a SD200 prior to use. RbN constructs were expressed as His6 fusion proteins in *Escherichia coli*, induced overnight at room, purified over Ni^{2+} resin, cut from the tag with GST-TEV and then purified using anion exchange over a source Q. The N-terminal loop was removed through a limited proteolysis reaction with 3% trypsin at room temperature for 1 hour. Reactions were quenched and diluted in low-salt buffer with 1 mM PMSF then loaded directly onto a source Q for purification. Additional details concerning limited proteolysis of RbN have been published (Hassler et al. 2007).

3.4.2. SAXS

All proteins used in SAXS experiments were purified over a SD200 column in a buffer containing 100 mM NaCL, 25mM Tris-HCL pH 8, 1 mM TCEP and 2% glycerol. Glycerol can help reduce radiation damage to the protein sample. Proteins were eluted at approximately 10 mgs/ml and diluted in elution buffer as needed. SAXS data were collected at the SIBYLS beamline (12.3.1) at the Advanced Light Source, Lawrence Berkeley National Laboratory. Scattering data are plotted as a function of q = 4p [sin(u/2)]/l,

where u is the scattering angle, and l is the X-ray wavelength in angstroms. An automated pipeline was applied for collection and partial analysis as previously described (Hura et al. 2009). Three concentrations of each sample were collected with three exposure times to check for concentration dependence and radiation damage. No concentration dependence was observed. Data were merged using PRIMUS (Konarev et al. 2003), maximizing signal to noise but excluding radiation-affected data points. The radius of gyration was determined to better than an angstrom of precision by using the Guinier approximation. GNOM (Svergun 1992) was used to determine the P(r) function and assign a Dmax. The output of GNOM was used as input into GASBOR (Svergun et al. 2001) for shape calculations. Ten runs of GASBOR were averaged together using the program DAMMAVER. The suite of programs is collectively assembled in the ATSAS suite (Konarev et al. 2006).

3.4.3. Crystallization, X-ray data collection, structure determination, model refinement

Proteins were prepared for crystallization by elution from a Superdex 200 column in a buffer containing 25 mM Tris, 200 mM NaCl, and 5 mM DTT. Proteins were crystallized by sitting drop vapor diffusion at 4°C. $Rb^{N–P}$ crystals grew over 2-3 weeks in a solution containing 100 mM HEPES, 100 mM ammonium fluoride, and 16% PEG 4K (pH 6.5). Notably, AmF was key to

obtaining crystals, and was either included in well condition or added directly to the protein sample prior to setting up drops. Crystals and were soaked in a cryoprotectant solution made by mixing the well precipitant solution with 30% ethylene glycol. Data were collected on Beamline 23-IDB at the Advanced Photon Source, Argonne National Laboratory. Reflections were integrated with Mosflm (Leslie 2006) and scaled with SCALE-IT (Howell and Smith 1992). Phases were solved by molecular replacement using PHASER (Mccoy et al. 2007). Both the N-terminus domain (PDB: 2QDJ) and unliganded pocket domain (PDB: 3POM) structures were used together as a search model (Balog et al. 2011; Hassler et al. 2007). Helix αP1 and other unique structural features were built into the model with Coot (Emsley and Cowtan 2004). The structure solution was refined with Phenix (Adams et al. 2010). Several rounds of position refinement with simulated annealing and individual temperature factor refinement with default restraints were applied. Stereochemical restraints were also increased over the course of refinement. The $Rb^{N–P}$ structure has one molecules in the asymmetric unit. Notably, there is a crystal-packing interface at the location where the “bar motif” is seen in a majority of Rb pocket structures; this is a possible reason that the “bar motif” is not present in this structure The conformational change we observe in this structure may also disrupt the “bar motif”. An electron density feature corresponding to two to three water molecules is visible at the smaller RbN–pocket interface in $Rb^{N–P}$. We had difficulty refining water at this site, which

may be due to heterogeneity in the precise water geometry throughout the crystal so we left the density here un-modeled. Buried surface areas were calculated using Chimera (Pettersen et al. 2004), and the pocket subdomain rotation was calculated using the program DynDom (Hayward and Berendsen 1998). Coordinates and structure factors for RbN-P have been deposited in the PDB under the code 4ELJ.

3.5. References

Adams PD, Afonine PV, Bunkoczi G, Chen VB, Davis IW, Echols N, Headd JJ, Hung LW, Kapral GJ, Grosse-Kunstleve RW, McCoy AJ, Moriarty NW, Oeffner R, Read RJ, Richardson DC, Richardson JS, Terwilliger TC, Zwart PH. "PHENIX: A comprehensive Python-based system for macromolecular structure solution."
Acta Crystallogr D Biol Crystallogr. 66, 213–221. (2010)

Andrew CD, Warwicker J, Jones GR, Doig AJ. "Effect of phosphorylation on alpha-helix stability as a function of position."
Biochemistry 41(6), 1897-905. (2002)

Balog ER, Burke JR, Hura GL, Rubin SM. Crystal structure of the unliganded retinoblastoma protein pocket domain." *Proteins.* 79(6), 2010-4. (2011)

Brown VD, Phillips RA, Gallie BL. "Cumulative effect of phosphorylation of pRB on regulation of E2F activity."
Mol Cell Biol. 19(5), 3246-56. (1999)

Brown VD, Gallie BL. "The B-domain lysine patch of pRB is required for binding to large T antigen and release of E2F by phosphorylation."
Mol Cell Biol. 22(5), 1390-401. (2002)

Burke JR, Deshong AJ, Pelton JG, Rubin SM. "Phosphorylation-induced conformational changes in the retinoblastoma protein inhibit E2F transactivation domain binding."
J Biol Chem 285(21):16286-93. (2010)

Burke JR, Hura GL, Rubin SM. “Structures of inactive retinoblastoma protein reveal multiple mechanisms for cell cycle control.” *Genes Dev.* 26(11):1156-66. (2012)

Dale GE, Oefner C, D'Arcy A. “ The protein as a variable in protein crystallization.” *J Struct Biol.* 142(1), 88-97. (2003)

Dick FA, Sailhamer E, Dyson NJ. “Mutagenesis of the pRB pocket reveals that cell cycle arrest functions are separable from binding to viral oncoproteins.” *Mol Cell Biol.* 20(10), 3715-27. (2000)

Dyson HJ, Wright PE. “Intrinsically unstructured proteins and their functions.” *Nat Rev Mol Cell Biol.* 6(3), 197-208. (2005)

Emsley P, Cowtan K. 2004. “Coot: Model-building tools for molecular graphics.” *Acta Crystallogr D Biol Crystallogr.* 60, 2126–2132. (2004)

Felsani A, Mileo AM, Paggi MG. “Retinoblastoma family proteins as key targets of the small DNA virus oncoproteins.” *Oncogene* 25(38), 5277-85. (2006)

Fera D, Schultz DC, Hodawadekar S, Reichman M, Donover PS, Melvin J, Troutman S, Kissil JL, Huryn DM, Marmorstein R. “Identification and characterization of small molecule antagonists of pRb inactivation by viral oncoproteins.” *Chem Biol.* 19(4), 518-28. (2012)

Gorges LL, Lents NH, Baldassare JJ. “The extreme COOH terminus of the retinoblastoma tumor suppressor protein pRb is required for phosphorylation on Thr-373 and activation of E2F. “ *Am J Physiol Cell Physiol.* 295(5), 1151-60. (2008)

Grafstrom RH, Pan W, Hoess RH. “Defining the substrate specificity of cdk4 kinase-cyclin D1 complex.” *Carcinogenesis* 20(2), 193-8. (1999)

Harbour JW, Luo RX, Dei Santi A, Postigo AA, Dean DC. “Cdk phosphorylation triggers sequential intramolecular interactions that progressively block Rb functions as cells move through G1.” *Cell* 98(6), 859-69. (1999)

Hassler M, Singh S, Yue WW, Luczynski M, Lakbir R, Sanchez-Sanchez F, Bader T, Pearl LH,Mittnacht S. “Crystal structure of the retinoblastoma protein N domain provides insight into tumor suppression, ligand i nteraction, and holoprotein architecture.”

Mol Cell. 28(3), 371-85. (2007)

Hayward S, Berendsen HJ. “Systematic analysis of domain motions in proteins from conformational change: New results on citrate synthase and T4 lysozyme.” *Proteins* 30, 144–154. (1998)

Hensey CE, Hong F, Durfee T, Qian YW, Lee EY, Lee WH. “Identification of discrete structural domains in the retinoblastoma protein. Amino-terminal domain is required for its oligomerization.”
J Biol Chem. 269(2), 1380-7. (1994)

Hirsch AK, Fischer FR, Diederich F. “Phosphate recognition in structural biology.” *Angew Chem Int Ed Engl.* 46(3), 338-52. (2007)

Holt LJ, Tuch BB, Villén J, Johnson AD, Gygi SP, Morgan DO. “Global analysis of Cdk1 substrate phosphorylation sites provides insights into evolution.” *Science.* 325(5948), 1682-6. (2009)

Howell PL, Smith GD. “Identification of heavy-atom derivatives by normal probability methods.” *J Appl Crystallogr* 25, 81–86. (1992)

Huang PS, Patrick DR, Edwards G, Goodhart PJ, Huber HE, Miles L, Garsky VM, Oliff A, Heimbrook DC. “Protein domains governing interactions between E2F, the retinoblastoma gene product, and human papillomavirus type 16 E7 protein.”
Mol Cell Biol. 13(2), 953-60. (1993)

Hura GL, Menon AL, Hammel M, Rambo RP, Poole FL II, Tsutakawa SE, J enney FE Jr, Classen S, Frankel KA, Hopkins RC, et al. 2009. Robust, high-throughput solution structural analyses by small angle X-ray scattering (SAXS). *Nat Methods* 6, 606–612. (2009)

Knudsen ES, Wang JY. “Dual mechanisms for the inhibition of E2F binding to RB by cyclin-dependent kinase-mediated RB phosphorylation.”
Mol Cell Biol. 17(10), 5771-83. (1997)

Konarev PV, Volkov VV, Sokolova AV, Koch MHJ, Svergun DI. “PRIMUS: A Windows PC-based system for small-angle scattering data analysis.”
J Appl Crystallogr 36: 1277–1282. (2003)

Konarev PV, Petoukhov MV, Volkov VV, Svergun DI. “ATSAS 2.1, a program package for small-angle scattering data analysis.” *J Appl Crystallogr* 39, 277–286. (2006)

Lee C, Chang JH, Lee HS, Cho Y. “Structural basis for the recognition of the E2F transactivation domain by the retinoblastoma tumor suppressor.” *Genes Dev.* 16(24), 3199-212. (2002)

Lee JO, Russo AA, Pavletich NP. “Structure of the retinoblastoma tumour-suppressor pocket domain bound to a peptide from HPV E7.” *Nature* 391, 859-65. (1998)

Lents NH, Gorges LL, Baldassare JJ. “Reverse mutational analysis reveals threonine-373 as a potentially sufficient phosphorylation site for inactivation of the retinoblastoma tumor suppressor protein (pRB).” *Cell Cycle* 5(15),1699-707. (2006)

Leslie AG. “The integration of macromolecular diffraction data.” *Acta Crystallogr D Biol Crystallogr* 62, 48–57. (2006)

Liu X, Clements A, Zhao K, Marmorstein R. “Structure of the human Papillomavirus E7 oncoprotein and its mechanism for inactivation of the retinoblastoma tumor suppressor.” *J Biol Chem.* 281(1), 578-86. (2006)

Mccoy AJ, Grosse-Kunstleve RW, Adams PD, Winn MD, Storoni LC, Read RJ. “Phaser crystallographic software.” *J Appl Crystallogr* 40, 658–674. (2007)

Petoukhov MV, Svergun DI. “Global rigid body modeling of macromolecular complexes against small-angle scattering data.” *Biophysical Journal* 89, 1237-1250. (2005)

Pettersen EF, Goddard TD, Huang CC, Couch GS, Greenblatt DM, Meng EC, Ferrin TE. “UCSF Chimera- a visualization system for exploratory research and analysis.” *J Comput Chem* 25, 1605–1612. (2004)

Phelps WC, Münger K, Yee CL, Barnes JA, Howley PM. “Structure-function analysis of the human papillomavirus type 16 E7 oncoprotein.” *J Virol.* 66(4), 2418-27. (1992)

Putnam CD, Hammel M, Hura GL, Tainer JA. “ X-ray solution scattering (SAXS) combined with crystallography and computation: defining

accurate macromolecular structures, conformations and assemblies in solution." *Q Rev Biophys.* 40(3), 191-285. (2007)

Qin XQ, Chittenden T, Livingston DM, Kaelin WG Jr. "Identification of a growth suppression domain within the retinoblastoma gene product." *Genes Dev.* 6(6), 953-64. (1992)

Rubin SM, Gall AL, Zheng N, Pavletich NP. "Structure of the Rb C-terminal domain bound to E2F1-DP1: a mechanism for phosphorylation-induced E2F release." *Cell* 123(6),1093-106. (2005)

Svergun DI. 1992. "Determination of the regularization parameter in indirect-transform methods using perceptual criteria." *J Appl Crystallogr* 25, 495–503. (1993)

Svergun DI, Petoukhov MV, Koch MH. 2001. "Determination of domain structure of proteins from X-ray solution scattering." *Biophys J* 80, 2946–2953. (2001)

Singh M, Krajewski M, Mikolajka A, Holak TA. "Molecular determinants for the complex formation between the retinoblastoma protein and LXCXE sequences." *J Biol Chem.* 280(45), 37868-76. (2005)

Wright PE, Dyson HJ. "Linking folding and binding." *Curr Opin Struct Biol.* 19(1), 31-8. (2009)

Zarkowska T, Mittnacht S. "Differential phosphorylation of the retinoblastoma protein by G1/S cyclin-dependent kinases." *J Biol Chem.* 272(19), 12738-46. (1997)

Chapter 4: Dual effects of RBC^N phosphorylation (S788/S795)

4.1. Introduction

The C-terminal region of Rb (RbC) is critical for growth suppression (Qin et al. 1992). RbC is a 145-residue, intrinsically unstructured "tail" directly attached to the pocket domain. Although RbC has no stable structure by itself, residues 829-872 form a strand-loop-helix motif in the presence of the marked box and coiled coil domains of the E2F1-DP1 heterodimer (Rubin et al. 2005). These residues comprise a small conserved segment of RbC we term RbC^{core}. Additional residues, 786-801, in RbC (termed RbC^N) increase the affinity of the RbC^{core}-E2F1-$DP1^{MB/CC}$ interaction 30-fold and likely contribute to the structured interaction, however the structural nature of the interaction between RbC^N and E2F1-$DP1^{MB/CC}$ has not been characterized.

RbC also has many features important for the reversal of its growth suppression function. RbC hosts half of Rb's phosphorylation sites and phosphorylation of RbC is necessary for the release of E2F and full activation of E2F-mediated promotors (Knudsen and Wang 1997; Brown et al. 1999). Six of these phosphorylation sites come in closely-spaced pairs, and studies have shown that each of these pairs contributes to the regulation of E2F in cells (Brown et al. 1999). Quantitative binding studies have further shown that S788/S795 phosphorylation reduces the affinity between $RbC^{786-928}$ and E2F1-$DP1^{MB/CC}$ 20-fold (Rubin et al. 2005). RbC also contains a highly-

conserved and overlapping kinase/phosphatase docking site as well as a cyclin docking motif; each of these are critical for Rb function (Adams et al. 1999; Hirschi et al. 2010). Therefore, while RbC is critical for the full growth-suppression effect of Rb, it also has the tools to turn off this function.

As a precursor to the mechanistic investigations presented in this thesis, we evaluated the extent to which cyclinA-CDK2 phosphorylates full-length Rb using LC-MS/MS. The results of this study are presented in the beginning of this chapter. The rest of this chapter explores the role of RBC^{N} phosphorylation in inhibiting $E2F^{TD}$ binding to Rb pocket. Quantitative $E2F^{TD}$-Rb pocket binding studies are used in combination with mutation and truncation studies to show that phosphorylation of S788 and S795 inhibit the Rb pocket-$E2F^{TD}$ interaction. Attempts to crystallize the phosphorylated interaction with the pocket have largely failed, but are described here nonetheless. NMR studies characterize how phosphorylation causes RbC^{N} to both dissociate from E2F1-$DP1^{MB/CC}$ and bind to Rb pocket in a manner that competitively displaces $E2F^{TD}$; uniquely this indicates phosphorylation of RbC^{N} disrupts two separate Rb-E2F interfaces. Additionally, we find RbC^{N} phosphorylation is complementary to Rb^{PL} phosphorylation, so that together Rb^{PL} and RBC^{N} have a large, 40-fold effect in inhibiting $E2F^{TD}$ binding to Rb pocket. Finally, we identify an interaction between Rb's "LxCxE-binding site" and E2F1's marked box domain.

4.2. Results

4.2.1. Analysis of full-length Rb phosphorylation by LC-MS/MS

All of our investigations into the effects of phosphorylation require the use of *in vitro* recombinant kinase reactions. In order to study the effects of different phosphorylation events we require a kinase with broad activity toward Rb. Therefore, we selected CDK2-cyclin A, which is thought to maintain high Rb phosphorylation levels non-specifically during S-phase. To determine which sites CDK2-cyclin A (K2A) is able to phosphorylate in near full-length $Rb^{55\text{-}928}$ *in vitro*, we treated 2-3 mg protein with 5% kinase (% mass of the total substrate) for 1hr, then 3% trypsin or chymotrypsin for 30 minutes to produce peptide fragments for analysis by LC-MS/MS. MS/MS spectra were individually inspected for parent ion peaks and charge ladders which correlate to each phosphorylated peptide (Figure 4.1). For our recombinant K2A reaction, we find that Rb is phosphorylated at 12 of its 15 CDK consensus sites (Table 4.1). In the case of S230 and S567, we recover only the unphosphorylated version of each peptide, indicating that these two sites are not phosphorylated in our kinase reaction. Significantly, both of these CDK consensus sites exist within structured domains of Rb and appear to be inaccessible to kinase (Hassler et al. 2007; Lee et al. 1998); furthermore, neither site has been observed phosphorylated *in vivo*. However, one study did indicate that S567 can be phosphorylated by CDK in the presence of a phosphorylated RbC peptide (Harbour et al. 1999). To explore this possibility,

we repeated our reaction to the specifications of the experiment described by Harbour et al, but fail to observe phosphorylation at S567 (data not shown).

Several phosphorylation sites were difficult to observe because the peptide fragments produced by trypsin are too small for detection; these include T356 and S788. Using chymotrypsin, however, we are able to overcome this limitation and observe phosphorylation at S788. The phosphorylation sites T252, S612, S811 are also closely flanked by positively charged residues and were expected to be similarly excluded; however, due to the inefficiency of trypsin digestion at some of these sites, we were are able to recover these phosphopeptides. It is worth noting that the chymotrypsin and trypsin used in these reactions each seem contaminated with the other enzyme, as we observe N-terminal chymotrypsin cleavage for S608 treated with trypsin, and N-terminal trypsin cleavage for T373 treated with chymotrypsin. It is also notable that a few of the peptides recovered are not fully-phosphorylated. For example, the T826 peptide is not phosphorylated T821. Another example is the S612 peptide, which is not phosphorylated at S608. For these peptides it was important to evaluate the MS-MS spectra for evidence that the phosphate mass is attributed to the correct residue. These mixed phosphorylation results also suggests that our kinase reaction is not quantitative. We did try to observe quantitative changes to the overall mass of full-length Rb after the kinase reaction using MS-ESI, however, this near full-length $Rb^{55\text{-}928}$ (expressed in insect cells) is

mildly degraded which contributed to noise and prohibited us from observing quantitive overall changes in mass. We were able to observe quantitative phosphorylation for many bacterially-expressed Rb constructs. These revealed our kinase assay can quantitatively phosphorylate Rb at: 249, 252, 356, 373, 608, 612, 788, 795, 807 and 811. The MS-ESI spectra for some of these results are presented elsewhere (Figure 2.11; Figure 3.14; Figure 3.16). The one notable exception to quantitative phosphorylation is S780, which can be only partially phosphorylated in our reaction (see discussion section 4.3.5.). Because of this, all crystallography constructs used in these studies include S780A mutations, which facilitate quantitative phosphate incorporation and avoid problems associated with protein heterogeneity.

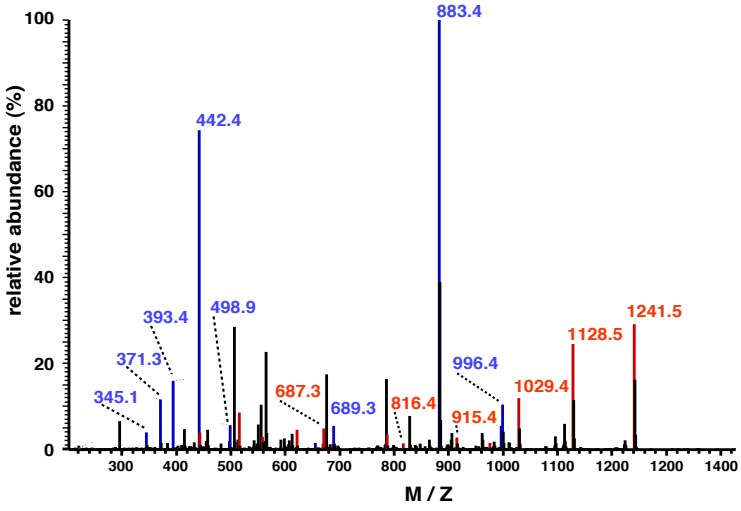

A.A.	b^{+1}	y^{+1}	y^{+2}
K 359	129.1	-	-
S 360	216.1	1995.9	998.5
N 361	330.2	1908.9	954.9
L 362	443.3	1794.9	897.9
D 363	558.3	1681.8	841.4
E 364	687.3	1566.8	783.9
E 365	816.4	1437.7	719.4
V 366	915.4	1308.7	654.8
N 367	1029.4	1209.6	605.3
V 368	1128.5	1095.6	548.3
I 369	1241.5	996.5	498.8
P 370	1338.7	883.4	442.2
P 371	1435.7	786.4	393.4
H 372	1572.8	689.3	345.1
*T 373	1753.8	552.3	276.6
P 374	1850.9	371.3	186.1
V 375	1949.9	274.2	137.6
R 376	-	175.1	88.1

Figure 4.1. Sample MS/MS spectrum. Peptide fragments corresponding to a M/Z of 883.4 and 442.2 confirm that this peptide is phosphorylated at T373.

A.A.	Ⓟ	Trypsin (85% recovered)	Chymotrypsin (63% recovered)
230	N	not recovered	F.IKLSPPML.L
249	Y	K.TAVIPINGS*PR.T	Y.KTAVIPINGS*PR.T
252	Y	K.TAVIPINGS*PRT*PR.R	not recovered
356	-	not recovered	not recovered
373	Y	R.KSNLDEEVNVIPPHT*PVR.T	R.KSNLDEEVNVIPPHT*PVRTVM.N
567	N	R.IMESLAWLSDSPLFDLIK.Q	W.LSDSPLF.D
608	Y	L.NLPLQNNHTAADMYLS*PVRS*PK.K	not recovered
612	Y	L.NLPLQNNHTAADMYLSPVRS*PK.K	Y.LSPVRS*PK.K
780	Y	K.TNILQYASTRPPTLS*PIPHIPR.S	Y.ASTRPPTLS*PIPHIPRSPY.K
788	Y	not recovered	L.SPIPHIPRS*PY.K
795	Y	Y.KFPSS*PLR.I	Y.KFPSS*PL.R
807	Y	R.IPGGNIYIS*PLKS*PYK.I	L.RIPGGNIYIS*PL.K
811	Y	R.IPGGNIYIS*PLKS*PYK.I	L.RIPGGNIYISPLKS*PY.K
821	Y	K.ISEGLPT*PTK.M	Y.KISEGLPT*PTKM.T
826	Y	K.ISEGLPTPTKMT*PR.S	not recovered

Table 4.1. A map of Rb phosphorylation: Rb phosphopeptides recovered from the K2A kinase reaction.

4.2.2. S788/S795 phosphorylation inhibits E2F1^{TD} binding to Rb pocket by ITC

Our studies into the function of Rb^{PL} reveal a consensus motif (DxYLSP) is required for S608 phosphorylation to inhibit E2F1^{TD} binding to Rb pocket (Chapter 2). In light of this finding, it occurred to us that motifs which are similar, and maybe functionally-redundant, may exists in different flexible regions of Rb similar to Rb^{PL}. In RbC, S807 is part of a highly-conserved xxYISP motif, which is similar to the Rb^{PL} motif, DxYLSP. We therefore conducted a series of ITC experiments using a Rb construct which lacks Rb^{PL} but retains part of RbC with S807 (RbC^{N}), so to selectively observe the effect of RbC^{N} phosphorylation on E2F1^{TD} binding to Rb pocket. We find that phosphorylation of Rb$^{380\text{-}816\Delta PL}$, which contains five RbC phosphorylation sites, is able to inhibit E2F1^{TD} binding to Rb pocket 7-fold (Table 4.1, rows 1-2; Figure 4.1, A-B); however, when we mutate S807 and S811 to alanine, we find that these sites are not necessary for this effect (Table 4.1, row 3; Figure 4.2, C). When we mutate S788 and S795 to alanine, we find that phosphorylated Rb$^{380\text{-}816\Delta PL}$ binds E2F1^{TD} similar to unphosphorylated Rb$^{380\text{-}816\Delta PL}$,indicating that S788/S795 are responsible for inhibiting E2F1^{TD} binding to Rb pocket (Table 4.1, row 1&4; Figure 4.2, D). Mutation of S780 to alanine maintains the 7-fold effect, but when we also mutate S795 to alanine, the effect is reduced to almost 4-fold (Table 4.1, row 5-6, Figure 4.2 E-F). Thus, these results indicate that phosphorylation of

S788/S795, but not S807/S811, inhibits of binding between E2F1^{TD} and Rb pocket.

	Rb construct	mutations	phos. sites	K_d E2F1^{TD}-Rb	panel
1	u. Rb$^{380\text{-}816\Delta PL}$	none	-	0.07 ± 0.03 μM	A
2	p. Rb$^{380\text{-}816\Delta PL}$	none	780/788/795/ 807/811	0.47 ± 0.04 μM	B
3	p. Rb$^{380\text{-}816\Delta PL}$	S807A/ S811A	780/788/795	0.51 ± 0.07 μM	C
4	p. Rb$^{380\text{-}816\Delta PL}$	S788A/ S795A	780/807/811	0.13 ± 0.06 μM	D
5	p. Rb$^{380\text{-}800\Delta PL}$	S780A	788/795	0.51 ± 0.10 μM	E
6	p. Rb$^{380\text{-}794\Delta PL}$	S780A/ S795A	788	0.27 ± 0.02 μM	F

Table 4.2. ITC analysis of the effect of RbC phosphorylation on binding between E2F1^{TD} and Rb pocket.

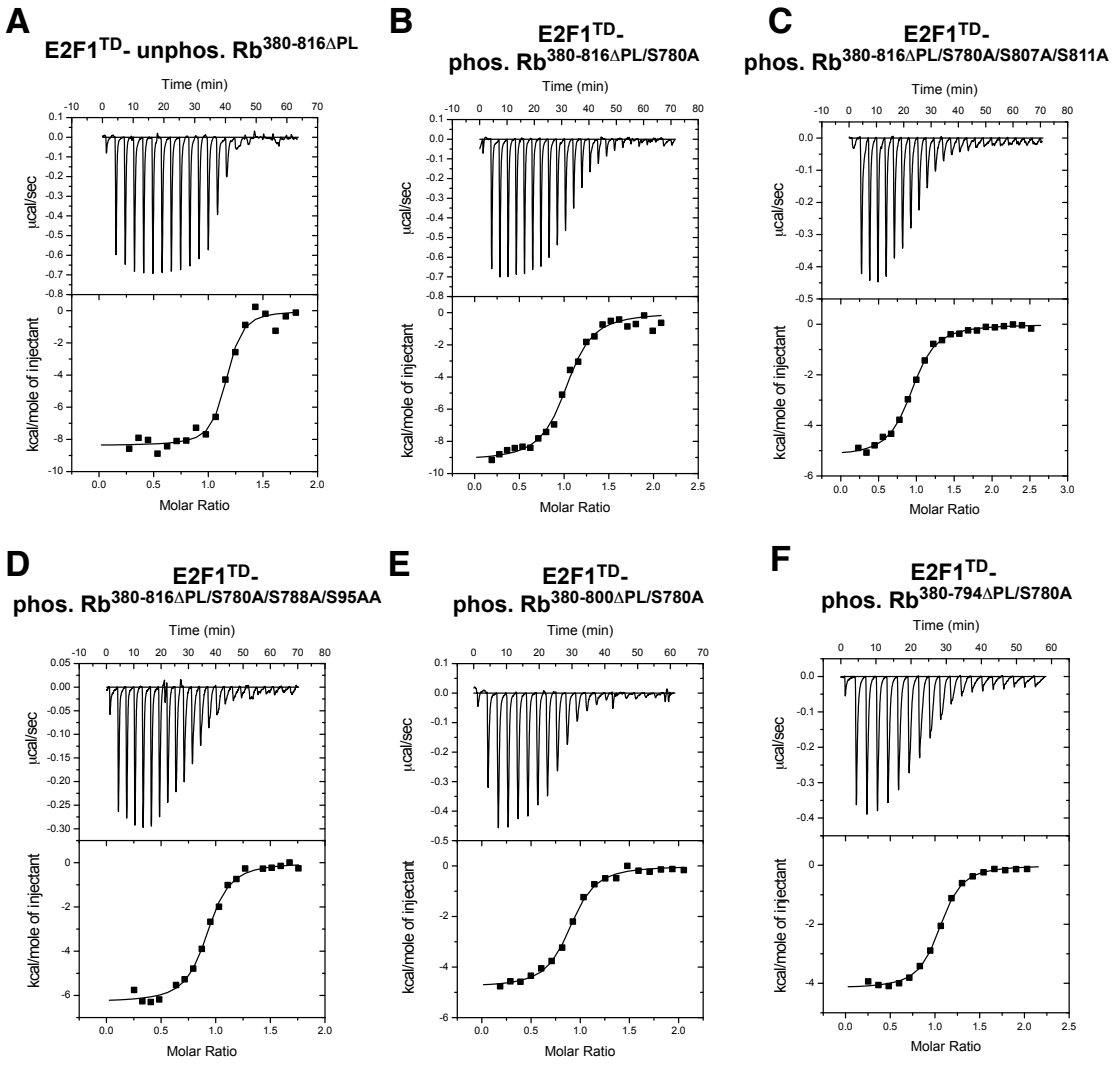

Figure 4.2. Representative ITC data presented in table 4.2.

4.2.3. Efforts toward the crystallization of the Rb pocket-RbC interaction

Many attempts have been made to obtain decent crystals of the phosphorylation-dependent interaction between RbC and Rb pocket (Table 4.3). Initially, we used an Rb pocket construct lacking the pocket linker and containing a 28-reside portion of RbC; however, this construct, which includes sites S788, S795, S807, S811, did not crystallize (Table 4.3, row 1). Next, we

trimmed the RbC tail back 16 residues to include only S788 and S795; this also failed to produce crystals (Table 4.3, row 2). Several Rb constructs were designed to include the shortened pocket linker with a S608E mutation, which previously crystallized so well, but this also did not help facilitate crystal formation (Table 4.3, rows 4-7). Glutamate mutations to S788/S795 turned out to be non-helpful, as well as non-functional (Table 4.3, row 8; Figure 4.3, A). Finally, we turned to a construct lacking the pocket linker but containing a 17-residue portion of RbC, in which the only phosphorylation site is S788 (Table 4.3, row 3). This construct produced bunches of slightly amorphous needles (Figure 4.3, B). Attempts to optimize this hit produced larger needles, but these needles have failed to diffract.

	Rb crystallography construct	phos. sites	x-tals
1	$Rb^{380\text{-}816\Delta PL/S780A}$	788/795/807/811	no
2	$Rb^{380\text{-}800\Delta PL/S780A}$	788/795	no
3	$Rb^{380\text{-}794\Delta PL/S780A}$	788	yes
4	$Rb^{380\text{-}800\Delta 616\text{-}642/S608E/S780A}$	788/795	no
5	$Rb^{380\text{-}794\Delta 616\text{-}642/S608E/S780A}$	788	no
6	$Rb^{380\text{-}800\Delta 616\text{-}642/S608E/S780A/S788E/S795E}$	-	no
7	$Rb^{380\text{-}795\Delta 616\text{-}642/S608E/S780A/S788E/S795E}$	-	no
8	$Rb^{380\text{-}795\Delta PL//S780A/S788E/S795E}$	-	no

Table 4.3. Rb pocket-RbC crystallography constructs.

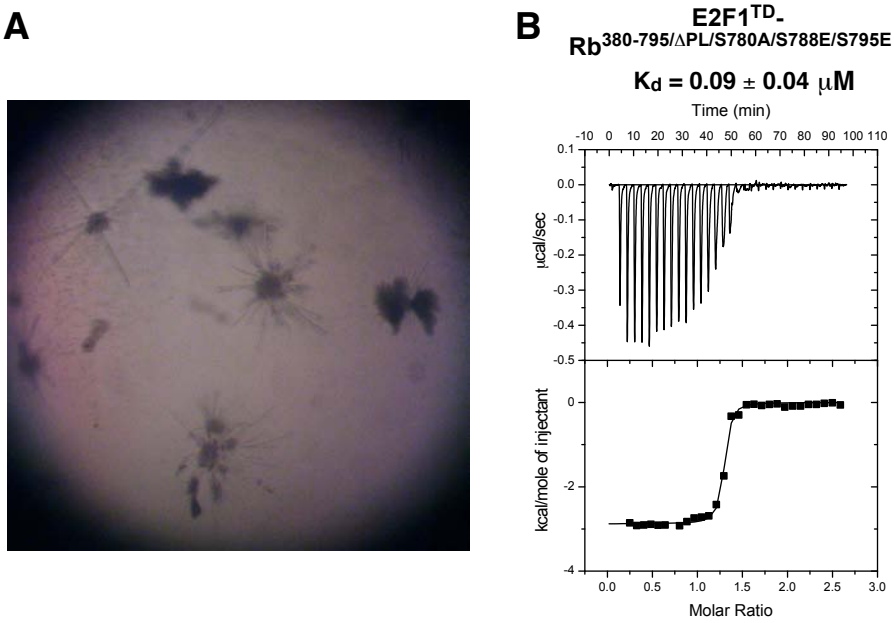

Figure 4.3. Rb pocket-RbC crystallography. (**A**) Crystals of phosphorylated $Rb^{380\text{-}794\Delta PL/S780A}$. Initial hits were obtained: 0.2M NaCl, 0.1M Na cacodylate pH 6.5, 2M AmSO4 (JCSG 2-D10); and 1M NaCitrate, 0.1M Na cacodylate (JSCG 3-D12). Hits were optimized and were most reproducible around the condition JCSG2-D10. Crystallization of $Rb^{380\text{-}794\Delta PL/S780A}$ in this condition is largely pH independent. (**B**) $Rb^{380\text{-}795\Delta PL//S780A/S788E/S795E}$ binds $E2F1^{TD}$ with an affinity of: $K_d = 0.09 \pm 0.04$ μM. This is similar to the affinity of $E2F1^{TD}$ for unphosphorylated $Rb^{380\text{-}795}$: $K_d = 0.05 \pm 0.01$ μM (Figure 2.1); indicating that S788E/S795E are not functional phosphate mimetics in the context of this construct.

4.2.4. Phosphorylation of RbC^N dissociates E2F1-$DP1^{MB/CC}$ and associates Rb pocket to inhibit $E2F1^{TD}$ binding.

In the absence of suitable protein crystals, we turned to NMR to further explore the phosphorylation-dependent interaction between RbC^N and Rb pocket. For these experiments we generated an expressible RbC peptide ($RbC^{787\text{-}816}$), which contains four RbC phosphorylation sites: S788, S795, S807 and S811. Even though S807 and S811 do not have an effect in the

inhibition of E2F1^{TD} binding by ITC, we included these sites to observe possible differential binding effects between S788/S795 and S807/S811. Notably, this peptide is difficult to express as a GST fusion: it produces low yields and one particular truncation is common (RbC$^{787-806}$). When we acquire a ^{1}H-^{15}N HSQC spectrum of phosphorylated, ^{15}N-labeled RbC$^{787-816}$ alone and in the presence of Rb pocket, we observe selective peak broadening effects to several spectral peaks (Figure 4.4, A). Significantly, three or four of the peaks with a ^{1}H chemical shift greater than 8.5 p.p.m. most likely represent phosphoserines, although this spectrum has not been formally assigned. Interestingly, chemical shift changes and peak broadening effects are evident for three of these four peaks, suggesting that two or three phosphoserines interact with Rb pocket. Since our ITC results indicate RBC^{N} phosphorylation inhibits E2F^{TD} binding to Rb pocket, we next tested for competitive binding between phosphorylated RbC$^{787-816}$ and E2F^{TD} by looking for chemical shift changes to phosphorylated RbC$^{787-816}$ when both Rb pocket and E2F^{TD} are present. Here we observe reduced peak broadening effects and chemical shift changes to phosphorylated RbC$^{787-816}$ than we previously observed without E2F^{TD}; this indicates an increased concentration of unbound, phosphorylated RbC$^{787-816}$, consistent with model in which E2F^{TD} competes with phosphorylated RbC$^{787-816}$ in binding to Rb pocket (Figure 4.4, B; compare to Figure 4.4, A). To confirm that binding between RbC$^{785-816}$ and Rb pocket is dependent upon phosphorylation, we examine the spectrum of

unphosphorylated, ^{15}N-labeled RbC$^{787\text{-}816}$ in the presence of unlabeled Rb pocket and observe no chemical shift changes or peak broadening effects (Figure 4.4, C).

Previous work has suggested that RbC$^{787\text{-}816}$ binds the heterodimer E2F1-DP1$^{MB/CC}$ in a phosphorylation-dependent manner (Rubin et al. 2005). Accordingly, when we look for binding between unphosphorylated, ^{15}N-labeled RbC$^{787\text{-}816}$ and unlabeled E2F1-DP1$^{MB/CC}$, we see extensive peak broadening indicative of complex formation (Figure 4.4, D). When we repeat this experiment using phosphorylated, ^{15}N-labeled RbC$^{787\text{-}816}$, we see less-extensive signal broadening, but notably, some selective broadening remains (Figure 4.4, E). This is consistent with ITC studies which show that S788/S795 phosphorylation reduces the overall binding affinity between RbC$^{771\text{-}928}$ and E2F1-DP1$^{MB/CC}$ 20-fold (Rubin et al. 2005). Intriguingly, this result further suggests that phosphorylated S807/S811 may remain bound to E2F1-DP1$^{MB/CC}$, as the peaks which broaden in the presence of Rb pocket are largely distinct from the peaks which broaden in the presence of E2F1-DP1$^{MB/CC}$(Compare Figure 4.4 A&E). In summary, these NMR studies support a unique role for S788/S795 phosphorylation in both dissociating RbC-E2F1-DP1$^{MB/CC}$, complexes as well as disrupting Rb pocket-E2F1^{TD} complexes (Figure 4.4, F).

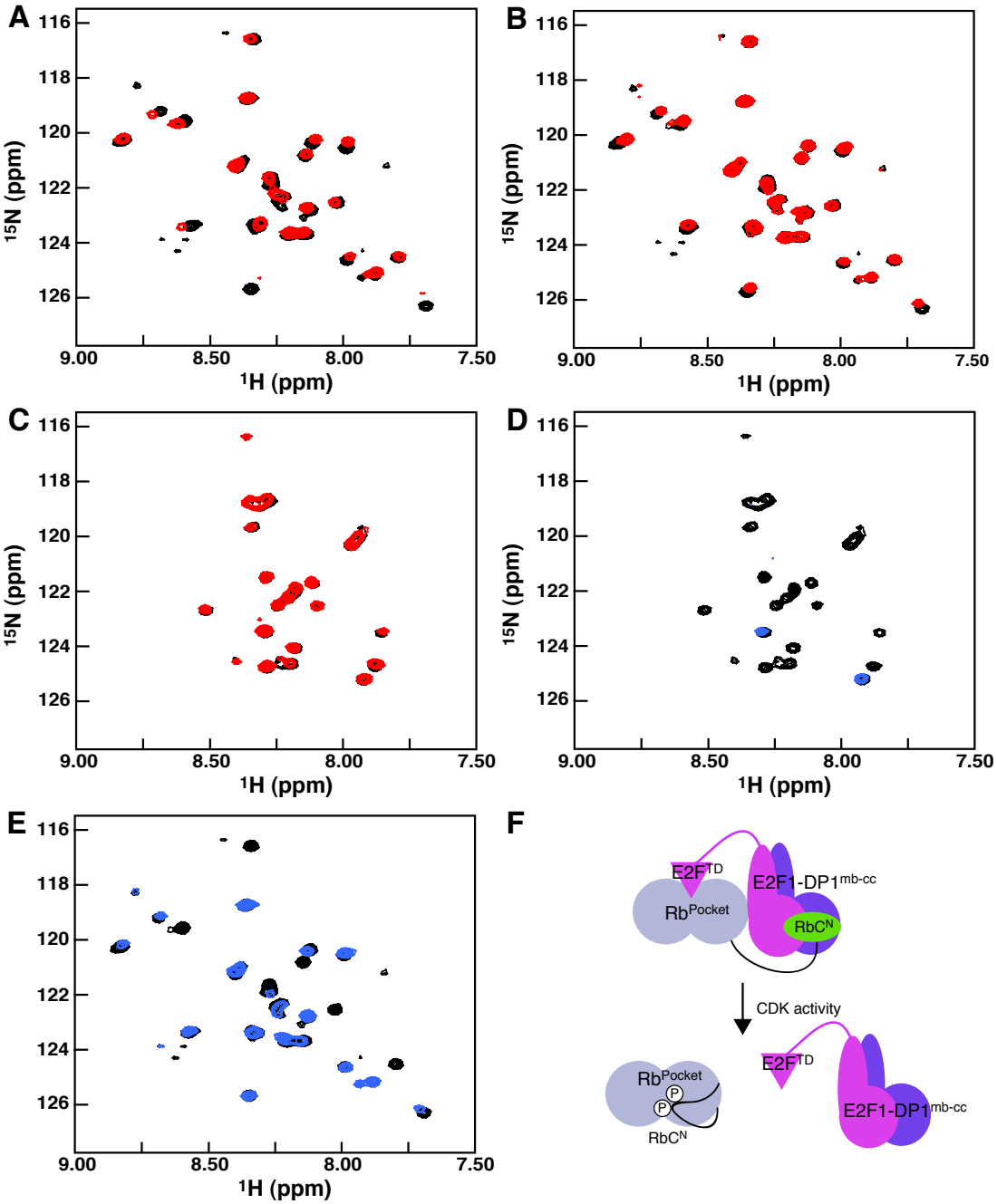

Figure 4.4. Phosphorylation of RbC$^{787\text{-}816}$ causes the dissociation of RbC-E2F1-DP1$^{MB/CC}$ and association of RbC-Rb pocket to inhibit E2F1^{TD} binding. (**A**) ^{1}H-^{15}N HSQC spectra of 50 µM ^{15}N-labeled phosphorylated RbC$^{787\text{-}816}$ alone (black) and in the presence of 900 µM unlabeled Rb pocket$^{380\text{-}787\Delta PL}$ (red). Broadening of selective peaks indicates an association between the phosphorylated RbC peptide and the pocket domain. (**B**) HSQC

spectra of 50μM ^{15}N-labeled phosphorylated RbC$^{787\text{-}816}$ alone (black) and in the presence of 900μM unlabeled Rb pocket$^{380\text{-}787\Delta PL}$ and 900 μM unlabeled E2F4^{TD} (red). Peak broadening is less extensive than in (A), indicating that phosphorylated RbC$^{787\text{-}816}$ and E2F4^{TD} have overlapping binding sites on Rb pocket. (**C**) HSQC spectra of 60μM ^{15}N-labeled unphosphorylated RbC$^{787\text{-}816}$ alone (black) and in the presence of 900μM unlabeled Rb pocket$^{380\text{-}787\Delta PL}$ (red). The absence of peak broadening effects indicates RbC$^{787\text{-}816}$ binding to Rb pocket is dependent upon phosphorylation. (**D**) HSQC spectra of 60 μM ^{15}N-labeled unphosphorylated RbC$^{787\text{-}816}$ alone (black) and in the presence of 300 μM unlabeled E2F1-DP1$^{MB/CC}$(blue). The dramatic peak broadening observed in this spectrum is suggestive of binding. Attempts were made to quantify this binding interaction by ITC, however, this binding interaction produced no detectible signal. (**E**) HSQC spectra of 100 μM ^{15}N-labeled phosphorylated RbC$^{787\text{-}816}$ alone (black) and in the presence of 300 μM unlabeled E2F1-DP1$^{MB/CC}$(blue). Less peak broadening is observed here than in (D), suggesting that phosphorylation of RbC$^{787\text{-}816}$ dissociates RbC-E2F1-DP1$^{MB/CC}$ complexes. (**F**) Summary of interactions identified by NMR: Phosphorylation of RbC$^{787\text{-}816}$ dissociates it from E2F1-DP1$^{MB/CC}$ and re-associates it with Rb pocket in a manner that perturbs E2F1^{TD} binding.

4.2.4. RbC and Rb^{PL} have an additive effect in inhibiting E2F1^{TD}-Rb pocket binding

Since phosphorylated Rb^{PL} and RbC^{N} each inhibit E2F^{TD} binding to Rb pocket through competitive inhibition, we next sought to determine if Rb^{PL} and RbC^{N} together have an additive effect. For this experiment, we used a Rb construct with both Rb^{PL} sites as well as five RbC phosphorylation sites (S608, S612, S780, S788, S795, S807, S811). We find that unphosphorylated Rb$^{380\text{-}816}$ binds E2F1^{TD} with and affinity of: K_d = 0.07 ± 0.03 μM (Figure 4.5, A). When we phosphorylate Rb$^{380\text{-}816}$, E2F1^{TD} binds with an affinity of: K_d = 3.06 ± 0.52 μM (Figure 4.5, B). This 40-fold difference in binding corresponds to a 2.6 Kcal/mol change in the free energy of binding. Previously, we determined that Rb^{PL} and RbC^{N} phosphorylation reduce the

free energy of binding by 1.4 Kcal/mol and 1.2 Kcal/mol, respectively (Figure 4.5, C). If the mechanisms of Rb^{PL} and RbC^{N} are independent, and the effects are additive, we would expect to see an overall change in the free energy of binding is 2.6 Kcal/mol, which is exactly what we see in this experiment.

Overall, our results suggest that phosphorylated RbC^{N} competes for Rb pocket binding with $E2F^{TD}$, and adds to the effect of Rb^{PL} phosphorylation. Previously, we showed that phosphorylation of Rb^{PL} promotes an interaction with the pocket domain that is structurally analogous to the C-terminal half of $E2F^{TD}$. Therefore, we suspect that phosphorylated RbC^{N} binds Rb pocket in a manner that is structurally analogous to the N-terminal half of $E2F^{TD}$. Remarkably, there is a consensus sequence of highly-conserved residues that is similar between RbC^{N} and $E2F2^{TD}$. These include: D410 of $E2F2^{TD}$, which is positionally similar to S788 of RbC^{N}, and makes a salt bridge with K548 of Rb pocket; Y412 of $E2F2^{TD}$ is similar to Y790 of RbC^{N}, and forms a buried hydrogen bond with K653 of Rb pocket; W414 of $E2F2^{TD}$ is similar to F792 of RbC^{N}, and binds a within a conserved pocket partially formed by E2F's Y412; E416 of $E2F2^{TD}$ is similar to S795 of RbC^{N}, and forms a critical stabilizing salt bridge with K652 of Rb pocket (Figure 4.5, D). Therefore, these structural similarities along with the binding data strongly suggest that phosphorylated RbC^{N} directly competes with the N-terminal half of $E2F2^{TD}$ for binding to Rb pocket.

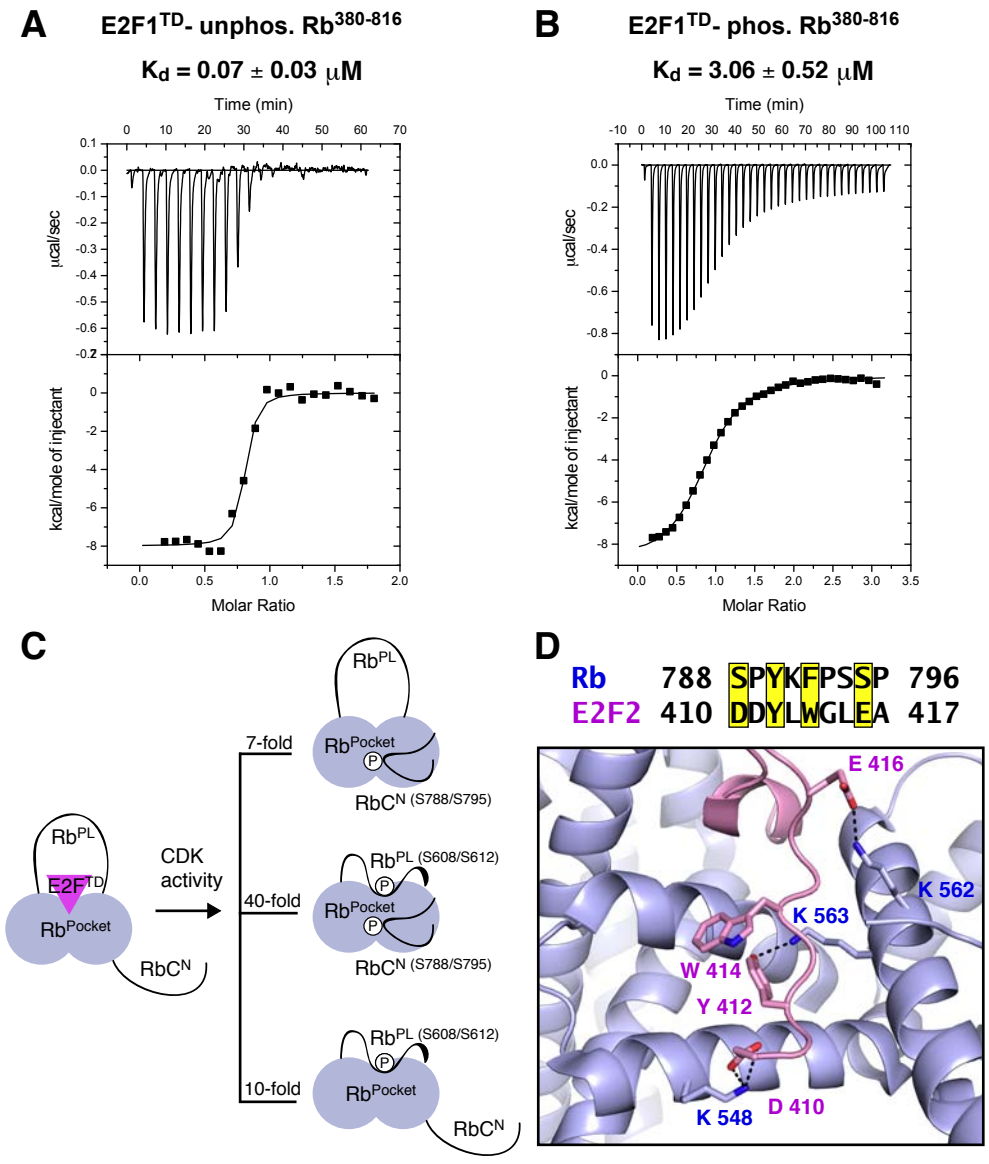

Figure 4.5. The role of RbC^{N} phosphorylation in E2F1^{TD} inhibition. (**A-B**) The binding affinity of E2F1^{TD} for Rb$^{380-816}$ is reduced 40-fold upon Rb$^{380-816}$ phosphorylation. (**C**) Scheme depicting the effects of Rb^{PL} and RbC^{N} phosphorylation separately and together. (**D**). RbC^{N} and E2F2^{TD} have many important sequence similarities and therefore may bind in an analogous fashion to Rb pocket.

4.2.5. E2Fs interact with Rb via the “LxCxE-binding site”

The “LxCxE-binding site” on Rb pocket is intriguing in that it is so structurally accessible yet so functionally inaccessible. The first crystal structure of Rb’s pocket domain detailed the binding requirements of HPV’s $E7^{LxCxE}$ peptide, and also quantified the high-affinity binding interaction at this site (Lee et al. 1998). This structure, coupled with the knowledge of the tightly-binding viral peptide, led some to assume that the functional role of $E7^{LxCxE}$ must be to disrupt a similar high-affinity interaction between Rb and a cellular protein with an ‘LxCxE’ sequence. This line of thinking has further led to the entirely speculative claim that Rb has “hundreds” of functional “LxCxE” binding partners in the cell; a claim which would no doubt require hundreds of grant renewals to investigate (Morris and Dyson 2001). Statistically, there should be between 200-400 different cellular proteins with “LxCxE” somewhere in their sequence. Therefore, this review boldly suggests that Rb binds nearly every cellular protein with an LxCxE motif. Certain studies have actually endeavored to characterize direct binding interactions between Rb and functionally-related cellular proteins with LxCxE motifs, however, many of the results which claim a direct LxCxE-mediated interaction have later been refuted (Dick et al, 2000; Harbour et al, 1999; Kennedy et al, 2001; Rayman et al, 2002).

The full E7 viral protein has several domains, each of which selectively disrupts an important Rb-E2F interface (Liu et al. 2006; Huang et al. 1993;

Phelps et al. 1992). Therefore, since E7 is largely devoted to disrupting Rb-E2F, logic would follow that it's central, most highly-conserved motif would be devoted to the same function; however, there are several reasons why this logic has never caught on. First, the $E7^{LxCxE}$ peptide alone is not sufficient to disrupt Rb-E2F complexes in pull down assays (Huang et al. 1993). Second, E2F does not have a canonical "LxCxE motif". Third, Rb's LxCxE-binding surface seems dispensable for normal Rb-E2F mediated control of the cell cycle (Chen et al. 2000; Dick and Dyson 2000). While these results together seem oddly definitive, they do not exclude the possibility of a less-potent, yet functionally important binding interaction between E2F and Rb at this site. Indeed, the same studies which purport Rb's LxCxE site is dispensable for E2F regulation also include results which indicate Rb's ability to repress E2F-mediated transcription is significantly, but not fully, compromised when the LxCxE-binding site is mutated (Chen et al. 2000; Dick and Dyson 2000). Furthermore, a separate study has shown that an Rb-$E7^{LxCxE}$ complex can directly inhibit $E2F^{MB}$ binding to Rb pocket (Xiao et al. 2003). On a structural note, three different Rb pocket crystal structures feature non-LxCxE sequences unintentionally bound to this site; these structures therefore further specify that the leucine is probably the only strict binding determinant at Rb's putative "LxCxE site. (Burke et al. 2012; Lee et al. 2002; Liu et al. 2007).

In exploring the distinct functions of Rb's many phosphorylation sites, it has become apparent that most of them are important for regulating E2F

binding. It is well-established that phosphorylation of T821/T826 disrupts viral protein binding to Rb's "LxCxE-binding site" (Harbour et al. 1999; Knudsen and Wang, 1996; Rubin et al. 2005); however, it is also interesting that when T821/T826 is mutated to alanine, Rb phosphorylation is less effective at activating E2F in a transcription reporter assay (Brown et al. 1999). This result suggests that E2F interacts with Rb's "LxCxE-binding" site, and, similar to other Rb-E2F interfaces, this interface is regulated by phosphorylation.

To attempt to detect this interaction, we designed a binding experiment similar to, but distinct from, the one described by Xiao et al. (2003). In the previous experiment, the authors used an E2F construct including the transactivation and marked box domains of E2F, but they excluded the coiled-coil domain. A crystal structure of Rb's marked box domain reveals it is stabilized through extensive contacts with it's coiled-coil domain and it's heterodimeric binding partner, DP1 (Rubin et al. 2005). While E2F homodimers may be functional in the cell, the missing coiled-coil domain suggests the protein used by Xiao et al. (2003), may have not been properly folded. We wanted to repeat this experiment in essence, but avoid the uncertainty caused by the use of this truncated E2F construct; therefore, we used the E2F1-DP1$^{MB/CC}$ heterodimer from the crystal structure (Rubin et al. 2005). We find that E7^{LxCxE} peptide binds Rb$^{380\text{-}787\Delta PL}$ with an affinity similar to what has been previously reported: K_d = 0.14 ± 0.04 μM (Figure 4.6, A; Lee et al. 1998). When we pre-bind Rb$^{380\text{-}787\Delta PL}$ to 2 molar excess E2F1-DP1$^{MB/}$

$^{CC\text{-}TD}$, we find that E7^{LxCxE} binding is inhibited 10-fold: K_d = 1.4 ± 0.07 μM (Figure 4.6, B). Notably, this complex retains the high-affinity Rb pocket-E2F^{TD} interaction. When we repeat the experiment with E2F1-DP1$^{MB/CC}$, which lacks E2F1^{TD}, we find that E7^{LxCxE} binding to Rb$^{380\text{-}787\Delta PL}$ is no longer inhibited: K_d = 0.10 ± 0.01 μM (Figure 4.6, C). Similarly, when we use only E2F1^{TD}, we find that E7^{LxCxE} binding to Rb$^{380\text{-}787\Delta PL}$ is not inhibited: K_d = 0.05 ± 0.02 μM; this is also consistent with previously published work (Figure 4.6, C; Xiao et al. 2003). These results suggest that E2F1-DP1$^{MB/CC}$ interacts at the "LxCxE-site" so to weaken E7^{LxCxE} binding, but only if the E2F^{TD}-Rb pocket domain interaction is also present to tether it there. Notably, both RbC^{N} and RbC^{core} bind E2F1-DP1$^{MB/CC}$; when these interactions are present they may further increase the stability of the Rb pocket-E2F1-DP1$^{MB/CC}$ complex at the LxCxE binding site. The specific interactions at the Rb pocket-E2F1-DP1$^{MB/CC}$ interface might come from E2F's marked box domain, which contains several highly-conserved, solvent exposed leucine side chains as well as a significant density of highly-conserved glutamates. These glutamates can potentially interact at the adjacent "lysine patch" on Rb pocket. Notably, the lysine patch and "LxCxE-binding site" pocket interfaces are disrupted by both T821/T826 and T373 phosphorylation. This is consistent with the role that many Rb phosphorylation events have in disrupting Rb-E2F interfaces.

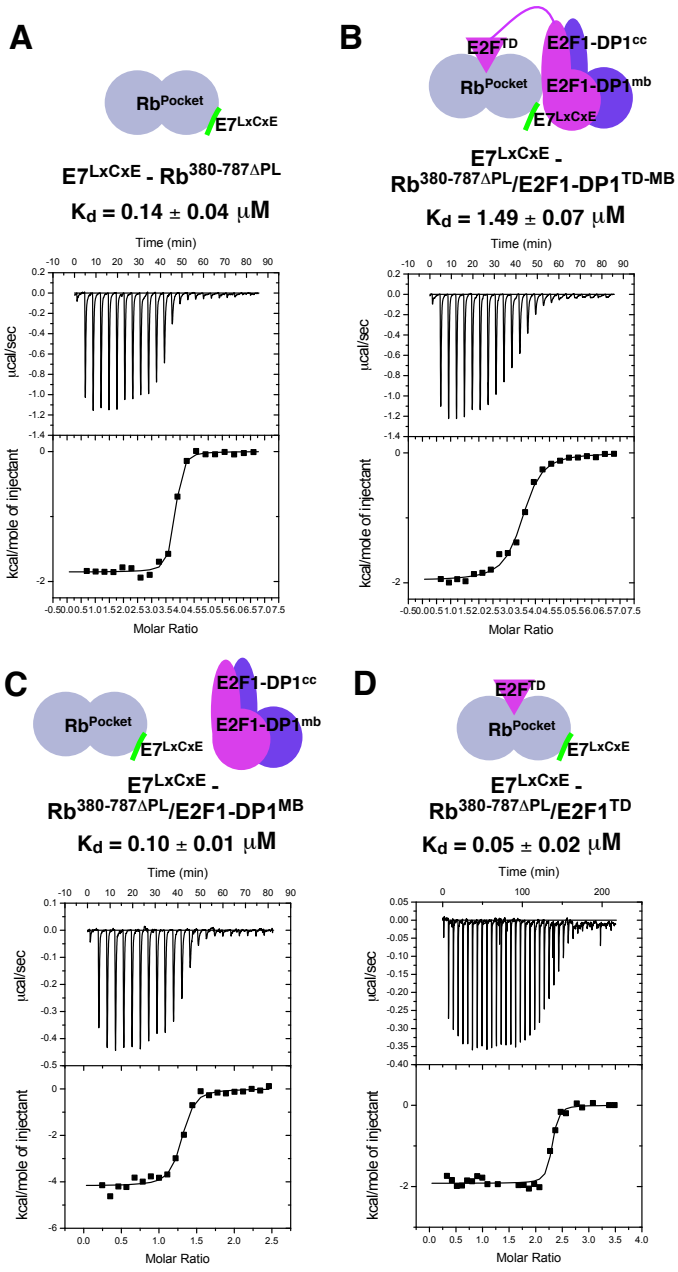

Figure 4.6. E7^{LxCxE} binding to Rb pocket is inhibited by E2F1-DP1$^{TD-MB/CC}$. (**A**) E7^{LxCxE} binds Rb pocket with an affinity of K_d = 0.14 ± 0.04 μM. (**B**) E7^{LxCxE} binds Rb pocket in the presence of 2 molar excess E2F1-DP1^{TD-MB} with an affinity of K_d = 1.49 ± 0.07 μM. (**C**) E7^{LxCxE} binds Rb pocket in the presence of 2 molar excess E2F1-DP1^{MB} with an affinity of K_d = 0.10 ± 0.01 μM. (**D**) E7^{LxCxE} binds Rb pocket in the presence of 2 molar excess E2F1^{TD} with an affinity of K_d = 0.05 ± 0.02 μM.

Rb's pocket protein homologues, p107 and p130, also contain conserved LxCxE binding pockets; although, direct binding between these proteins and $E7^{LxCxE}$ has not been quantified (Lee et al, 1998). p107 and p130 do not bind E2F1 in the cell, and Rb's interaction with E2F1-$DP1^{MB/CC}$ may be specific for E2F1 (Dick and Dyson 2003); therefore, it is interesting to ask how else the "LxCxE-binding site" might be utilized by E2Fs. All E2Fs contain highly-conserved " pre-transactivation domain sequences" adjacent to the the well-characterized 18-residue transactivation domain (Hagemeier et al. 1993; Lee et al. 2002; Xiao et al. 2003). The different E2Fs can be grouped together based on their similarities of this "pre transactivation domain" sequence: E2F2/E2F3 are similar, E2F4/E2F5 are similar, and E2F1 is unique. Binding studies have indicated that a 57-residue $E2F1^{380-437}$ peptide binds to Rb pocket with only a slight, 2-fold greater affinity than the 18-residue crystallized fragment, $E2F1^{409-426}$ (Xiao et al. 2003); therefore, while conserved, this sequence in E2F1 is not important for binding to Rb pocket. Importantly, this conserved non-transactivation domain sequence may be important for E2F1-mediated apoptosis (Hallstrom et al. 2003). When we test E2F2 binding to Rb pocket, we find that a longer $E2F2^{380-427}$ binds with only a 2-fold greater affinity than a shorter $E2F2^{410-427}$. This suggests that the conserved, pre-transactivation domain sequences of E2F2 and E2F3 are not important for binding to Rb pocket (Table 4.4, row 1-2; Figure 4.7, A-B). E2F4 and E2F5 are a little different: these "inactivating E2Fs" both

contain highly-conserved LxCxE-like motifs adjacent to their transactivation domain sequences; however, these motifs differ from the classic “LxCxE motif” in that they each have a serine instead of a cystine (ELxSxExF). These sequences also include additional features which are important for binding, these include: an acidic residue directly preceding the leucine, and a hydrophobic residue two places after the glutamic acid (Signh et al. 2005). We therefore wanted to test whether these sequences bind directly to Rb, and, by adding a closely-tethered weak interaction to the well-characterized transactivation domain interaction, enhance the overall affinity of these transactivation domains for Rb. We find that the short, classic transactivation domain (TD) fragment, E2F4$^{390-407}$, binds Rb pocket with an affinity of: K_d = 2.20 ± 0.22 μM (Table 4.4, row 3; Figure 4.7, C). The N-terminal fragment alone, which is excludes the classic TD fragment but includes the highly-conserved LxCxE-like motif, E2F4$^{366-391}$, binds Rb with an affinity of: K_d = 47.8 ± 10.9 μM (table 4.4, row 4; figure 4.7, D). A longer version, E2F4$^{366-407}$, which includes both sequences, binds to Rb with an affinity of: K_d = 2.05 ± 0.54 μM. Therefore, the LxCxE-like sequence included in E2F4$^{366-391}$ does not substantially increase the affinity of E2F4$^{366-407}$ for Rb pocket (table 4.4, row 5; figure 4.7, E). This indicates these E2F4 sequences cannot bind to Rb pocket simultaneously; if they could, the combined binding affinities would result in an overall subnanomolar affinity between E2F4$^{366-391}$ Rb pocket.

	Rb construct	$E2F^{TD}$ construct	K_d Rb-E2F	panel
1	$Rb^{380\text{-}787\Delta PL}$	$E2F2^{410\text{-}427}$	0.08 ± 0.01 μM	A
2	$Rb^{380\text{-}787\Delta PL}$	$E2F2^{380\text{-}427}$	0.04 ± 0.02 μM	B
3	$Rb^{380\text{-}787\Delta PL}$	$E2F4^{390\text{-}407}$	2.20 ± 0.22 μM	C
4	$Rb^{380\text{-}787\Delta PL}$	$E2F4^{366\text{-}391}$	47.8 ± 10.9 μM	D
5	$Rb^{380\text{-}787\Delta PL}$	$E2F4^{366\text{-}407}$	2.05 ± 0.54 μM	E

Table 4.4. Rb binding to E2F2/E2F4 extended transactivation domains.

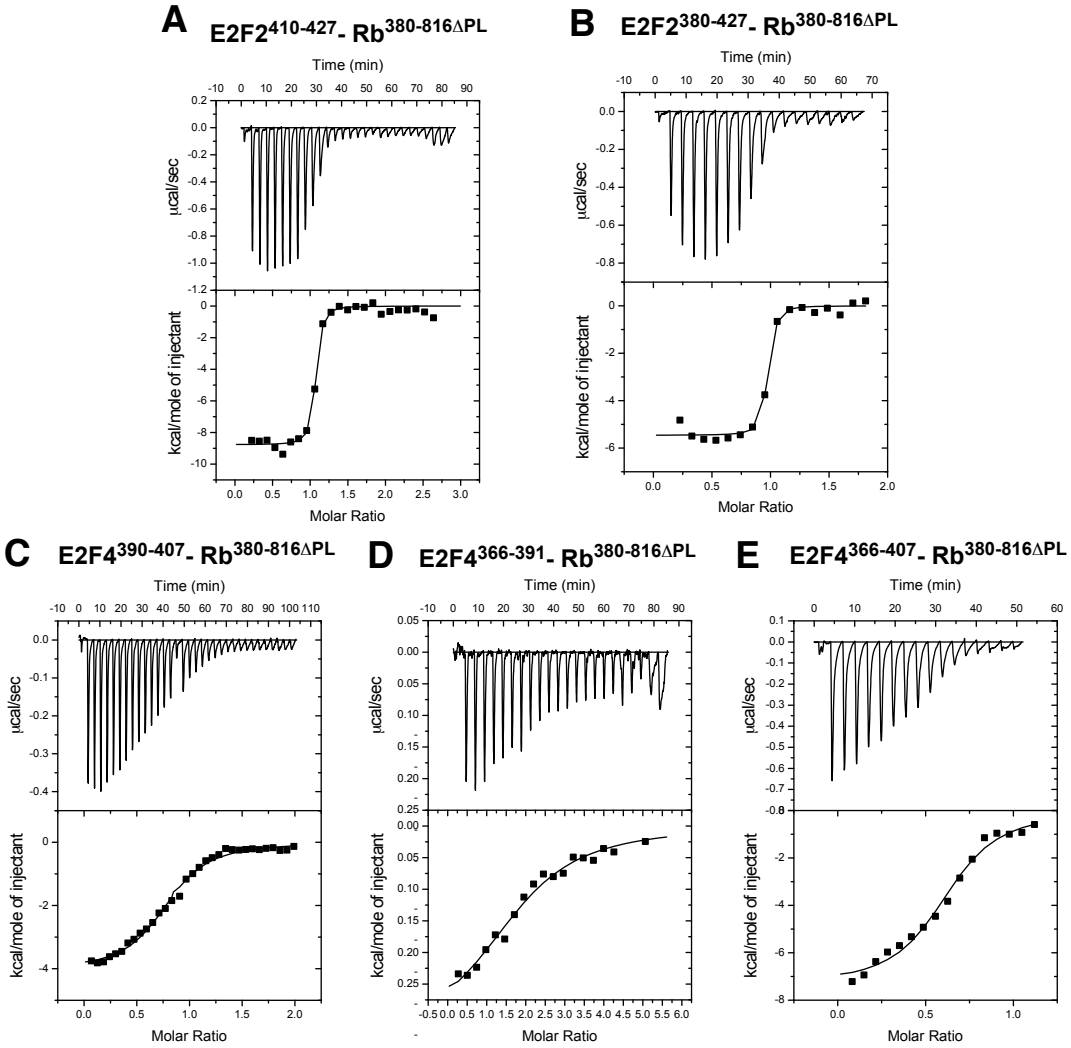

Figure 4.7. Representative ITC data from table 4.4.

4.3. Discussion

The results presented in this chapter reveal that Rb phosphorylation at S788/S795 has a special role in both dissociating RbC^{N} from E2F1-$DP1^{MB/CC}$ and competitively inhibiting the $E2F^{TD}$-Rb pocket interaction. Additionally, we find that RbC^{N} phosphorylation has an additive effect with Rb^{PL} phosphorylation, which inhibits $E2F^{TD}$ binding to Rb pocket 40-fold. Finally, $E7^{LxCxE}$ binding studies show that large Rb-E2F complexes can inhibit binding of this peptide 10-fold; an indication that-in the context of normal cellular functions-Rb's "LxCxE-binding site" may more appropriately be considered an "E2F-binding site".

4.3.1. The interplay of different phosphorylation sites

The work presented in this chapter demonstrates that certain phosphorylation events have an additive effects, and suggests mechanisms by which others may cancel each other out. Importantly, we have found another example of specific phosphorylation sites which exhibit additive effects. Previously, we found that phosphorylation of T356 and T373 are additive and occur through independent mechanisms. Experiments have shown that phosphorylation of Rb^{PL} also contributes to this effect, possibly through S612 since the structures presented in Chapters 2 and 3 suggest the effects of S608 and T373 are not compatible (see discussion 3.3.2.). Here

we find that the effect of S788/S795 is additive with S608. This suggests a mechanism whereby the bipartite binding interface of $E2F^{TD}$ is disrupted through separate competitive binding mechanisms: phosphorylation of S608 competes off the C-terminal half of $E2F^{TD}$, as seen in the Rb^{PL-P} structure, while phosphorylation of S788/S795 competes off N-terminal half of $E2F^{TD}$. We have not directly tested the compatibility of S788/S795 phosphorylation with T373 phosphorylation; however, if phosphorylation of S788/S795 causes RbC^{N} to bind the interface between the A and B subdomains similar to $E2F^{TD}$, then we would expect that these events are incompatible because T373 phosphorylation disrupts this interface. Unfortunately, it is not entirely clear what the role of T356 phosphorylation is, however it is possible that it also disrupts binding of the $E2F^{TD}$ N-terminus interface with Rb pocket. Several observations suggest this: First, the structure of Rb^{N-P} indicates that phosphorylated T356 could extend to the E2F binding site to disrupt the salt bridge between K548 and E2F's D410; an effect that would be both independent from, but additive to, the effect of T373 phosphorylation. Second, both T356 phosphorylation and a K548Q mutation cause Rb to bind $E2F1^{TD}$ with an affinity of 300nM (K548Q data not shown). If T356 and S788 both target K548 upon phosphorylation, this might disrupt the overall effect of RbC^{N} phosphorylation, however, it is possible that these two events could have an additive effect as well.

This chapter also details an interaction between Rb's "LxCxE-binding site" and E2F1-DP1$^{MB/CC}$. Specifically we find E7^{LxCxE} binding is inhibited 10-fold in the presence of E2F1-DP1$^{MB/CC-TD}$. It is probable that phosphorylation of T821/T826 negatively regulates this interaction, as it has been shown to disrupt binding between viral antigens and Rb (Knudsen and Wang 1996). Since T373 phosphorylation also negatively regulates binding to the LxCxE site and the lysine patch, the effects of T821/T826 and T373 could be additive. In support of this idea, work in our lab has shown that binding of phosphorylated RbC$^{818-842}$ (T821/T826) to Rb^{N-P} is not affected by phosphorylation of T356/T373 (Burke et al. 2012). Therefore, this is a strong indication that these two events are cooperative in disrupting Rb-E2F binding at the "LxCxE-binding site" and lysine patch.

Finally, there is an interesting symmetry in the way that all of these phosphorylation events function. Rb has three core "domains": RbN, Rb pocket and RbC. The pocket is the central domain and hosts the critical interaction with E2F^{TD}. Distinct phosphorylation events on RbN (T356/T373) and RbC (S788/S795) each specifically target the E2F^{TD} N-terminal interface with Rb pocket, and in a way that is most likely incompatible. Similarly, RbN (T373) and RbC (821/826) each individually target the Rb pocket - E2F1-DP1$^{MB/CC}$ interaction at the LxCxE site; however, this set of events is probably compatible. Rb^{PL} targets an interaction that neither RbN or RbC seem to target directly: the interface between E2F^{TD} C-terminus and Rb pocket.

Significantly, however, the pocket linker sites contribute to the overall effects of either RbN or RbC through phosphorylation of S608 (which is synergistic with RbC) or phosphorylation of S612 (which is synergistic with RbN). In light of this apparent pattern, it will be interesting to see if there are additional symmetrical functions between RbC and the lesser-studied RbN.

4.3.2. S788/S795 and T821/T826 phosphorylation in cell-based studies

In cell-based reporter assays, S795 phosphorylation alone is not sufficient to induce E2F activity (Gorges et al. 2008). Similarly, mutation of S788/S795 to alanine does not suppress E2F activity in the presence of kinase (Brown et al. 1999). However, in the context of other phosphorylation events, the significance of S788/S795 phosphorylation is more apparent. For example, Rb phosphorylated at only S608/S795/S821 has 5-fold greater E2F reporter activity than unphosphorylated Rb, and 2-fold greater activity than Rb phosphorylated at only S795/S821 (Lents et al. 2006). Similarly, mutation of T252/T356/S608/S612 to alanine barely suppresses E2F activity when compared to wild-type; however, add S788/S795 to the mix and Rb now suppresses E2F activity 25-fold more than wild-type (Brown et al. 1999). These cell-based results correlate well with our ITC data, which also suggests that S608 and S788/S795 phosphorylation together have a synergistic effect in inhibiting $E2F^{TD}$ binding to Rb pocket.

Our model for how S788/S795 phosphorylation inhibits Rb-E2F seems incompatible with the large structural change that results from T373 phosphorylation. In an E2F reporter assay, the effect T373 phosphorylation alone seems trump the effects of other phosphorylation events so that E2F activity resulting from phosphorylation of T373 alone is similar to the effect of T373 with either S249, T252, T356, or T821 (Gorges et al. 2008). The single exception to this trend is S795 with T373, which dramatically reduces E2F reporter activity when compared to the effect of phosphorylating T373 alone (Gorges et al. 2008). This result suggests that S795 phosphorylation can attenuate the effect of T373 phosphorylation, and, although the mechanism for this is not obvious, this is nevertheless a strong indication that these two events are not compatible for E2F inhibition. Furthermore, this result intriguingly implies S795 phosphorylation can counteract T373 phosphorylation to allow Rb to re-uptake E2F. While this idea is counterintuitive on many levels, it is actually consistent with one study which shows that DNA damage and oncogenic stress promote the formation of Rb-E2F complexes, and this correlates with phosphorylation of Rb at S780/S795/S807/S811 (Ianari et al. 2009).

S795 phosphorylation is the darling of Rb phosphorylation western blot analysis, and is frequently used to indicate cell cycle progression or arrest in response to different stimuli. The number of studies that specifically mention any of Rb's other phosphorylation sites is pale by comparison. This is a

somewhat fascinating trend, considering that we barely understand the function of S795, and what we do understand is that it is only able to regulate E2F in the context of additional phosphorylation events. However, one likely reason for the popularity of S795 may be that it has been repeatedly identified as specific target of CyclinD-CDK4 activity (Connell-Crowley et al. 1997; Grafstrom et al. 1999; Zarkowska et al. 1997).

Finally, work presented in this chapter suggests a functional interaction between Rb pocket and E2F1-DP1$^{MB/CC}$ at Rb's "LxCxE-binding site". Several studies have suggested this interface is regulated by T821/T826 phosphorylation (Harbour et al. 1999; Knudsen and Wang. 1996; Rubin et al. 2005). Furthermore, it's been shown that mutation of T821/T826 partially suppress E2F activity in the presence of kinase; this suggests Rb is unable to fully release E2F without phosphorylation of T821/T826 (Brown et al. 1999). Mutation of T821/T826 in combination with other RbC sites dramatically suppresses E2F activity 25-fold more than wild-type (Brown et al, 1999). This result suggests that T821/T826 cooperates with S788/S795 and S807/S811 to fully release E2F. In comparison, mutation of S807/S811 or S821/S826 alone produces only modest effects, and mutation of S788/S795 alone has no effect (Brown et al. 1999). Therefore these results emphasize that these three sets of sites have a greatly enhanced combined effect in disrupting Rb-E2F complexes. Significantly, we have not been able to identify a role for S807/S811 in the regulation of Rb-E2F complexes; however, at this point we also

barely understand the structural nature of the interaction between RbC^N and E2F1-$DP1^{MB/CC}$, so there may be some important discoveries to be made here. A different possibility is that S807/S811 function in a manner unrelated to the negative regulation of Rb-E2F interfaces. While this seems unlikely, one recent study suggests that 807/811 phosphorylation facilitates the G_0-G_1 cell cycle transition (Ren and Rollins 2004).

4.3.3. Differential E2F binding and regulation by phosphorylation imparts specificity

Throughout our studies we have identified several biochemical indicators of Rb-E2F complex-specific regulation. Buried residues in $E2F2^{TD}$ which are important for Rb binding and transcription initiation are also highly-conserved in E2Fs 1-5. Interestingly, E2Fs 1-3 are transcription factors, while E2Fs 4 and 5 are considered “active repressors” of transcription and functionally interact with Rb’s pocket protein homologues p107 and p130. Our work has shown a 50-fold difference between the affinity of $E2F2^{TD}$ and $E2F4^{TD}$ for Rb pocket (Table 4.4, rows 2-3). This suggests the different affinities for pocket-$E2F^{TD}$ interactions form a primary basis for specificity which correlates to the different pocket-E2F complexes that are found in the cell.

A second surprising result, which also suggests functional specificity at the Rb pocket-$E2F^{TD}$ level, is that T356/T373 phosphorylation inhibits $E2F1^{TD}$

binding to Rb pocket 40-fold and E2F2^{TD} binding to Rb pocket only 5-fold (Table 3.4, rows 1-2, 6-7). Therefore, this particular phosphorylation event is perhaps specific for the regulation of E2F1, while additional phosphorylation events or different combinations of events might be required to effectively release and activate E2F2. Indeed, this idea fits with the model of progressive Rb phosphorylation by different kinases though G1 phase, of which the relevance has never been well-understood. By combining these models, its conceivable that early phosphorylation events, such as T373, selectively release and activate E2F1, before a combination of subsequent events (such as Rb^{PL} phosphorylation) release and activate E2F2 at a distinct set of promoters. This type of phospho-specific E2F regulation by Rb may also extend to the Rb-E2F1-DP1$^{MB/CC}$ interfaces, which are regulated by S788/S795 and T821/T826 and may be specific for certain E2Fs (Cecchini and Dick 2011; Dick and Dyson 2003; Rubin et al. 2005).

4.3.4. Glutamic acid as a phosphomimetic in Rb

Throughout the course of our structural studies, we have often employed glutamic acid phospho-mimmetic mutations to bypass the need for phosphorylation. These mutations allow us to avoid additional protein purification steps, which is a great advantage in protein crystallography. We find that the glutamic acid substitution works well for S608, and here we are able to observe weak E2F1^{TD} binding to Rb pocket by ITC that is proportional

to the effect of phosphorylating S608 (Figure 2.14,C). However, when we use glutamic acid substitution for T356/T373, we do not observe the same conformational change in Rb that we observe upon T373 phosphorylation; although, strangely, T356E/T373E does cause significant inhibition of E2F1^{TD} binding to Rb pocket by ITC (Figure 3.9, A-B). When we use the glutamic acid substitutions for S788/S795, we observe no inhibition of E2F1^{TD} binding to Rb pocket by ITC (Figure 4.3, B). Therefore, these results are sort of a mixed bag: S608E works well, T356E/T373E partially works, and S788E/S795E does not work at all. Accordingly, it is unclear from a structural standpoint why some phospho-mimmetics work and others don't. In SAOS-2 cells, mutation of all Rb CDK consensus sites to glutamate partially inhibits Rb's ability to control cell cycle progression (Barrientes et al. 2000). Therefore, in a cellular context, certain glutamate mutations do serve as functional imitations of Rb phosphorylation; however, our studies also reveal the functional viability of each mutation is highly variable.

4.3.5. The deal with S780 phosphorylation

Many of the Rb constructs used throughout this thesis contain CDK-consensus phosphoacceptor site, S780. Previous work has established that phosphorylation of S780 occurs *in vitro* and *in vivo* (Kitagawa et al. 1996; Lees et al. 1992; Zarkowska et al. 1997). The role of S780 phosphorylation in regulating E2F is difficult to discern using our system because we find it is

impossible to quantitatively phosphorylate S780 using either recombinant cyclinA-CDK2 or cyclinK-CDK6. As one example, $Rb^{380-787}$ contains 3 well-established CDK consensus phosphorylation sites: S608, S612 and S780. When $Rb^{380-787}$ is phosphorylated in our standard kinase reaction, most of the resulting protein corresponds to a mass that indicates the incorporation of two phosphates, while a small fraction-often one third-of the protein corresponds to a mass that indicates the incorporation of three phosphates. In comparison, phosphorylation of $Rb^{380-787/S780A}$ results in a near-homogenous population of doubly phosphorylated protein. Because of this, we frequently mutate S780 to alanine in protein constructs used for crystallography, SAXS and ITC.

In the majority of Rb pocket crystal structure solutions, the S780 sidechain hydroxyl makes direct contacts with the pocket domain and therefore does not seem accessible for phosphorylation. Notably, S780 is part of the “bar motif” (residues 773-785), which wraps around the pocket domain in an odd structural fashion, similar to the tail of a sleeping cat (Figure 2.16, A). The bar is present in the majority of pocket structures, although a few pocket structures also lack the bar, which suggests that the bar is not critical for the stability of the pocket domain. However, whether the bar is present or absent does not correlate with any particular functional feature of the structure, such as LxCxE binding, and therefore the presence of the bar is probably dictated by crystal packing forces.

Based on the studies presented in chapter 4, we suggest that the bar may play a functional role in Rb-E2F complexes, and this may allow for phosphorylation at S780. The bar motif (residues 773-785) is directly adjacent to RbC^{N} (residues 788-801), which we show binds to E2F1-$DP1^{MB/CC}$ (Figure 4.4, D). E2F1-$DP1^{MB/CC}$ also binds to Rb's "LxCxE-binding site", which is proximal to the bar motif. Several structures show that the bar motif points away from the "LxCxE-binding site", and would therefore direct RbC^{N} toward the pocket A subdomain, unless it were to adopt a different conformation. Therefore, a complex involving simultaneous interactions between E2F1-$DP1^{MB/CC}$, RbC^{N} and Rb pocket would require an unknown conformation of Rb's bar, and this change in conformation might expose S780 for phosphorylation. Thus, it stands to reason that S780 can be better phosphorylated in an experiment in which $Rb^{380-801}$ is in complex with E2F1-$DP1^{MB/CC-TD}$.

An alternative hypothesis is offered up by a new study which proposes that the peptidylprolyl isomerase, Pin-1, is important for phosphorylating S780 in cells (Rizzolio et al. 2012). Notably, S780 is in a proline-rich coil, and therefore Pin-1 may be required to alter the bar conformation so that S780 becomes accessible to kinase.

In summary, we do observe that S780 is phosphorylated by CDK2-cyclin A *in vitro* by LC-MS/MS (Table 4.1); however, full-protein ESI-MS indicates that unlike the other phosphorylation events we study, this

phosphorylation event is not quantitative (data not shown). Interestingly, our structural studies hint that the large Rb-E2F1 complex might be required for more robust S780 phosphorylation.

4.4. Materials and Methods

ITC and NMR experiments were performed as described in chapters 2.2.3 and 2.2.4.

4.4.1. Protein Expression and Purification

$RbC^{787-816}$ is expressed as a GST-fusion proteins in *e. coli* and induced with 1 mM IPTG for three hours at 37C. Expression of this construct is generally poor one particular truncation is common: $RbC^{787-806}$. Lysate is purified over GS4B, then Q, then cut with GST-TEV and re-purified over GS4B to obtain pure peptide.

$E2F2^{TD}$ and $E2F4^{TD}$ peptides are expressed as GST-fusion proteins in *e. coli* and induced overnight at RT with 1 mM IPTG. Lysate is purified over GS4B, then Q, then cut with GST-TEV and re-purified over GS4B to obtain pure peptide. $E2F4^{366-407}$ co-purifies from the initial GS4B step with an *e. coli* heat shock protein (identified by MS/MS). The heat shock protein can be purified away through multiple runs over a SD200 column. Expression of $E2F4^{366-407}$ is also less robust than expression of the shorter protein,

E2F4$^{390\text{-}407}$. Expression and purification of E2F2$^{380\text{-}427}$ is straight forward and comparable to expression of the shorter version, E2F2$^{410\text{-}427}$. E2F1-DP1$^{MB/CC}$ and E2F1-DP1$^{MB/CC\text{-}TD}$ were expressed and purified as described (Rubin et al. 2005). All Rb pocket constructs were expressed and purified as previously described (Chapter 2, materials and methods). Notably, Rb$^{380\text{-}816\Delta PL}$ does not express as well as Rb pocket constructs, perhaps due to the presence of a troublesome IYI motif in RbC (residues 804-806). The E7^{LxCxE} peptide (DLYCYQLN) was purchased from biopeptides.com

4.4.2. Liquid Chromatography Mass Spectrometry (LC-MS/MS)

Rb$^{55–928}$ was expressed in insect cells, purified, concentrated to 1–5 mg/ml and then phosphorylated in a reaction containing 10 mM $MgCl_2$, 10 mM ATP, 250 mM NaCl, 25 mM Tris (pH 8.0), 5% Cdk2-Cyclin A (percentage of mass of the total substrate in the reaction). Kinase reactions were incubated at room temperature for 1 hr, then digested at room temperature for an hour with 3% trypsin or chymotrypsin and no denaturing agents. Reactions were quenched and diluted in buffer containing 1 mM PMSF, loaded on to a C18 column, and eluted at 1 ml/min for 30 minutes over a gradient of 5% ACN to 50% ACN on to a Thermo Finnegan liquid chromatography MS/MS (LTQ) linear ion trap. All MS/MS spectra were processed using Bioworks 3.3. Peptide identifications with better than 0.01 peptide probability were accepted and manually inspected for the appropriate peptide fragments.

4.5. References

Adams PD, Li X, Sellers WR, Baker KB, Leng X, Harper JW, Taya Y, Kaelin WG Jr. "Retinoblastoma protein contains a C-terminal motif that targets it for phosphorylation by cyclin-cdk complexes." *Mol Cell Biol.* 19, 1068–80. (1999)

Brown VD, Phillips RA, Gallie BL. "Cumulative effect of phosphorylation of pRB on regulation of E2F activity." *Mol Cell Biol.* 19(5), 3246-56. (1999)

Burke JR, Hura GL, Rubin SM. "Structures of inactive retinoblastoma protein reveal multiple mechanisms for cell cycle control." *Genes Dev.* 26(11):1156-66. (2012)

Cecchini MJ, Dick FA. "The biochemical basis of CDK phosphorylation-independent regulation of E2F1 by theretinoblastoma protein." *Biochem J.* 434(2):297-308. (2011)

Chen TT, Wang JYJ. "Establishment of irreversible growth arrest in myogenic differentiation requires RB LxCxE-binding function." *Mol. Cell. Biol.* 20(15), 5571-80. (2000)

Connell-Crowley L, Harper JW, Goodrich DW. "Cyclin D1/Cdk4 regulates retinoblastoma protein-mediated cell cycle arrest by site-specific phosphorylation." *Mol Biol Cell.* 8(2), 287-301. (1997)

Dick FA, Sailhamer E, Dyson NJ. "Mutagenesis of the pRB pocket reveals that cell cycle arrest functions are separable from binding to viral oncoproteins." *Mol Cell Biol.* 20(10), 3715-27. (2000)

Dick FA, Dyson N. "pRB contains an E2F1-specific binding domain that allows E2F1-induced apoptosis to be regulated separately from other E2F activities." *Mol Cell.* 12(3), 639-49. (2003)

Felsani A, Mileo AM, Paggi MG. "Retinoblastoma family proteins as key targets of the small DNA virus oncoproteins." *Oncogene* 25(38), 5277-85. (2006)

Gorges LL, Lents NH, Baldassare JJ. "The extreme COOH terminus of the retinoblastoma tumor suppressor protein pRb is required for

phosphorylation on Thr-373 and activation of E2F. " *Am J Physiol Cell Physiol.* 295(5), 1151-60. (2008)

Grafstrom RH, Pan W, Hoess RH. "Defining the substrate specificity of cdk4 kinase-cyclin D1 complex." *Carcinogenesis* 20(2), 193-8. (1999)

Hagemeier C, Cook A, Kouzarides T. "The retinoblastoma protein binds E2F residues required for activation in vivo and TBP binding in vitro." *Nucleic Acids Res.* 21(22), 4998-5004. (1993)

Hallstrom TC, Nevins JR. "Specificity in the activation and control of transcription factor E2F-dependent apoptosis." *Proc Natl Acad Sci* 100(19), 10848-53. (2003)

Harbour JW, Luo RX, Dei Santi A, Postigo AA, Dean DC. "Cdk phosphorylation triggers sequential intramolecular interactions that progressively block Rb functions as cells move through G1." *Cell* 98(6), 859-69. (1999)

Hassler M, Singh S, Yue WW, Luczynski M, Lakbir R, Sanchez-Sanchez F, Bader T, Pearl LH,Mittnacht S. "Crystal structure of the retinoblastoma protein N domain provides insight into tumor suppression, ligand i nteraction, and holoprotein architecture." *Mol Cell.* 28(3), 371-85. (2007)

Hirschi A, Cecchini M, Steinhardt RC, Schamber MR, Dick FA, Rubin SM. "An overlapping kinase and phosphatase docking site regulates activity of the retinoblastoma protein." *Nat Struct Mol Biol.* 17(9), 1051-7. (2010)

Huang PS, Patrick DR, Edwards G, Goodhart PJ, Huber HE, Miles L, Garsky VM, Oliff A, Heimbrook DC. "Protein domains governing interactions between E2F, the retinoblastoma gene product, and human papillomavirus type 16 E7 protein." *Mol Cell Biol.* 13(2), 953-60. (1993)

Ianari A, Natale T, Calo E, Ferretti E, Alesse E, Screpanti I, Haigis K, Gulino A, Lees JA. "Proapoptotic function of the retinoblastoma tumor suppressor protein." *Cancer Cell.* 15(3), 184-94. (2009)

Kennedy BK, Liu OW, Dick FA, Dyson N, Harlow E, Vidal M. "Histone deacetylase-dependent transcriptional repression by pRB in yeast occurs independently of interaction through the LXCXE binding cleft." *Proc Natl Acad Sci* 98(15), 8720-5. (2001)

Kitagawa M, Higashi H, Jung HK, Suzuki-Takahashi I, Ikeda M, Tamai K, Kato J, Segawa K, Yoshida E, Nishimura S, Taya Y. "The consensus motif for phosphorylation by cyclin D1-Cdk4 is different from that for phosphorylation by cyclin A/E-Cdk2." *EMBO J.* 15(24),7060-9. (1996)

Knudsen ES, Wang JY. "Differential regulation of retinoblastoma protein function by specific Cdk phosphorylation sites." *J Biol Chem.* 271(14), 8313-20. (1996)

Knudsen ES, Wang JY. "Dual mechanisms for the inhibition of E2F binding to RB by cyclin-dependent kinase-mediated RB phosphorylation." *Mol Cell Biol.* 17(10), 5771-83. (1997)

Lee C, Chang JH, Lee HS, Cho Y. "Structural basis for the recognition of the E2F transactivation domain by the retinoblastoma tumor suppressor." *Genes Dev.* 16(24), 3199-212. (2002)

Lee JO, Russo AA, Pavletich NP. "Structure of the retinoblastoma tumour-suppressor pocket domain bound to a peptide from HPV E7." *Nature* 391, 859-65. (1998)

Lees JA, Buchkovich KJ, Marshak DR, Anderson CW, and Harlow E. "The retinoblastoma protein is phosphorylated on multiple sites by human cdc2." *EMBO J.* 10**,** 4279- 4290. (1991)

Lents NH, Gorges LL, Baldassare JJ. "Reverse mutational analysis reveals threonine-373 as a potentially sufficient phosphorylation site for inactivation of the retinoblastoma tumor suppressor protein (pRB)." *Cell Cycle* 5(15),1699-707. (2006)

Liu X, Clements A, Zhao K, Marmorstein R. "Structure of the human Papillomavirus E7 oncoprotein and its mechanism for inactivation of the retinoblastoma tumor suppressor." *J Biol Chem.* 281(1), 578-86. (2006)

Liu X, Marmorstein R. "Structure of the retinoblastoma protein bound to adenovirus E1A reveals the molecular basis for viral oncoprotein inactivation of a tumor suppressor." *Genes Dev.* 21(21), 2711-6. (2007)

Morris EJ, Dyson NJ. “Retinoblastoma binding partners.” *Adv Cancer Res.* 82, 1-54. (2001)

Phelps WC, Münger K, Yee CL, Barnes JA, Howley PM. “Structure-function analysis of the human papillomavirus type 16 E7 oncoprotein.” *J Virol.* 66(4), 2418-27. (1992)

Qin XQ, Chittenden T, Livingston DM, Kaelin WG Jr. “Identification of a growth suppression domain within the retinoblastoma gene product.” *Genes Dev.* 6(6), 953-64. (1992)

Rayman JB, Takahashi Y, Indjeian VB, Dannenberg JH, Catchpole S, Watson RJ, te Riele H, Dynlacht BD. “E2F mediates cell cycle-dependent transcriptional repression in vivo by recruitment of an HDAC1/mSin3B corepressor complex.” *Genes Dev.* 16(8), 933-47. (2002)

Ren S, Rollins BJ. “Cyclin C/cdk3 promotes Rb-dependent G0 exit.” *Cell* 17(2), 239-51. (2004)

Rizzolio F, Lucchetti C, Caligiuri I, Marchesi I, Caputo M, Klein-Szanto AJ, Bagella L, Castronovo M, Giordano A. “Retinoblastoma tumor-suppressor protein phosphorylation and inactivation depend on direct interaction with Pin1.” *Cell Death Differ.* 19(7), 1152-61. (2012)

Rubin SM, Gall AL, Zheng N, Pavletich NP. “Structure of the Rb C-terminal domain bound to E2F1-DP1: a mechanism for phosphorylation-induced E2F release.” *Cell* 123(6),1093-106. (2005)

Singh M, Krajewski M, Mikolajka A, Holak TA. “Molecular determinants for the complex formation between the retinoblastoma protein and LXCXE sequences.” *J Biol Chem.* 280(45), 37868-76. (2005)

Xiao B, Spencer J, Clements A, Ali-Khan N, Mittnacht S, Broceño C, Burghammer M, Perrakis A, Marmorstein R, Gamblin SJ. “Crystal structure of the retinoblastoma tumor suppressor protein bound to E2F and the molecular basis of its regulation.” *Proc Natl Acad Sci* 100(5), 2363-8. (2003)

Zarkowska T, Mittnacht S. “Differential phosphorylation of the retinoblastoma protein by G1/S cyclin-dependent kinases.” *J Biol Chem.* 272(19), 12738-46. (1997)